College Note No. 33

THE COLLEGE OF AERONAUTICS

CRANFIELD

INCOMPRESSIBLE FLOW PAST BODIES OF REVOLUTION

by

T. NONWEILER

NOTE NO. 33
JULY, 1955.

THE COLLEGE OF AERONAUTICS

CRANFIELD

Incompressible Flow Past Bodies of Revolution

-by-

T. Nonweiler, B.Sc.

List of Contents

MEP

List of Contents (Contd.)

---

1. Introduction

In this paper we shall attempt to review the existing information, both theoretical and experimental, which relates to some of the more important aerodynamic problems arising in the study of the flow over bodies of revolution. Many of these problems can only be explained by including an account of the effects of the air viscosity on the flow, but this can more easily be accomplished if we first consider the simpler conditions existing in inviscid, irrotational flow. In common with many other branches of aerodynamics, potential flow theory provides a basic framework of knowledge, helping to suggest likely effects of viscosity, which we can modify to explain and predict the behaviour of a real fluid.

Thus the first part of this paper is taken up with a study of the various methods which have from time to time been devised to enable the calculation of the properties of axi-symmetric potential flow. We shall first concern ourselves with more or less exact, rigorous theories, and afterwards with the approximate methods. Space does not permit a full discussion of the exact techniques but it is not considered that any single approach possesses advantages above all others to warrant exclusive attention: so a brief review is given of most of those which have been developed. The theory of potential flow about inclined bodies of revolution is next discussed, and leads to an account of the manner in which these results can be used to derive the surface pressure distribution, and the magnitude of the theoretical destabilising moment on a body in a simple translational motion.

The second part of the paper is concerned in the main with the modifications introduced by viscosity effects. These manifest themselves in the presence of a drag force which can be readily assessed in axi-symmetric flow, and also of a lift force whose magnitude cannot be so accurately predicted. In

relation to this latter problem, we give a brief description of the various changes in the flow pattern which have been observed to take place as the body incidence is increased. A detailed account of the theory of boundary layer flow, which lies behind many of the results quoted, has been avoided.

Finally, brief sections are appended devoted to the problems of the flow over bodies in curved motion, and to the external flow about ducted bodies of revolution.

We shall for the most part concern ourselves only with the steady motion of slender bodies in an incompressible fluid of small viscosity. Thus we exclude from discussion the flow about spheres or planetary ellipsoids, and we make no reference to phenomena typical of low Reynolds numbers.

2. The Flow about an Ellipsoid of Revolution

The most important of the exact solutions of the equation of continuity for potential flow about bodies of revolution is, no doubt, the classical treatment of the motion of an ovary ellipsoid of revolution or spheroid, given, for instance, by Lamb (1879) and Munk (1934). A short summary of this treatment will be of interest here, as it introduces the use of certain techniques which have been extended to the solution of other problems to be discussed later.

The method depends essentially upon the use of semi-elliptic coordinates (μ,ζ,θ) defined in terms of the cylindrical polars (r,θ,x) by the relations

$$r = l_f (1-\mu^2)^{\frac{1}{2}} (\zeta^2-1)^{\frac{1}{2}} ; \quad x = l_f \mu\zeta . \qquad \ldots\ldots\ldots(1)$$

The system of surfaces ζ = constant, for $\zeta \geqslant 1$, define a family of confocal ellipsoids of revolution, centre the origin (see fig.1); the surface $\zeta = 1$ is degenerate, being the line joining the foci $x = \pm l_f$, on $r = 0$. The surfaces μ = constant for $-1 \leqslant \mu \leqslant 1$ define an orthogonal system of confocal hyperboloids

of revolution.

The metric for this system of coordinates is found to be

$$d\zeta^2 = l_f^2 \left[\left(\frac{\zeta^2-\mu^2}{1-\mu^2} \right) d\mu^2 + \left(\frac{\zeta^2-\mu^2}{\zeta^2-1} \right) d\zeta^2 + (1-\mu^2)(\zeta^2-1)d\theta^2 \right];$$

and the equation of continuity, which is the Laplace equation for the velocity potential ϕ, may be accordingly written as

$$\frac{\partial}{\partial\mu} \left[(1-\mu^2) \frac{\partial\phi}{\partial\mu} \right] + \frac{\partial}{\partial\zeta} \left[(\zeta^2-1) \frac{\partial\phi}{\partial\zeta} \right] + \frac{\zeta^2-\mu^2}{(1-\mu^2)(\zeta^2-1)} \frac{\partial^2\phi}{\partial\theta^2} = 0.$$

Using the method of separation of variables, a general solution for ϕ may be shown to be obtained by linear superposition of solutions of the type:

$$\phi = \phi_{nm} K_n^m(\mu) K_n^m(\zeta) \cos(m\theta + \theta_{nm}), \quad \ldots\ldots\ldots\ldots(2)$$

where ϕ_{nm} and θ_{nm} are constants, and K_n^m denotes Legendre associated functions of either the first or second kind, (which we later distinguish as P_n^m and Q_n^m respectively).

We suppose that the spheroid $\zeta = \zeta_w$, a constant > 1, is to be a stream surface of a motion of the fluid in which the velocity at infinity is parallel to its axis and of magnitude u_∞. This motion will have an axial symmetry, and accordingly we need only consider those solutions of ϕ independent of θ. The boundary condition on the surface is that

$$\frac{\partial\phi'}{\partial\zeta} = -u_\infty \frac{\partial x}{\partial\zeta} = -u_\infty l_f \mu, \quad \text{on} \quad \zeta = \zeta_w,$$

supposing that ϕ' denotes the perturbation velocity potential, so that ϕ' tends asymptotically to a constant value (say, zero) at infinity. Accordingly we infer that ϕ' is not only independent of θ, but linearly dependent on μ. We can select the appropriate form of solution from (2) by noting that $m = 0$ and $P_1^0(\mu) = \mu$, and consequently we can deduce that

$$\phi' = -u_\infty l_f (\zeta_w^2 - 1)^{\frac{1}{2}} P_1^0(\mu) Q_1^0(\zeta) \Big/ Q_1^1(\zeta_w) \quad \ldots\ldots\ldots(3)$$

The value of ζ_w may be identified with the reciprocal of the eccentricity of the given spheroid, and $(2l_f)$ is of course its focal distance, so that $l_f(\zeta_w^2 - 1)^{\frac{1}{2}}$ is the length of its minor semi-axis (i.e. its maximum radius).

Similarly the flow over a spheroid moving laterally to its axis may be treated by considering it to be a stream surface of a motion of the fluid in which the velocity at infinity is parallel to the z-axis, say, and of magnitude w_∞. The boundary condition for the perturbation velocity potential is then

$$\frac{\partial \phi'}{\partial \zeta} = - w_\infty \frac{\partial z}{\partial \zeta} = - w_\infty l_f \left(\frac{1-\mu^2}{\zeta^2 - 1} \right)^{\frac{1}{2}} \zeta \cos\theta, \quad \text{on } \zeta = \zeta_w ;$$

and it is found that

$$\phi' = - w_\infty l_f P_1^1(\mu) Q_1^1(\zeta) \cos\theta \Big/ \left[\frac{dQ_1^1(\zeta_w)}{d\zeta_w} \quad \frac{(\zeta_w^2 - 1)^{\frac{1}{2}}}{\zeta_w} \right] \qquad \ldots\ldots\ldots\ldots (4)$$

The appropriate linear superposition of the solutions (3) and (4) yields the potential of the disturbed flow for any translational motion, combining axial and lateral movement. The most general motion of a spheroid can be treated by inclusion of the effect of a rotation with angular velocity Ω about the axis $\theta = \theta_o$ through its centre, say, due to which the disturbed flow is given by the potential

$$\phi' = - \frac{1}{3} \Omega l_f^2 P_2^1(\mu) Q_2^1(\zeta) \sin(\theta - \theta_o) \Big/ \left[(\zeta_w^2 - 1)^{\frac{1}{2}} \frac{dQ_2^1(\zeta_w)}{d\zeta_w} \right].$$

3. The Stokes Stream Function

In flows possessing axial symmetry, - due to the motion of a body of revolution parallel to its axis, - it is sometimes convenient to introduce the Stokes stream function Ψ, related to the velocity potential by the equations

$$\frac{\partial \Psi}{\partial r} = r \frac{\partial \phi}{\partial x} , \quad \frac{\partial \Psi}{\partial x} = - r \frac{\partial \Psi}{\partial r} . \qquad \ldots\ldots\ldots\ldots (5)$$

The definition of this function ensures that the flow satisfies the continuity equation, and Ψ = constant represents the stream surfaces (Stokes, 1842, and Sampson 1891). The condition of irrotational flow becomes

$$r \frac{\partial}{\partial r} \left(\frac{1}{r} \frac{\partial \Psi}{\partial r} \right) + \frac{\partial^2 \Psi}{\partial x^2} = 0 . \qquad \text{.....(6)}$$

Corresponding to the general axially-symmetric solution for the velocity potential given by putting $m = 0$ in (2), i.e.

$$\phi = \phi_{no} K_n^o(\mu) K_n^o(\zeta) , \qquad \text{.....(7)}$$

- there exists an equivalent solution of (6) which can be written as

$$\Psi = \frac{\phi_{no} l_f}{n(n+1)} (1-\mu^2)(\zeta^2-1) \frac{dK_n^o(\mu)}{d\mu} \frac{dK_n^o(\zeta)}{d\zeta} . \qquad \text{.....(8)}$$

The stream function for a uniform stream of speed u_∞ parallel to the axis is $\frac{1}{2}u_\infty r^2 = \frac{1}{2}u_\infty l_f^2(1-\mu^2)(\zeta^2-1)$, so that after superposing solutions we find that the expression

$$\Psi = l_f(1-\mu^2)(\zeta^2-1) \left[\sum_n \frac{\phi_{no}}{n(n+1)} \frac{dK_n^o}{d\mu} \frac{dK_n^o}{d\zeta} + \tfrac{1}{2}u_\infty l_f \right] \qquad \text{.....(9)}$$

represents the Stokes stream function for an axial motion about an arbitrary body of revolution. Its surface has a point on the axis $r = 0$ (or $\mu = 1$) so that it is represented by $\Psi = 0$. The Stokes stream function for the flow about a spheroid can be found to be given by

$$\Psi = \tfrac{1}{2} l_f^2 u_\infty (1-\mu^2)(\zeta^2-1) \left\{ 1 - \left[\frac{dQ_1^o(\zeta)}{d\zeta} \right] \Big/ \left[\frac{dQ_1^o(\zeta_w)}{d\zeta_w} \right] \right\} .$$

Evidently $\zeta = \zeta_w$ is a stream surface ($\Psi = 0$), as required.

4. Kaplan's Method

Kaplan (1934) has used equation (9), with $\frac{dK_n^o}{d\mu}$ and $\frac{dK_n^o}{d\zeta}$ replaced by $\frac{dP_n^o}{d\mu}$ and $\frac{dQ_n^o}{d\zeta}$ respectively, to determine the axial flow about a surface of revolution represented by

$$\zeta_w = \sum_{r=0}^{\infty} a_r \mu^r \,. \qquad \text{.....(10)}$$

Expanding the expression for the Stokes stream function,

$$\frac{\Psi}{l_f(1-\mu^2)(\zeta^2-1)} = \tfrac{1}{2} u_\infty l_f + \sum_{n=1}^{\infty} \frac{\phi_{no}}{n(n+1)} \frac{dP_n^o}{d\mu} \frac{dQ_n^o}{d\zeta} \,, \qquad (11)$$

on the surface of the body as a power series in μ with the help of (10), and equating to zero the coefficient of each power of μ, - as is necessary if the surface is to be a stream surface of the motion, - yields a set of linear equations for the unknowns ϕ_{no}. The multiple of each term ϕ_{no} in these equations can consequently be obtained from a knowledge of the values of a_r in (10). As a computational method, it is of practical value if the given body shape closely corresponds to an ellipsoid, so that the first few terms of the series of equation (10) are adequate to describe its shape, and likewise all but the first few unknowns ϕ_{no} may be neglected in the expression for the potential or Stokes stream function.

Kaplan also describes a similar method applicable to the calculation of the transverse flow about the body of revolution, in which a set of linear equations is obtained for the coefficients ϕ_{n1} of the general expression for the corresponding perturbation potential :

$$\phi' = \sum_{n} \phi_{n1} P_n^1(\mu) Q_n^1(\zeta) \cos\theta \qquad \text{.....(12)}$$

As the flow has no longer an axial symmetry, Stokes stream function cannot of course be employed.

A more convenient computational method for evaluation of the coefficients ϕ_{no} in equation (11) has been independently suggested by R.H. Smith (1935): it is simply to substitute the values of the coordinates of m chosen points (ζ_n, μ_n) on the body profile $(\Psi = 0)$ in (11), and by neglect of all but the first m coefficients $\phi_{1o}, \phi_{2o}, \ldots, \phi_{mo}$, to obtain m

non-homogeneous linear equations for these coefficients, which can be solved by usual methods. The knowledge of a form of relation between ζ and μ like equation (10) assumed in Kaplan's method, is of course unnecessary to this technique, but the accuracy of both approaches is alike sensitive to the choice of the position of the foci of the coordinate system relative to the body (see page 21).

An alternative and later suggestion by Kaplan for the solution of the longitudinal flow involves an extension of the use of special coordinate systems, and brief details are given in the next section.

5. The Use of Generalised Orthogonal Coordinates for Axially Symmetric Flows. (Kaplan, 1943)

An axial flow about a body can be described by treating ϕ, the velocity potential, as a function of the cylindrical polar coordinates (r,x). Suppose however we now treat x and r as if they were rectangular, or cartesian , coordinates of a plane: then the equation of continuity for ϕ,

$$\frac{\partial}{\partial r}\left(r\,\frac{\partial \phi}{\partial r}\right) + \frac{\partial}{\partial x}\left(r\,\frac{\partial \phi}{\partial x}\right) = 0 \ ,$$

may be said to be the two-dimensional form of the equation

$$\nabla.(r\nabla\phi) \ = \ 0,$$

valid in two dimensional space for all values of r and x. It may be noted that we can suppose ϕ to exist for $r < 0$, by analytical continuation, as an even function of r. If a new set of two-dimensional orthogonal coordinates (ξ,η) is introduced to replace the cartesians (z,r), the continuity equation becomes

$$\frac{\partial}{\partial \xi}\left(\frac{rh_2}{h_1}\,\frac{\partial \phi}{\partial \xi}\right) + \frac{\partial}{\partial \eta}\left(\frac{rh_1}{h_2}\,\frac{\partial \phi}{\partial \eta}\right) = 0,$$

where $\quad ds^2 = dx^2 + dr^2 = h_1 d\xi^2 + h_2 d\eta^2.$

In particular, if the transformation is conformal, i.e.

$$x + ir = f(\xi + i\eta), \qquad \text{.....(13)}$$

where f is some specified function different from a constant, then $h_1 = h_2$, so that the continuity equation simplifies to :

$$\frac{\partial}{\partial \xi}\left(r \frac{\partial \phi}{\partial \xi}\right) + \frac{\partial}{\partial \eta}\left(r \frac{\partial \phi}{\partial \eta}\right) = 0 . \qquad \text{.....(14)}$$

Let us choose the transformation of equation (13) so that the region external to the contour in the (x,r) plane, representing the meridian plane of the body, maps into the upper half-plane, $\eta \geq 0$. This may best be effected by mapping this region of the (x,r) plane onto that exterior to a circle, $|Z| = R$, in the Z-plane, by a conformal transformation :

$$x + ir = Z + a_o R + \frac{a_1 R^2}{Z} + \frac{a_2 R^3}{Z^2} + \dots , \qquad \text{.....(15)}$$

and then placing

$$Z = R \exp\left[-i\,(\xi + i\eta)\right] . \qquad \text{.....(16)}$$

The coefficients in the series (15) may be determined by Theodorson's method. We have seen that ϕ is an even function of r, so that accordingly, the contour representing the body profile in the (x,r) plane is symmetrical about the x-axis, and consequently the coefficients $a_o, a_1, a_2, \dots$ will be real. Separating (15) into real and imaginary parts with the help of (16), we find that

$$\left.\begin{aligned} x &= R\left[e^{\eta}\cos\xi + a_o + a_1 e^{-\eta}\cos\xi + \dots\right] \\ r &= -R\left[e^{\eta}\sin\xi + a_1 e^{-\eta}\sin\xi + a_2 e^{-2\eta}\sin 2\xi + \dots\right] \end{aligned}\right\} \text{for } \eta \geq 0. \qquad \text{.....(17)}$$

The boundary condition satisfied at the surface by the perturbation potential (ϕ') in terms of the conformal orthogonal coordinates (ξ,η), is given by

$$\frac{\partial \phi'}{\partial \eta} = -u_\infty \frac{\partial x}{\partial \eta} , \quad \text{on } \eta = 0 , \qquad \text{.....(18)}$$

where u_∞ is the velocity of the body relative to the undisturbed stream, in the direction of its axis of symmetry; at infinity ϕ' must tend asymptotically to a constant value, and so this describes its behaviour as $\eta \longrightarrow \infty$. The simplicity of these boundary conditions is a result of the special choice of coordinate system, and leads to an iterative process of solution of the differential equation (14) involving only simple quadratures.

The substitution of the expression for r' from (17) in (14) gives the equation for the perturbation potential in the form

$$\sinh(\eta-\chi)\sin\xi\left(\frac{\partial^2\phi'}{\partial\xi^2}+\frac{\partial^2\phi'}{\partial\eta^2}\right)+\sinh(\eta-\chi)\cos\xi\,\frac{\partial\phi'}{\partial\xi}+\cosh(\eta-\chi)\sin\xi\,\frac{\partial\phi'}{\partial\eta}$$

$$=\sum_{n=1}^{\infty} b_n\,\varepsilon^n\,e^{-(n+1)\eta}\left[\sin(n+1)\xi\left(\frac{\partial^2\phi'}{\partial\xi^2}+\frac{\partial^2\phi'}{\partial\eta^2}\right)\right.$$

$$\left.+(n+1)\cos(n+1)\xi\,\frac{\partial\phi'}{\partial\xi}-(n+1)\sin(n+1)\xi\,\frac{\partial\phi'}{\partial\eta}\right], \quad \ldots\ldots(19)$$

where $2\chi = \log a_1$, and $2a_1^{\frac{1}{2}} b_n\,\varepsilon^n = a_{n+1}$. Likewise the boundary condition (18) can be expressed as

$$\left.\frac{\partial\phi'}{\partial\eta}\right|_{\eta=0} = 2u_\infty \mathrm{Re}^{\chi}\left[\sinh\chi\cos\xi+\sum_{n=1}^{\infty}(n+1)b_n\,\varepsilon^n\cos(n+1)\xi\right] \quad (20)$$

A solution of (19) subject to (20) is sought by putting

$$\phi' = \sum_{n=0}^{\infty}\phi_n\,\varepsilon^n,$$

and equating the powers of ε on each side of the equations. Kaplan, in this manner, arrives at the differential equations for ϕ_0, ϕ_1 and ϕ_2 and their appropriate boundary values on $\eta = 0$. These equations he solves by separation of variables after introducing new independent variables $\cos\xi$ and $\cosh(\eta-\chi)$, which render the separated parts of the homogeneous left-hand-side of equation (19) solvable in terms of Legendre functions. The

solution for ϕ_o is for instance, found as

$$\phi_o = - u_\infty R(e^{2\chi} - 1)\, P_1^o(\cos\xi) Q_1^o\left[\cosh(\eta - \chi)\right] \Big/ Q_1^1(\cosh\chi),$$

but the expressions for ϕ_1, ϕ_2, ... become increasingly involved.

The value of ϕ_o is by itself sufficient to describe the flow about an ellipsoid of revolution when ξ and η can be identified with the semi-elliptic coordinates used in the classical treatment (of section 2). As an application of the general method, Kaplan considers the axial flow about a body whose meridian section is of the form of a symmetrical Joukowski profile. The resulting surface velocity distribution obtained is practically indistinguishable from that obtained by Kaplan's earlier method, but the computations involved are less formidable. The chosen body meridian section is particularly suitable to this method, as of course it is the result of a well known conformal transformation of a circle. The computational advantages are less obvious for an arbitrary shape.

6. Source and Doublet Distributions

The most profitably exploited alternative technique to the use of special coordinate methods has been found in the simulation of the flow about bodies by distributions of singularities, such as sources and doublets. We shall begin with a brief discussion of the flow described by such isolated singularities and then pass on to a discussion of the several methods developed to find the manner of their distribution required to describe the flow conditions about an arbitrary but stipulated shape of body.

The velocity potential and Stokes stream function of the three-dimensional source at the origin is given in terms of cylindrical coordinates (r,x) by

$$\phi = \frac{-m}{4\pi(r^2+x^2)^{\frac{1}{2}}}, \qquad \Psi = \frac{-mx}{4\pi(r^2+x^2)^{\frac{1}{2}}}. \qquad \text{.....(21)}$$

The equivalent expression for a double source or doublet may be obtained by differentiating with respect to x

$$\text{i.e.,} \qquad \phi = \frac{M x}{4\pi(r^2+x^2)^{3/2}}, \qquad \Psi = \frac{-Mr^2}{4\pi(r^2+x^2)^{3/2}}; \quad \ldots\ldots(22)$$

and corresponding solutions of higher order singularities, or quadrupoles, may be easily found in terms of Legendre functions as :

$$\left.\begin{aligned} \phi &= (-1)^{n-1} n!\,(x^2+r^2)^{-\left(\frac{n+1}{2}\right)} P_n^0\left(\frac{x}{\sqrt{x^2+r^2}}\right) \\ \Psi &= (-1)^n (n-1)!\,(x^2+r^2)^{-\left(\frac{n+1}{2}\right)} r\, P_n^1\left(\frac{x}{\sqrt{x^2+r^2}}\right) \end{aligned}\right\} \text{ for } n > 0 ;$$

$$\left.\begin{aligned} \phi &= -(x^2+r^2)^{-\left(\frac{n+1}{2}\right)} Q^0_{-(n+1)}\left(\frac{x}{\sqrt{x^2+r^2}}\right) \Big/ (-n-1)! \\ \Psi &= -(x^2+r^2)^{-\left(\frac{n+1}{2}\right)} r\, Q^1_{-(n+1)}\left(\frac{x}{\sqrt{x^2+r^2}}\right) \Big/ (-n)! \end{aligned}\right\} \text{ for } n < 0 . \quad \ldots\ldots\ldots\ldots(23)$$

By superposition of sources and sinks in a uniform stream the axially symmetric flow about various closed bodies of revolution can be simulated. This was first suggested by Rankine (1871) and the concept was elaborated by D.W. Taylor (1894). A single source in a uniform stream produces a flow about the so-called Blasius-Fuhrmann half-body(fig.2). The addition of an equal sink downstream of the source serves to close the streamtube representing the body. (For any closed body the algebraic sum of the strengths of the enclosed sources must, of course, be zero.) Fuhrmann (1911) computed several bodies using continuous axial distributions of sources and sinks. Thus, denoting by $q(x)$ the density of the source distribution per unit length along the axis $(r = 0)$, in the interval $-l \leq x \leq l$, the potential and Stokes stream functions of the resulting flow

are evidently given from equation (21) by

$$\phi = \frac{-1}{4\pi}\int_{-l}^{+l} \frac{q(t)\,dt}{\left[(x-t)^2 + r^2\right]^{\frac{1}{2}}} \; ; \; \Psi = \frac{-1}{4\pi}\int_{-l}^{+l} \frac{(x-t)q(t)dt}{\left[(x-t)^2 + r^2\right]^{\frac{1}{2}}} \; .$$

Fuhrmann employed a step function or a piecewise linear function of x for $q(x)$. His method can be shown to be equivalent to the superposition of a discreet number of singularities of the type given by (23) with $n = -1$ and $n = -2$; for we note, for instance, that the potential due to a finite line of sources of uniform density is proportional to

$$\int_0^{+l} \frac{dt}{\left[(x-t)^2+r^2\right]^{\frac{1}{2}}} = \cosh^{-1}\left(\frac{x}{r}\right) - \cosh^{-1}\left(\frac{x-l}{r}\right)$$

$$= Q_0^0\left(\frac{x}{\sqrt{x^2 + r^2}}\right) - Q_0^0\left(\frac{x-l}{\sqrt{(x-l)^2+r^2}}\right)$$

Recently, the Rankine method has been applied by Munzer and Reichardt (1944) to obtain bodies with nearly uniform surface pressure distributions; the techniques employed appear to be essentially peculiar to this problem, but certain generalisations have been suggested by Riegels and Brandt (1944).

Another development of the use of source-sink distributions has been initiated by Weinstein (1948) who considered the body shape generated by axi-symmetric source-sink distributions on rings, and over discs and cylinders. The fundamental solution is that for a source ring, the others being obtained by superposition. Weinstein employed an operational approach in his analysis, representing the velocity potentials and stream functions in terms of improper integrals involving Bessel functions. Sadowsky and Sternberg (1950) have considered the alternative approach, using elliptic integrals: it may be shown for instance, that the potential of the source ring of total strength m, situated on $r = a$ in the plane $x = 0$, is given by

$$\phi = \frac{-m}{2\pi^2\left[x^2+(r+a)^2\right]^{\frac{1}{2}}} K\left(\frac{4ar}{x^2+(r+a)^2}\right) \quad , \quad \ldots\ldots\ldots(24)$$

where K is the complete elliptic integral of the first kind.

Although flows obtained from distributions of source rings involve in their analysis considerable complications, it is possible by their use to simulate the axi-symmetric flow over a far wider class of body shapes than is possible merely with the use of axial distributions of sources. Thus, a source disc placed in a uniform stream produces a flow about a body (fig. 2) which has a much blunter nose than is obtainable by any axial distribution of sources (Van Tuyl, 1950). The assumption that the axial flow about a certain body of revolution can be simulated by a line distribution of sources, or of any other single type of singularity, implies an analytical continuation of the flow into the interior of the body which is only possible if the body shape satisfies certain conditions. It precludes, for instance, the consideration of the flow about bodies of revolution with discontinuities in their surface slope. On the other hand, it has been shown by Lamb (1879), that any continuous acyclic irrotational motion of an incompressible fluid can be regarded as due to a distribution of simple sources over the boundary; in particular, therefore, a surface distribution of source rings exists which would simulate the axi-symmetric flow past any body of revolution, whatever the shape of its meridian section. The method of von Karman, outlined in the next section, is based on the representation of the flow by axial distributions of sources, whilst that of Miss Flügge-Lotz (section 8) employs the less restrictive, but more involved, analysis of source ring distributions.

7. The Method of von Karman

We have mentioned above some indirect methods of obtaining the flow about bodies using stipulated singularity distributions. The direct problem - to determine the distribution of singularities which will simulate the axi-symmetric

flow over a given body appears first to have been assailed by von Karman (1927).

For a body of given meridian shape, an approximation to the axi-symmetric flow about it is obtained by subdividing its axis into a finite number of intervals, along each of which a distribution of sources of constant density is assigned. The profile is thus simulated by a finite number of axial source lines, the potential and stream function of each being obtained, as before, from the use of the relations of equation (23) with n=-1. Thus, superposing this distribution on a uniform stream, the stream function of the resulting motion may be quoted in the form

$$\Psi = \tfrac{1}{2}u_\infty r^2 + \frac{1}{4\pi}\sum_{k=1}^{m} q_k \left\{ \left[r^2+(x-x_k-l_k)^2 \right]^{\frac{1}{2}} - \left[r^2+(x-x_k)^2 \right]^{\frac{1}{2}} \right\},$$

where q_k is the density of sources per unit length assigned to the segment $x_k < x < x_k + l_k$. The value of Ψ on the body is the same as that on the axis r=0 upstream of the body, i.e. $\frac{1}{4\pi}(\sum q_k l_k)$; in particular, if the body is closed it is zero. Thus if Ψ is equated to this value at m prescribed points on the surface (taken at $x = x_k+\frac{1}{2}l_k$) where the value of r is known, a set of m non-homogeneous linear equations for $q_1, q_2, \ldots q_m$ is obtained, which can then be solved. The process may be made as accurate as desired by increasing the number of intervals, although such refinement is only obtained at the expense of greatly increased labour in the numerical solution: nevertheless it is the best known, and most frequently used, of the direct methods. Von Karman's method in application to the flow over bodies at incidence is described later. Modifications to his methods have been recently suggested by Bilharz and Hölder (1947) and Wijngaarden (1948).

8. The Method of Flügge-Lotz

The most important alternative source distribution

method is that originated by Mrs. Flügge-Lotz (1931), which employs a generation of the body by a distribution of sources over its surface. We have noted that this representation avoids the restriction inherent in using an axial distribution - that the latter is possible only if an analytic continuation of the flow into the body exists which is free from singularities except on the axis. On the other hand, the method of Mrs. Flügge-Lotz, although applicable to any type of body, has the practical disadvantage of requiring much greater labour in computation.

The potential for a surface distribution of sources can be obtained by superposition of a continuous distribution of ring-sources, so that using equation (24), the perturbation potential of the motion can be written as

$$\phi' = -\frac{1}{2\pi^2}\int_{-l}^{+l}\frac{q(t)K(k^2)\,dt}{\left[(x-t)^2+(r+a)^2\right]^{\frac{1}{2}}} \quad ,$$

where $$k^2 = 4ar \Big/ \left[(x-t)^2+(r+a)^2\right] \quad ,$$

$q(t)$ is the source intensity per unit axial length in the plane $x=t$, and $a = r_w(t)$ is the radius of the body at $x=t$, (where $|t| < l$ on the surface). The boundary condition to be satisfied is that, in an axial flow of speed u_∞,

$$\frac{\partial\phi'}{\partial n} = -u_\infty \frac{\partial x}{\partial n} \quad .$$

The algebra involved in finding the normal derivative of the potential is a little tedius, and care needs to be exercised, but this boundary condition leads finally to an integral equation for $q(t)$:

$$q(x) = 4\pi u_\infty r_w r_w' - \frac{2r_w}{\pi}\int_{-l}^{+l}\left\{2aD(k^2)+\frac{\left[r_w-a-(x-t)r_w'\right]}{(1-k^2)}E(k^2)\right\}\frac{q(t)\,dt}{\left[(x-t)^2+(r_w+a)^2\right]^{3/2}} \quad ..(25)$$

where k^2 and a are defined as before, $r_w \equiv r_w(x)$, $r'_w = \frac{d}{dx} r_w(x)$, and $D(k^2)$ is the complete elliptic integral

$$\int_0^{\pi/2} \frac{\sin^2\theta \, d\theta}{(1-k^2\sin^2\theta)^{\frac{1}{2}}} .$$

Vandrey (1953) has done much to reduce the work involved in the numerical solution of this type of equation. He suggests an iteration scheme of the type

$$q_o(x) = \tfrac{1}{2} f(x),$$

$$q_n(x) = \tfrac{1}{2} q_{n-1}(x) + \tfrac{1}{2} f(x) + \tfrac{1}{2} \int q_{n-1}(t) K(x,t) dt, \quad (n=1,2,\ldots),$$

supposing that the integral equation is of the form

$$q(x) = f(x) + \int q(t) \, K(x,t) dt,$$

to which (25) plainly corresponds. The main difficulty of this scheme of iteration, which Vandrey finds rapidly convergent, lies in the evaluation of the integral which involves the complicated kernal shown in (25); to aid this evaluation, Vandrey derives an integration formula of the type

$$\int q(t) \, K(x,t) dt = \sum_m p_m q(t_m) \, K(x,t_m),$$

for which he calculates the weighting coefficients taking proper account of the singularities in the kernal, by suitable transformation of the variable of integration t.

For full details, the reader is referred to Vandrey's paper, which contains computational instructions and programmes. However, to quote the author, 'the work is still so laborious that a single computor is likely to get tired of it'. Nevertheless the accuracy is high; for a spheroid, for instance, the calculated surface velocity is practically indistinguishable from that obtained from the classic theory.

If the body is slender - with a large (length/diameter) ratio and small surface slope - then the local source surface

density is proportional to the local surface slope, or more precisely,

$$q(x) \equiv q_o(x) = 2\pi u_\infty r_w r_w' = u_\infty S'(x) \quad \ldots\ldots\ldots\ldots (26)$$

This result, which has been shown by Ward (1954) to be true for all types of slender body (and not merely bodies of revolution), is one which we shall frequently meet in the ensuing pages.

9. Doublet Distribution Methods

Other attempts to solve the direct problem have been made using axial doublet distributions: such a distribution can be easily shown to be equivalent to a continuous axial source distribution, with the addition of a finite number of simple sources or sinks at the points of discontinuity in the doublet distribution (such as its end points). Plainly the method is therefore of slightly greater generality than that proposed by von Karman.

The stream function describing the flow due to the axial doublet distribution placed in a uniform stream (moving parallel to the axis) may be found from equation (22) in the form

$$\Psi = \tfrac{1}{2} u_\infty r^2 + r^2 \int_a^b \frac{m(t)\, dt}{\left[r^2+(x-t)^2\right]^{3/2}} , \quad (a < b) .$$

On the surface $\Psi = 0$, so that the doublet intensity may be found by solving an integral equation for $m(t)$:

$$\int_a^b \frac{m(t)\, dt}{\left[r_w^2(x) + (x-t)^2\right]^{3/2}} = -\tfrac{1}{2} u_\infty . \quad \ldots\ldots\ldots\ldots (27)$$

Of the various methods of solution of this type of equation which have been suggested, the iteration techniques due to Landweber (1951) appear to be the most satisfactory. The successive approximations $m_1(x)$, $m_2(x)$, etc., to the value of $m(x)$ are constructed by using the iteration formula

$$m_{n+1}(x) = m_n(x) + \tfrac{1}{2} r_w^2(x) \left[\tfrac{1}{2} u_{\infty} + \int_a^b \frac{m_n(t)\, dt}{\left[r_w^2(x) + (x-t)^2 \right]^{3/2}} \right] .$$

The computations are most conveniently carried out in terms of the differences between successive approximations to $m(x)$, which also furnish a measure of the error at each stage in the process. Two methods of integration are suggested, one semi-graphical, and the other completely arithmetic, but both involving the use of Gaussian quadrature formulae.

As the first approximation to $m(x)$, Landweber uses a variation of doublet intensity in proportion to the cross-sectional area $r_w^2(x)$, which is equivalent to the slender-body approximation of equation (26). In application to bodies with bluff noses and tails, a slight modification to this approximation is suggested, so as to give the appropriate values to $m(x)$ at the end-points $x=a$ and $x=b$ of the doublet distribution, which can be calculated independently. Landweber shows that for such bodies these end-points do not coincide with the extremities of the body axis, there being a small length of the axis at the nose and at the tail over which the doublet intensity vanishes. A prior knowledge of the extent of these regions greatly increases the rate of convergence of the successive approximations, and their accuracy. Landweber shows, for instance, that if the nose of the body is, say, at $x=0$, and if

$$\pi r_w^2(x) = S(x) = S'(0)x + \tfrac{1}{2} S''(0)x^2 + \frac{1}{6} S'''(0)x^3 + \ldots ,$$

then a good approximation to the lower distribution limit $\underline{a}$ at that end is given by

$$a = S'(0) \Big/ \left\{ 4\pi + \tfrac{1}{2} S''(0) + \left[\frac{1}{24} S'(0) S'''(0) \right]^{\frac{1}{2}} \right\} \qquad (28)$$

The dominant term $\underline{a} = \frac{1}{4\pi} S'(0)$ corresponds to a point half-way between the centre of curvature of the nose and the nose itself. Figure 3 shows the results of (28) applied to the spheroid in comparison with the exact theory.

More accurate data for the determination of the distribution limits will be found in Landweber's paper.

Such data are also of use in other methods employing either doublet or some distributions along the axis. For instance, Kaplan's early method (§4) can be shown to be equivalent to the simulation of the flow by a source distribution extending along the axis between the foci of the chosen system of semi-elliptic coordinates, whose local intensity per unit length is

$$q(x) = -2\pi \sum_{n=1}^{\infty} \phi_{no} P_n^o(\mu)$$

in the notation of equation (11): a knowledge of the proper limits of such a distribution therefore leads to the appropriate choice of the positions of the foci.

10. Simulation of the Flow by Vortex Distribution

Any continuous irrotational motion, whether cyclic or not, of an incompressible fluid occupying a region extending to infinity may be regarded as due to a distribution of vortices over the interior boundaries, provided the fluid be at rest at infinity. This theorem (proved by Lamb, 1879) provides an alternative model to that of surface source distributions by which one may attempt to simulate the axial flow about a body of revolution. The perturbed flow in this particular case may be obtained by supposing the surface to be replaced by a continuous distribution of vortex rings, enclosing fluid which is at rest relative to the body. Now a vortex ring of circulation $V ds$ in the plane $x=0$, and of radius $r=r_w$ produces, in particular, on the axis $r=0$ an axial velocity

$$\tfrac{1}{2} r_w^2 V ds \Big/ \left(x^2 + r_w^2\right)^{3/2},$$

(as is shown for instance, by Sadowsky and Stemberg, 1950). Thus the resultant axial velocity due to a distribution of such vortex

rings extending over the surface of a body, $r=r_w(x)$ between $x = \pm l$, may be obtained by integration in the usual way. But the fluid velocity on the axis is equal to the velocity of the body, (or, in other words, equal and opposite to the free stream velocity, u_∞, relative to the body). Thus

$$\int_{-l}^{+l} \left\{ \frac{V'(x)\, r_w^2(x)}{\left[(x-t)^2+r_w^2(x)\right]^{3/2}} \right\} \frac{ds}{dx}\, dx = -2u_\infty, \quad \text{for all } |t| < l, \qquad \ldots\ldots\ldots\ldots(29)$$

where $V'(x)$ is here the circulation per unit distance along the body surface, designated by s, so that

$$s = \int_{-l}^{x} \left\{ 1 + \left[r_w'(x) \right]^2 \right\}^{\frac{1}{2}} dx .$$

Thus $V'(x)$ is in fact the fluid velocity at the surface, and (29) is an integral equation for $V'(x)$ if the body shape is known.

To find the complete flow field away from the body would require the evaluation of the velocity components induced at an arbitrary point by the vorticity distribution thus obtained, and this would involve some difficulties. But in problems where only a distribution of surface velocity is required, the solution of (29) gives the desired information more directly and rapidly than any of the other exact techniques proposed.

Landweber (1951) obtained the integral equation (29) by applying a Green's function method to the solution of the boundary value problem for the potential, and he has suggested a method of successive approximation to its solution which is identical in principle with that which he employed in solving the integral equation for the doublet distribution (given by equation (27) in the previous section).

11. Slender Body Theory

The methods so far described have been exact in the sense that generally any desired accuracy could be achieved by their use, for the expenditure of sufficient labour in computation, always provided, of course, that the body is appropriate to the assumed singularity distribution. However the labour, in most instances, is so heavy that other methods have been, and continue to be, suggested, where approximations are introduced into the analysis at an early stage, providing simplified computation at the expense of rigour and ultimate accuracy. The choice of the level of compromise, thus introduced, will depend of course upon the particular application of the results envisaged by the investigator; but it often falls in favour of the simplified techniques. The inherent approximation in nearly all these methods has been that the body is slender, and it has been appreciated, in the course of time, that they can all be absorbed into a generalised and rigorously developed single 'Slender Body' theory, which is the subject of the present section.

This theory is one in which the properties of the flow over a body, whose radius is small compared with the length, are discussed by expanding these properties as a series in terms of the (radius/length) ratio. It is applicable to all types of flows, - those due to lateral, axial or curved motion, - and to various types of pointed bodies; for instance, we have met it before in terms of the theory of R.T. Jones for Slender wings. We shall here attempt a general statement of the theory, deriving it by the method of operational transforms initiated by Ward (1949) in relation to the supersonic flow problem, and extended by Adams and Sears (1953) to the present problem.

We define the Fourier Transform of the perturbation velocity potential as $\bar{\phi}$: that is

$$\bar{\phi} \equiv \bar{\phi}(r,\theta,p) = \frac{1}{(2\pi)^{\frac{1}{2}}} \int_{-\infty}^{+\infty} \phi'(r,\theta,x) e^{ipx}\, dx, \text{ say.} \quad (30)$$

The resulting equation of continuity then becomes

$$\frac{1}{r}\frac{\partial}{\partial r}\left(r\frac{\partial \bar{\Phi}}{\partial r}\right) + \frac{1}{r^2}\frac{\partial^2 \bar{\Phi}}{\partial \theta^2} = p^2 \bar{\Phi} \ ,$$

using the boundary condition that ϕ' and ϕ'_x vanish at $x = \pm\infty$. A solution of this equation by separation of variables, including the appropriate condition at infinity, yields the expression

$$\bar{\Phi} = \sum_{n=0}^{\infty} K_n(|p|r)\, \bar{\phi}_n(p) \cos\left[n\theta + \Theta_n(p)\right], \quad (\Theta_0 \equiv 0), \qquad \ldots\ldots\ldots\ldots(31)$$

where K_n is the modified Bessel function of the second kind and the $\bar{\phi}_n$'s and Θ_n's are arbitrary functions of p. On the body surface $|p|r$ is a small quantity of general order of magnitude r/l, so that in examining the behaviour of ϕ' or $\bar{\Phi}$, on or near the body surface we may replace the K_n's by their asymptotic forms:

$$K_n(\varepsilon) \sim \tfrac{1}{2}(n-1)! \left(\frac{2}{\varepsilon}\right)^n \left[1 + O(\varepsilon^2)\right] \ , \ (n = 2,3,\ldots),$$

$$K_1(\varepsilon) \sim \frac{1}{\varepsilon}\left[1 + O(\varepsilon^2 \log \varepsilon)\right] \ ,$$

and

$$K_0(\varepsilon) \sim \left[\log\left(\frac{2}{\varepsilon}\right) - \gamma\right]\left[1 + O(\varepsilon^2)\right] \ ,$$

where γ is Euler's constant. Substituting these relations in (31), for $r \longrightarrow 0$

$$\bar{\Phi} \sim \left\{\left[\log\left(\frac{2}{|p|r}\right) - \gamma\right]\bar{\phi}_0(p) + \sum_{n=1}^{\infty} \frac{2^{n-1}(n-1)!}{|p|^n r^n}\, \bar{\phi}_n(p)\cos\left[n\theta + \Theta_n(p)\right]\right\}\left[1 + O(r^2 \log r)\right].$$

The Fourier transforms having served their purpose we revert back to the variable x by taking the inverse transform of each term, giving from (30) for $r \longrightarrow 0$,

$$\phi' \sim \left\{\frac{q(x)}{2\pi}\log\left(\frac{r}{2l}\right) + \phi_0(x) + \sum_{n=1}^{\infty} \frac{l^n \phi_n(x)}{r^n}\cos\left[n\theta + \theta_n(x)\right]\right\}\left[1 + O(r^2 \log r)\right], \qquad \ldots\ldots\ldots\ldots(32)$$

where $\frac{-1}{2\pi}\, q(x)$ is the inverse transform of $\bar{\phi}_0(p)$, and the

functions $\phi_n(x)$, $\theta_n(x)$ can be related to $\bar{\Phi}_n(p)$, $\bar{\Theta}_n(p)$, although the precise nature of this relationship is of no consequence. An exception is the value of $\phi_o(x)$, which is the inverse transform of $\left[\log\left(\frac{1}{|p|\,l}\right) - \gamma\right]\bar{\Phi}_o(p)$; this can be calculated, using the product theorem for transforms, as

$$\phi_o = -\frac{1}{4\pi}\int_{-\infty}^{+\infty} \mathrm{sgn}(x-t)q'(t)\log\left|\frac{x-t}{l}\right| dt. \quad \ldots\ldots(33)$$

Equation (32) shows that the flow near the body in transverse planes x = constant is a two-dimensional potential motion. In particular, the asymmetrical flow terms $(n \geq 1)$ are independent of conditions up or down-stream of the transverse plane considered, and it is these terms (or, to be precise, merely the first of these terms) which determine the flow due to a lateral motion of a slender body of revolution: the implications of this fact will be considered later (see §15). However we are here concerned with the terms independent of θ which can be expected to describe the axi-symmetric flow due to a longitudinal motion of a body of revolution. This flow does not conform to the independence principle as the term $\phi_o(x)$, and so also the longitudinal component of velocity, u, depends near the body on the variation of $q(x)$ for all values of x, as is implicit in equation (33).

Now $q(x)$ describes the local density of a flow singularity on the x-axis which can be recognised as a source distribution, and its value may be readily found. Let ν,τ be distances in the plane x-constant measured along the outward normal, and along the circumference of the section of the body. The boundary condition to be applied at the surface in axi-symmetric flow shows that

$$\frac{\partial \phi'}{\partial \nu} = -\frac{\partial \nu}{\partial x}\left(u_\infty + \frac{\partial \phi'}{\partial x}\right) = -u_\infty \frac{\partial \nu}{\partial x}\left[1 + O(\bar{r}_w^2 l_n\, \bar{r}_w)\right],$$

where $\bar{r}_w$ is a length characteristic of the body radius. But

using Gauss's theorem, equation (33), and this condition in turn, we have for a body of arbitrary cross-section C,

$$\left.\begin{aligned}\int_C \frac{\partial \phi'}{\partial \nu}\, d\tau &= \int_0^{2\pi} r \frac{\partial \phi'}{\partial r}\, d\theta = q(x) \\ &= -u_\infty \int_C \frac{\partial \nu}{\partial x}\, d\tau = u_\infty S'(x)\end{aligned}\right\} \text{ i.e. } q(x) = u_\infty S'(x), \qquad \ldots\ldots\ldots\ldots(34)$$

where $S(x)$ is the area enclosed by the local cross-section. The error in this derivation is again of the order $(\bar{r}_w^2/l^2)$. This result can be of course obtained in various other ways for a body of revolution, and was given earlier in equation (26). We see that the source density $q(x)$ can be a discontinuous function, in which event the integral in (34) must accordingly be interpreted in the Stieltz sense. In particular, if $S'(x)$ is continuous for $|x| < l$, and zero elsewhere (describing a body whose axis extends a distance l on either side of the origin) we find from (32), (33) and (34) that on or near the body surface the perturbation potential of the axial flow is

$$\phi \sim \left\{ \frac{u_\infty}{4\pi} \int_{-l}^{+l} \frac{S'(x)-S'(t)}{|x-t|}\, dt + \frac{u_\infty S'(x)}{2\pi} \log\left(\frac{r}{2\sqrt{l^2-x^2}} \right) \right\} \left[1 + \mathcal{O}(r^2 \log r) \right], \qquad \ldots\ldots\ldots\ldots(35)$$

provided that $|x| \leqslant l$.

In some examples, (where, for instance, the cross-sectional area of the body is given by a polynomial in x), it is convenient to express the variation of $S'(t)$ in the form of a Taylor series

$$S'(t) = \sum_{n=0}^{\infty} \frac{1}{n!} S^{(n+1)}(x)\, (t-x)^n$$

and supposing that a term-by-term integration is permissible, equation (35) becomes

$$\phi \sim -\frac{u_\infty}{4\pi} \left\{ \sum_{n=1} \frac{(-1)^n}{n!\, n} S^{(n+1)}(x) \left[(l+x)^n + (x-l)^n \right] + S'(x) \log \left[\frac{4(l^2-x^2)}{r^2} \right] \right\}$$

The longitudinal perturbation velocity u' is then given by $\frac{\partial \phi'}{\partial x}$, and so on performing the differentiation, we find that

$$u' = + \frac{u_\infty}{4\pi} \sum_{n=0}^{\infty} \frac{(-1)^n}{n!} S^{(n+1)}(x)\, I_{n+1} ,$$

where $$I_n = \frac{1}{n-2} \left[(x+l)^{n-2} + (x-l)^{n-2} \right] , \quad (n \neq 2),$$

and $$I_2 = \log \left[\frac{4(l^2 - x^2)}{r^2} \right] - 2. \qquad \ldots\ldots\ldots\ldots (36)$$

This result was established by Laitone (1947), using an approximate method based on the axial source distribution, and later independently by Neumark (1950). There are of course various ways in which the results of Slender Body theory may be deduced, but the operational approach can be readily extended to higher orders of accuracy, if desired.

12. The Inverse Problem

The determination of the shape of body having a prescribed surface velocity distribution is a problem which has eluded exact solution. An approximate approach due to Young and Owen (1943) is however of interest: its original treatment was based on a simplification of the early work of Kaplan, but it can now be recognised as an approximation to Slender Body theory in which the longitudinal perturbation velocity on the body is written as

$$u' = - \frac{u_\infty}{2\pi} \log \left(\frac{4l}{d} \right) S''(x) , \qquad \ldots\ldots\ldots\ldots (37)$$

where $\frac{1}{2} d$ is the maximum radius of the body. The terms preserved are of order $(r^2 \log r)$ on the body, whereas for instance equation (36) shows that those neglected are of order r^2. Thus the approximation is a crude one, but nevertheless it provides a very rapid means of finding the cross-sectional area distribution corresponding to a given type of variation of u', which is at least qualitatively significant. To

this approximation the spheroid is the body of revolution which has a uniform surface velocity; again, in figure 4 we show the exact surface velocity distribution (calculated by the vortex distribution method) about the shape of body derived by this means so as to give a uniform favourable velocity gradient over the body length. The approximate method will be seen to provide some guide to the shape required.

13. Singularities representing the Transverse Flow over Bodies of Revolution

The incompressible flow over a body whose axis is inclined to the direction of motion can be obtained, of course, by a superposition of the flows due to the resolved components of longitudinal and lateral motion relative to the axis. We have noticed this earlier in the solution for the potential of the lateral flow about an ellipsoid, (equation (4)), and in the expression of Kaplan for the potential of the flow about a body of arbitrary meridian-section (equation 12). Kaplan's method of calculation of the transverse flow (i.e. that due to a motion perpendicular to the body axis) follows the lines of the approach he used in evaluating axially symmetric flows. In fact, in many instances analogous treatments of transverse flow exist which follow, in their analytical and computational development, the corresponding methods used by investigators in their treatment of the axial flow problem.

Many of the singularity distribution techniques can be applied to the calculation of the transverse flow. Thus, whereas axi-symmetric flows can be determined by an axial distribution of sources, or more generally of doublets (with the doublet axes lying along the axis of symmetry), transverse flows may be simulated by the superposition along the body axis of doublets - whose axes lie in the direction of the relative lateral motion. Assuming the motion to be parallel to the

z-axis, say, the potential of the doublet at the origin whose axis lies in this direction is obtained from elementary principles as

$$\phi = \frac{M z}{4\pi(x^2+y^2+z^2)^{3/2}} = \frac{M r \cos\theta}{4\pi(r^2+x^2)^{3/2}} .$$

Such a doublet placed in a uniform stream parallel to the z-axis produces a spherical closed stream surface.

A uniform distribution of such doublets along the complete x-axis simulates in the same uniform stream the flow about an infinite circular cylinder, the flow in any transverse plane corresponding, of course, to that of a two-dimensional doublet. A uniform semi-infinite distribution of such doublets along the positive x-axis, produces a flow given by the velocity potential

$$\phi = \frac{\gamma \cos\theta}{2\pi r}\left[1 + \frac{x}{(x^2+r^2)^{\frac{1}{2}}}\right] , \quad \ldots\ldots\ldots\ldots(38)$$

which will be recognised as the potential of an infinitesimal horseshoe vortex.

However, the use of axial singularity distributions is restricted to certain bodies, as in axi-symmetric flow, whereas the acyclic flow about <u>any</u> body can be represented by a surface distribution of sources, as we have noticed before. In application to the lateral flow over bodies of revolution, such a surface distribution can be made up from source rings each with sinusoidal variation of source density. Consequently, solutions can be developed by analogy with the methods initiated by Mrs. Flügge-Lotz for axial flow (in which source rings of uniform density are used). If the source density is assumed to vary as $(\cos\theta)$ round the circumference of a ring, of radius <u>a</u> in the plane $x = 0$, the potential may be calculated from elementary considerations of superposition as:

$$\phi = \frac{4 M r \cos\theta}{\pi^2\left[x^2+(r+a)^2\right]^{3/2}} C(k^2) , \quad \ldots\ldots\ldots\ldots(39)$$

where $k^2 = 4ar \Big/ \left[x^2+(r+a)^2\right]$ as before, and $C(k^2)$ is the complete elliptic integral

$$\int_0^{\pi/2} \frac{\sin^2\theta \cos^2\theta}{(1-k^2 \sin^2\theta)^{3/2}} \, d\theta \, .$$

This expression for ϕ may be compared with that for the source ring of uniform density given by equation (24).

14. The Methods of von Karman and Flügge-Lotz applied to the Determination of Lateral Flow

Von Karman's method for axial flows depends on a simulation of the flow by a superposition of a discreet number of line sources, and in application to lateral flows it depends on a superposition of a discreet number of line doublets with lateral axes. From (38), the corresponding velocity potential of the lateral flow is therefore of the form

$$\phi = w_{\infty} r \cos\theta + \frac{\cos\theta}{2\pi r} \sum_{k=1}^{n} \gamma_k \left\{ \frac{x-x_k}{\left[r^2+(x-x_k)^2\right]^{\frac{1}{2}}} - \frac{x-x_k-l_k}{\left[r^2+(x-x_k-l_k)^2\right]^{\frac{1}{2}}} \right\} ,$$

where γ_k is the doublet intensity per unit length assigned to the segment $x_k < x < x_k+l_k$, and where the term $w_{\infty} r \cos\theta$ denotes the free stream potential. The velocity components v_r and u may be found in a similar form by taking the appropriate derivative of ϕ, and the boundary condition to be satisfied at the surface is that the normal component of velocity to the surface vanishes, which is that

$$\frac{\partial\phi}{\partial n} = \frac{v_r - ur'_w}{\left[1+(r'_w)^2\right]^{\frac{1}{2}}} = 0, \quad \text{or} \quad v_r = ur'_w \, , \qquad \ldots\ldots(40)$$

where r'_w denotes the tangent of the angle of slope of the meridian section relative to the body axis. If this condition is satisfied in one meridian section θ = constant, it will evidently be satisfied at all such sections, as v_r and u both vary in direct proportion to $\cos\theta$; thus the boundary condition

may be satisfied by equating $(v_r - ur'_w)$ to zero at n points on any meridian line of the body. This results in a set of n non-homogeneous linear equations for the n unknown values of γ_k, which may therefore be calculated in the usual manner.

An analogous treatment to Mrs. Flügge-Lotz's technique for axial flows consists of the representation of the flow by a surface distribution of sinusoidal source rings placed in a uniform lateral stream, yielding a value of the velocity potential which can be calculated from (39) as

$$\phi = w_\infty r \cos\theta + \frac{8}{\pi^2} r \cos\theta \int_{-l}^{+l} \frac{\gamma(t)\, C(k^2)}{\left[(x-t)^2+(r+a)^2\right]^{3/2}}\, dt,$$

with $k^2 = 4ar \Big/ \left[(x-t)^2+(r+a)^2\right]$, and $a = r_w(t)$.

The normal derivative of ϕ at the surface needs care in its evaluation, owing to the surface singularities, but the boundary condition (40) can be expressed after performing the necessary algebra as an integral equation for $\gamma(t)$ which is, in all essential features, similar to that expressed by (25). The methods developed by Vandrey (1954) for the solution of that equation are therefore directly applicable to the one above, and involve the method of successive approximation previously described. Full computational details are to be found in Vandrey's paper.

15. The Lateral Flow about a Slender Body of Revolution

We have seen that Slender Body theory is applicable to the flow due to any type of motion of a slender body, and therefore in particular it will be applicable to the lateral flow about a body of revolution provided that it satisfies the requirements of slenderness. The general expression for the perturbation potential on or near the body is given by equation (32), where terms of order r^2/l^2 are neglected compared with

unity; to an equivalent degree of approximation, the boundary condition to be satisfied at the surface is found from (40) as

$$\frac{\partial \phi'}{\partial r} \sim - w_\infty \cos\theta$$

Such a condition is met by supposing that in the expression for the perturbation potential all terms vanish except that involving $\cos\theta$, and so we find that in accordance with the boundary condition,

$$\phi' \sim \frac{w_\infty S(x)}{\pi r} \cos\theta \left[1 + \mathcal{O}(r^2 \log r)\right] \quad \ldots\ldots\ldots\ldots (41)$$

This remarkable result expresses the fact that the flow may be approximated by a doublet distribution along the axis whose intensity per unit length varies locally as the body cross-sectional area; an equivalent variation for a doublet distribution in axially symmetric flow has been already noted. But more than this, in any plane normal to the body axis, the lateral flow perturbation potential, and so the perturbation velocity, depends near the body only on the local surface shape, and is independent of upstream or downstream conditions. In other words, the lateral flow may be adequately approximated, in any given transverse plane, by an appropriate two-dimensional motion about the infinite cylinder of the same local radius placed in a uniform stream. This representation of the flow seems first to have been used by Munk (1934), in discussing the aerodynamic forces on airship hulls, who derived it on the basis of physical reasoning.

16. The Pressure Distribution about Bodies in Steady Rectilinear Motion

The discussion so far has concerned itself with various ways in which the potential flow may be calculated. Broadly speaking, the methods discussed fall into two categories:

(i) those in which an integral equation is solved

to give a source or doublet intensity (the methods of Flügge-Lotz and Landweber), and

(ii) those in which the velocity potential, or stream function, is written as a series of terms whose coefficients may be evaluated (the methods of Kaplan, von Karman, and of Slender Body theory). The only exception is the Vortex distribution method, applicable to axi-symmetric flow, in which the surface velocity distribution is obtained directly as the solution of an integral equation. In all other methods, to find the surface velocity - which is of course necessary if the pressure distribution is required, - either the velocity must be expressed in terms of integrals involving the derived singularity distribution, or the terms of the derived series for the potential (or stream function) must be differentiated. In the former eventuality, the calculations are often simplified by the fact that the integrals to be evaluated are similar to those of the fundamental integral equation, for which a means of numerical quadrature is known.

A comparison of the results of the various 'exact' techniques, one with another, tells us very little, as - unless the body shape is so unusual that only the surface singularity representations are applicable, - all can give any desired accuracy at the expense of sufficient labour in computation. What is of more interest is a comparison of the results of the approximate but much more rapid Slender Body theory with those of exact methods. Such a comparison is tinged by the degree of 'slenderness' of the body, but a few examples are shown in figure 5, for axi-symmetric flow.

The pressure distribution is derived from Bernoulli's equation which can be written in the form

$$\frac{p - p_\infty}{\rho} = \underset{\sim}{V} \cdot \nabla\phi' - \tfrac{1}{2}(\nabla\phi')^2 ,$$

where ϕ' is the perturbation velocity potential and $-\underset{\sim}{V}$ is the velocity vector of the free-stream relative to the body.

For a slender body in axi-symmetric flow we find from (32) that on or near its surface

$$C_p = \frac{p - p_\infty}{\frac{1}{2}\rho u_\infty^2} = -2\left(\frac{u'}{u_\infty}\right) - \left[\frac{S'(x)}{2\pi r}\right]^2 + \mathcal{O}(r^4 \log r),$$

where u', the perturbation longitudinal velocity, is given for instance by equation (36) to the required accuracy. Thus, in particular, the pressure coefficient on the surface of a slender spheroid is

$$C_p = \frac{d^2}{4l^2}\left[\frac{x^2}{l^2-x^2} + 2 - \log\left(\frac{16l^2}{d^2}\right)\right] \quad \ldots\ldots\ldots\ldots(42)$$

where d is the maximum diameter.

We can compare this with the exact potential flow pressure distribution, which can be obtained from the expressions for the velocity potential derived in section 2. The algebra involved is a little tedius and we can do no better here than quote the result originally obtained by Jones (1925) in the form

$$C_p = \frac{p-p_\infty}{\frac{1}{2}\rho V_\infty^2} = 1 - (1+k_2)^2 \sin^2\alpha \sin^2\theta - \left[(1+k_1)\cos\alpha\cos\beta + (1+k_2)\sin\alpha\sin\beta\cos\theta\right]^2, \quad \ldots\ldots\ldots\ldots(43)$$

where
$$k_1 = \frac{-1}{\zeta_w} Q_1^0(\zeta_w) \Big/ \frac{dQ_1^0}{d\zeta_w},$$

$$k_2 = -\frac{\zeta_w}{\zeta_w^2 - 1} Q_1^1(\zeta_w) \Big/ \frac{dQ_1^1}{d\zeta_w} = 1/(1+2k_1)$$

and
$$\zeta_w^2 = 4l^2 / (4l^2 - d^2).$$

This applies to a spheroid in a free-stream of speed V_∞ inclined at an angle α to the body axis; β is the angular inclination of the meridian section to the axis. The values of k_1 and k_2 will later be identified with the longitudinal and lateral virtual mass coefficients, and their values are tabulated on p.41; Q_1^0 (and Q_1^1) can be identified as Legendre (associated) functions of the second kind. For axi-symmetric

flow, equation (43) simplifies into the relation

$$C_p = 1 - (1+k_1)^2 \cos^2\beta$$

$$= 1 - \left[(1+k_1)^2 \Big/ \left(1 + \frac{d^2}{4\,l^2}\,\frac{x^2}{l^2 - x^2}\right)\right]$$

This is compared in figure 6 with the corresponding result in equation (48) of slender body theory, which of course agrees with it only if the fineness ratio is large.

If the flow is inclined at a finite angle a to the axis of a body of revolution, we can derive from slender body theory an expression for the perturbation potential due to the lateral flow, which is given by equation (41), and using Bernouilli's equation, we can accordingly calculate the surface pressure distributions as

$$C_p = (1-4\sin^2\theta)\sin^2 a - 2r_w'(x)\cos\theta \sin 2a + \mathcal{O}(\bar{r}_w^2 \log \bar{r}_w) \quad \ldots\ldots\ldots\ldots (44)$$

This result is compared with that of the exact theory for a spheroid (equation 43) in figure 7 . As will be seen from the analogous expression for axi-symmetric flow, - equation (48), - the approximation of the Slender Body theory is such that the pressure changes due to the effect of lateral flow are of much larger magnitude.

The dominant term on the right hand side of equation (44) is the first one, which is of unit order, and simply describes a pressure variation proportional to that on an infinite circular cylinder. Being symmetrical it does not, however, contribute to any lateral force on the body; such a force arises from the second term, and acts in the direction of the resultant free-stream velocity component perpendicular to the body axis. It has a magnitude $\frac{dF}{dx}$ per unit length of the body, say, where we can calculate from (44) that for a sufficiently slender body

$$\frac{dF}{dx} = -\int_0^{2\pi} p \cos\theta \, r_w \, d\theta \,,$$

$$= \tfrac{1}{2} \rho V_\infty^2 \sin 2\alpha \, S'(x) \left[1 + \mathcal{O}\left(\bar{r}_w^2 \log \bar{r}_w\right)\right]. \quad ..(45)$$

For a spheroid we find, however, from equation (43) that the lateral force per unit length is exactly equal to

$$\frac{dF}{dx} = \tfrac{1}{2} \rho V_\infty^2 \frac{(1+k_1)(1+k_2)}{2} \sin 2\alpha \cos^2\beta \, S'(x) \quad ...(46)$$

A comparison of the slender body approximation with the exact variation for spheroids is shown in figure 8 . The result of slender body theory given by equation (45) suggests that the variation of lateral force is dependent only on local conditions (namely, on the variation of cross-section area). The exact expression for spheroids in equation (46) differs in the inclusion of the term $\cos^2\beta$ - which is also an effect of local geometry, as β is the surface slope, - and of the term $\frac{1}{2}(1+k_1)(1+k_2)$, - which represents an effect of overall geometry, namely the fineness ratio. Now the virtual mass factors for spheroids are tabulated on p. 41 , and it will be seen that this product varies monotonically from $\frac{9}{8}$ for a sphere, to unity for a slender body. Little accuracy is lost therefore by neglecting this change due to overall geometry, and Upson and Klikoff (1931) were prompted on this basis to suggest that the lateral force on any body could be expressed merely as a function of local conditions; thus, in accordance with the exact theory for the spheroids, we can put

$$\frac{dF}{dx} = \tfrac{1}{2} \rho V_\infty^2 \sin 2\alpha . \cos^2\beta \, S'(x),$$

for a body of revolution of arbitrary shape and fineness ratio. This result presents a slight modification to that of Slender Body theory, and to judge by experimental evidence, it is a modification in the right direction.

It will be seen from the distribution of lateral force

calculated by Slender Body theory in equation (45), that the resultant force is zero if the body is closed at the base. The same is also true, by symmetry, of the exact distribution calculated for the spheroid. In fact, as we shall show in the next section, this is a general result of potential theory.

17. Overall Forces and Moments

The potential theory we have developed fails, as is well-known, to account for a drag force on a body. The absence also of a lift force, may perhaps at first sight seem surprising; but it will be recognised that the essential difference between the approach to finite wing theory (where of course the 'body' has a lift acting on it) and the development of the theory for bodies of revolution has been in the inclusion in the former of the effects of a vortex wake. This wake, in a steady state of flow, is a direct consequence of the lift on the wing, and vice versa. In a potential flow, the wake can be represented by a distribution of flow singularities in the fluid, extending to infinity downstream of the body. In all mathematical interpretations of the flow about bodies of revolution we have so far described, however, all the flow singularities exist by direct design, or implication, within or on the surface of the body. Consequently there are no forces if the body is closed.

To particularise, we have seen that the general flow due to a translational motion of the body may be represented by a superposition of doublets, so that the magnitude of the perturbation velocity decreases at infinity inversely as the cube of the distance from the body; thus the pressure force on, and momentum flux through, a spherical surface of infinitely large radius is infinitesimally small. Thus, by the momentum theorem, there are no overall forces on the body necessary to sustain the flow.

This deduction is a consequence of the assumptions

made; in fact of course a lift force and a drag force are developed on a body of revolution in a real fluid, and a wake exists downstream of the body. The origin of these forces lies in the action of viscosity on the flow, and the measured magnitude of these forces and their prediction will be the subject of the later sections of this paper. Suffice it to say here that there is no generally accepted hypothesis, analogous say to that of Kutta and Joukowski in aerofoil theory, by which the action of viscosity may be adequately included in a description by potential flow methods; consequently its action is neglected.

Although there are no forces on a body in a steady motion there is nevertheless a moment. For let us consider the steady translational motion of the body (with velocity $+\underset{\sim}{V}$ say) through a fluid otherwise at rest; the body engenders a disturbance, which we have called the perturbation flow about the body, which will have a certain momentum and moment of momentum, and we represent these respectively by the vector quantities $\underset{\sim}{M}$ and $\underset{\sim}{N}$, measured relative to axes fixed in the body. There is no force on the body, as the momentum measured with respect to axes fixed in the undisturbed fluid, and likewise that measured with respect to the axes fixed on the body, do not change with time. On the other hand the rate of change of the moment of momentum about a point fixed relative to the undisturbed fluid is evidently $\frac{\partial \underset{\sim}{N}}{\partial t} + \underset{\sim}{V} \wedge \underset{\sim}{M}$, which is non-zero, although (as the motion is steady) we note that $\frac{\partial \underset{\sim}{N}}{\partial t}$ must vanish. This rate of change of momentum equals the resultant moment of the external forces, or since there is no resultant force on the body, it equals the external couple $\underset{\sim}{G}$, say, acting on the body; that is

$$\underset{\sim}{G} = \underset{\sim}{V} \wedge \underset{\sim}{M} \qquad \text{.....(47)}$$

The evaluation of the momentum of the perturbed flow presents some difficulties in interpretation, and it is more usual to work in terms of the energy of the perturbed field. To effect this change, we note that in an accelerated motion

the force on the body is $\frac{\partial \underset{\sim}{M}}{\partial t}$, so that a change in $\underset{\sim}{M}$ of amount $\delta\underset{\sim}{M}$, say, at an instant of time represents the impulse applied to the body system. The work done by an infinitesimal impulse is then $\underset{\sim}{V} \cdot \delta\underset{\sim}{M}$ which is equal to the increment in kinetic energy, δT. But the momentum of the perturbed flow varies in proportion to the magnitude of the perturbation velocity components of the fluid. These in turn vary with time in proportion to the components of the body velocity of which, therefore, $\underset{\sim}{M}$ is a homogeneous linear function. Whence

$$\underset{\sim}{V} \cdot \delta\underset{\sim}{M} = \underset{\sim}{M} \cdot \delta\underset{\sim}{V} = \tfrac{1}{2}\,\delta\,(\underset{\sim}{M} \cdot \underset{\sim}{V})$$

Thus integrating over all the impulses which have generated the motion from rest, the total kinetic energy of the fluid is

$$T = \tfrac{1}{2}\,\underset{\sim}{M} \cdot \underset{\sim}{V} \qquad \text{.....(48)}$$

We may suppose that $\underset{\sim}{V}$ has components $(-u_\infty, -v_\infty, -w_\infty)$ along the axes, where x is measured along the body axis. Now evidently T is a homogeneous quadratic function of the velocity components, and by symmetry it must accordingly have the form

$$T = \tfrac{1}{2}m_1 u_\infty^2 + \tfrac{1}{2}m_2(v_\infty^2 + w_\infty^2) \qquad \text{.....(49)}$$

where m_1 and m_2 are characteristic of the body shape and called its longitudinal and lateral virtual mass. From (48) we can evidently identify the components of $\underset{\sim}{M}$ as $(-m_1 u_\infty, -m_2 v_\infty, -m_2 w_\infty)$.

The physical interpretation of the 'virtual mass' is perhaps too well known to need restatement here, but we see that (47) now shows that the couple on the body necessary to maintain the motion has the single component

$$(m_1 - m_2)\, v_\infty^2 \sin a \cos a$$

in the plane of motion; or in other words, the flow produces a moment

$$(m_2 - m_1)\, v_\infty^2 \sin a \cos a$$

on the body. Defining the non-dimensional coefficients of virtual mass as

$$k_1 = \frac{m_1}{\rho(\text{Vol})} \quad , \quad k_2 = \frac{m_2}{\rho(\text{Vol})} \quad ,$$

where ρ is the fluid density and (Vol) the body volume, the pitching moment coefficient is

$$C_m = \frac{(\text{pitching moment})}{\frac{1}{2}\rho V_\infty^2 (\text{Vol})} = (k_2 - k_1) \sin 2\alpha \quad ..(50)$$

As we shall see, on elongated bodies the lateral virtual mass coefficient, k_2, exceeds k_1 so that the moment is generally destabilising.

To calculate k_1 and k_2 we note using Gauss's theorem, that since $\nabla^2\phi' = 0$,

$$T = \tfrac{1}{2}\rho \int_Q (\nabla\phi')^2 dQ = \tfrac{1}{2}\rho \int_Q \nabla.(\phi'\nabla\phi')\, dQ$$

$$= \tfrac{1}{2}\rho \int_R \phi'\nabla\phi'.\, \underset{\sim}{n}\, dS - \tfrac{1}{2}\rho \int_S \phi'\nabla\phi'.\, \underset{\sim}{n}\, dS \ ,$$

where Q denotes the fluid volume, bounded on the inside by the body surface S, and on the outside by a spherical surface R, say. The integral over R vanishes as the radius of the sphere becomes infinite, since $(\phi' \nabla\phi')$ decreases inversely as the fifth power of the distance from origin; thus

$$T = -\tfrac{1}{2}\rho \int_S \phi' \frac{\partial\phi'}{\partial n} dS = -\tfrac{1}{2}\rho\, \underset{\sim}{V}. \int_S \phi'\, \underset{\sim}{n}\, dS \ .$$

To evaluate the kinetic energy, T, of the flow induced by the translational motion of a spheroid, we can use the expressions for the perturbation potential previously found in equations (3) and (4), and in accordance with (49), we would deduce the relations for k_1 and k_2 given in equation (43); their values are tabulated below as a function of fineness ratio.

For a slender body, of arbitrary meridian section, we can calculate from (32) and (41) that $k_2 = 1 + \mathcal{O}(\bar{r}_w^2 \log \bar{r}_w)$ and k_1 vanishes to this order of approximation: thus

$$C_m = \frac{\pi}{2} \sin 2\alpha \qquad \ldots\ldots\ldots\ldots (51)$$

This is a result which can of course be obtained directly from (45), and which is in accordance with the particular results for a spheroid of infinitely large fineness ratio, as shown by the Table.

Table 1: Virtual Mass Coefficients of Spheroids

$\left(\frac{\text{Maximum Diameter}}{\text{Length}}\right)$	Coefficient of Longitudinal Virtual Mass, k_1	Coefficient of Lateral Virtual Mass, k_2	(k_2-k_1)	$\frac{1}{2}(1+k_1)(1+k_2)$
0	0	1	1	1
0.05	0.0068	0.9866	0.9798	1.0000
0.1	0.0207	0.9602	0.9395	1.0004
0.15	0.0386	0.9284	0.8898	1.0014
0.2	0.0591	0.8943	0.8352	1.0031
0.25	0.0815	0.8598	0.7782	1.0057
0.3	0.1054	0.8259	0.7204	1.0092
0.35	0.1304	0.7932	0.6627	1.0135
0.4	0.1563	0.7619	0.6056	1.0186
0.45	0.1829	0.7322	0.5494	1.0245
0.5	0.2100	0.7042	0.4942	1.0311
0.55	0.2376	0.6778	0.4401	1.0383
0.6	0.2657	0.6530	0.3872	1.0461
0.65	0.2942	0.6296	0.3354	1.0545
0.7	0.3230	0.6076	0.2846	1.0634
0.75	0.3520	0.5869	0.2349	1.0727
0.8	0.3812	0.5674	0.1862	1.0825
0.85	0.4106	0.5491	0.1384	1.0926
0.9	0.4402	0.5318	0.0915	1.1031
0.95	0.4700	0.5154	0.0454	1.1139
1	0.5	0.5	0	1.125

18. Comparison of Theory with Experiment

We have remarked on the absence of any overall forces on a body of revolution as a result of the assumption of potential flow. In any real flow there is however a lift force and a drag, which is not entirely due to the direct action of viscous shearing forces, and correspondingly the potential flow pressure distribution does not correspond exactly with that observed. However the discrepancies generally become appreciable only near the tail.

In figure 9 we show calculated pressures over a spheroid in axi-symmetric flow, compared with measured values (Jones, 1925). The comparison is typical of many which could be cited, and shows that the only significant difference lies in the absence in reality of the rapid recompression to stagnation conditions at the tail. This is due to the displacement effect of the boundary layer in the real flow, and of course a similar effect is well-known in the observation of the flow over a wing, or indeed any shape of body.

The difference between theory and measurement is more marked in the flow over bodies of revolution at incidence. Figure 10 shows the potential flow lateral force distribution for a model of the airship 'Akron' compared with experimental measurements (Freeman, 1932 (a)). The theory suggests a slightly smaller positive side force over the nose portion than actually exists, but greatly overestimates the negative lateral force on the tail. As a result there is, in a real flow, a resultant lateral force on a body of revolution, which grows rapidly with increase of incidence, with the result that the disparity between theory and experiment becomes greater at higher incidences. A comparison of the circumferential pressure distributions (figure 10) at various stations along the body shows that the disparity is caused mainly by the absence of the theoretical high pressures over the top surface of the body at the tail, suggesting a local separation of the boundary layer.

We shall have more to say about these effects of the boundary layer in the following sections. However for the most part the study of these effects has been aimed at providing a means of estimating the overall forces on the body, rather than their more particular effects upon the distribution of surface pressure.

Consequently, potential flow methods provide the best, and only, means of predicting the pressure distribution; the above remarks, however, will suggest the limitations of the theory. At least it appears from the discussion of the later sections that the inevitable differences between the potential and real flows become less accentuated at the larger Reynolds number of full-scale conditions than in model tests.

The Effects of Viscosity

19. Skin Friction Drag in Laminar Flow

It is not intended here to deal at any length with the various theories of the boundary layer on bodies of revolution. Rather we are concerned for the present with the results of the theories, and the manner in which the boundary layer modifies the picture of the fluid motion obtained from potential flow methods; consequently we shall, in the main, mention only briefly the method of derivation of the results which we shall have cause to cite.

Among the most fully discussed effects of the boundary layer is the skin friction drag, and some brief comments on this property may be appropriate here. We shall first consider the determination of the skin friction intensity in laminar flow. To the first order, at least, the skin friction drag is independent of incidence, and consequently we shall concern ourselves only with axi-symmetric flow. Perhaps the most useful theoretical approach to this problem is found in the use of Mangler's transformation (Mangler, 1946); this shows that the local shear stress at a distance x behind the nose of a body of revolution,

whose local radius is r_w, is (r_w/l) times that at a distance $\bar{x}$ from the nose of a two-dimensional contour, where

$$\bar{x} = \int_0^x \left(\frac{r_w}{l}\right)^2 dx$$

and where the pressure is identical at corresponding points on each surface. For a slender body at zero incidence we may ignore the change in pressure along the body, in which case the 'transformed' contour is a flat-plate, (i.e. one having a uniform surface pressure), and the shear stress over the slender body of revolution can accordingly be found from the well-known Blasius solution for laminar flow over a flat plate. It is given by:

$$\tau_w = 0.332\, \rho V_\infty \left(\nu V_\infty r_w^2 \Big/ \int_0^x r_w^2\, dx\right)^{\frac{1}{2}},$$

where V_∞ is the free stream velocity. By integration we can express the skin friction, developed upstream of the plane ahead of which the enclosed body volume is $V(x)$ by the formula

$$D = \frac{4.71}{R_V^{\frac{1}{2}}} \tfrac{1}{2} \rho V_\infty^2 V^{2/3}, \quad \text{where } V \equiv V(x) \text{ and } R_V = V_\infty V^{1/3}/\nu. \qquad \text{.....(52)}$$

Compared with a flat plate of the same length and wetted area, we can calculate that a spheroid of high fineness ratio has a skin friction drag 4 per cent higher, and a body with a parabolic meridian section a drag larger by $9\frac{1}{2}$ per cent. However it will be apparent that the body enclosed volume is the only important geometrical factor determining the absolute value of the drag.

The exact solution for the body with arbitrary, non-slender, meridian section evidently presents a difficult problem, as the appropriate pressure distribution is often difficult to describe, and the number of known solutions for two-dimensional boundary layer flow with varying pressure is few. Consequently

greater progress has been made using the approximate momentum equation methods. The momentum equation for axi-symmetric boundary layer flow is

$$\frac{U^2}{r_w}\,\frac{d(r_w\delta_{2x})}{dx} + (H+2)\,U\,\delta_{2x}\,\frac{dU}{dx} = \frac{\tau_w}{\rho}\,, \qquad \text{.....(53)}$$

where $U \equiv U(x)$ is the velocity outside the boundary layer along the body whose radius is r_w at a distance x downstream of the nose along the surface, and H is the ratio of displacement thickness to the momentum thickness, δ_{2x}, (Millikan, 1932). It differs from the two-dimensional form merely in the presence of the term r_w, the body radius. One of the earliest solutions for laminar flow about bodies of revolution is due to Millikan (1932), who used this equation together with a quadratic approximation to the variation of u (the boundary layer velocity) with z (the distance normal to the surface) to find the variation of δ_{2x}. A later paper by Tomotika (1935) assumed a quartic approximation, satisfying the conditions

$$u = U, \quad \frac{\partial u}{\partial z} = \frac{\partial^2 u}{\partial z^2} = 0, \quad \text{at } z = \delta, \quad \text{the outside of the boundary layer;}$$

$$u = 0, \quad \mu\frac{\partial u}{\partial z} = \tau_w, \quad \nu\frac{\partial^2 u}{\partial z^2} = -\,U\frac{dU}{dx}\,, \quad \text{at } y = 0, \quad \text{the surface.}$$

These conditions enable us to relate τ_w, H, and δ_{2x} with each other and with the known external velocity distribution; so we may determine any of these properties by solution of the differential equation (53).

More generally if we define a one-parametric family of velocity profiles, so that

$$\frac{u}{U} = l\left(\frac{z}{\delta_{2x}}\right) + \tfrac{1}{2}\,m\left(\frac{z}{\delta_{2x}}\right)^2 + \cdots\,,$$

where l, m, ... are supposed to be related to a single parameter, then it follows that

$$\tau_w = l\left(\frac{\mu U}{\delta_{2x}}\right), \quad m = -\frac{dU}{dx}\,\frac{(\delta_{2x})^2}{\nu}\,,$$

and the momentum equation becomes

$$\frac{U}{\nu\, r_w^2}\quad \frac{d(r_w \delta_{2x})^2}{dx} = 2l + 2(H+2)m = G, \text{ say.}$$

The assumption of a one-parametric family of velocity profiles implies that G, like l and H, is a function of m. Further, the use of the Mangler transformation (Rott and Crabtree, 1952) shows that these relations are identical with those existing between G, l, H and m in two-dimensional flow (where the 'growth parameter' G is obtained by putting r_w = constant in the above expression). Consequently we could invoke the results of Thwaites (1949) (obtained from a study of the various exact two-dimensional solutions) to obtain 'universal' relations between l and m, and between G and m, which are valid for axi-symmetric as well as two-dimensional flow. Using these relations the momentum thickness can again be found as the solution of a differential equation.

Thus, Thwaites puts $G = a+bm$, where $a = 0.45$ and $b = 6$ appear to be 'best values', and accordingly we can find that

$$r_w^2\, \delta_{2x}^2 = a\, \nu\, U^{-b} \int_0^x r_w^2\, U^{b-1}\, dx$$

Thwaites also tabulates the variation of l with m which permits the calculation of the skin friction intensity. The condition $l = 0$ denotes the onset of reversed flow in the boundary layer, and consequently a laminar flow separation: according to Thwaites this occurs where $m = +0.082$, and this value is achieved near the tail of the body in the region of recompression towards the stagnation point. The plane of laminar separation for spheroids, calculated by this method, is shown in figure 11 .

20. Turbulent Skin Friction

The skin friction within a turbulent boundary layer

is again generally found using momentum equation methods, although the assumptions made in solving the equation differ widely. The value of H is usually accepted as 1.4 for the turbulent layer, corresponding to the results of experimental observations (Lyon 1934); then the momentum equation (53) can be integrated if the relation is known connecting the shear stress at the surface with the momentum thickness. There are two such relations which are most commonly invoked: the first was originally used by Millikan (1932) and is based on the well-known seventh power law for the variation of boundary layer velocity with distance from the surface, which yields the relation

$$\frac{\tau_w}{\rho U^2} = 0.0128 \quad (U\delta_{2x}/\nu)^{-1/4}$$

The assumption of such a variation is justified at least by some boundary layer flow explorations (Freeman, 1932(b)) as shown in figure 12 . The power law formula has been more recently used by Truckenbrodt (see Schlichting, 1951) in a generalised form. The second is that used by Young (1939) based on an extension of von Karman's Logarithmic law for the velocity distribution, which implies the relation

$$\frac{U\delta_{2x}}{\nu} = 0.2454 \exp \left(0.3914 \sqrt{\frac{\rho U^2}{\tau_w}} \right)$$

This is evidently a much less simple form, though the law governing the velocity distribution on which it is based is valid at least for the flat plate up to higher Reynolds numbers than the power law. In either application, however, it is evident that the effects on the relation between shear stress and momentum thickness of the difference between two- and three-dimensional flow, and of the surface pressure distribution, have been ignored.

The power law for the velocity distribution yields a convenient explicit expression for the total turbulent skin

friction drag of a slender-body (i.e. one with negligible surface pressure changes), which is given by

$$D = 0.460\left(\frac{\nu}{V_\infty L}\right)^{0.2} \tfrac{1}{2}\rho V_\infty^2 L^2 ,$$

$$\text{where } L = \left(\int_0^x r_w^{5/4}\, dx\right)^{4/9}.$$

Accordingly, we can calculate that the skin friction coefficient, based on wetted area, exceeds that of a flat plate of the same length by 1.2 per cent for a slender spheroid, and by nearly 3 per cent for a slender body of parabolic meridian section. The inference is that to a good degree of approximation the skin friction intensity is the same as in two-dimensional flow at an equivalent Reynolds number: or in other words

$$D = \frac{0.230}{R_l^{0.2}} \tfrac{1}{2}\rho V_\infty^2 A \qquad \text{.....(54)}$$

where R_l is the Reynolds number based on body length, and A is the side area of the body.

21. Experimental Values of Skin Friction Intensity

We see by examining equations (52) and (54) that it is not possible to present the theoretical expressions for skin friction drag of slender bodies in both laminar and turbulent flow on any comparable basis, as they depend upon different geometrical properties of the body. The same can therefore be expected of the experimental results. Accordingly, it is most convenient to divide these results into those relevant to the two flow regimes, as is done is figure 13 .

There is plenty of experimental data to support the contention that the skin friction drag in turbulent flow can be calculated from the laws derived for two-dimensional motion, such as that of equation (54) above; only a small selection of the data is shown in the figure, indicating agreement over a wide range of Reynolds number. On the other hand, it is

difficult to adduce any confirmation of the theoretical laminar flow skin friction values, as given by equation (52). This is almost certainly due to the fact that only in very few tests can there have been conditions of laminar flow over the greater part body surface. The lowest values of drag coefficient appear to have been recorded in tests on the model of the airship R.101, as shown in the figure.

A great deal of other information exists (over a Reynolds number range from 0.1 to 10 million), giving values of drag intermediate between the theoretical results for laminar and turbulent flow, and differing from either by large factors. It is reasonable to imply that this is due to a transition from one state of flow to the other existing on the surface, but the data do not suggest that transition movement is regular or predictable in any way. The apparent chaos in the results, even for identical models in different tunnels, must be largely due to their varying free stream turbulence levels (Goldstein, 1938); transition position is particularly sensitive to this property, as well of course as to many others.

22. Form and Profile Drag

Skin friction is the main, but not the only, contribution to the profile drag of bodies of revolution. There is an additional resistance arising out of the displacement effect of the boundary layer on the potential flow, which is known as the form drag. This has been assessed theoretically by estimating the total momentum decrement of the wake far downstream of the body, although the form drag manifests itself physically, of course, in the slightly changed pressure distribution over the body. These theoretical discussions have concerned bodies over which the flow remains unseparated, and in particular this precludes the application of the results obtained to bodies of projectile shape - with flat bases - or indeed to any non-slender body. It is also difficult to find any reliable drag measurements

at low speeds on projectile shaped bodies, although of course their performance at high subsonic and supersonic speeds has been a topic much discussed and investigated.

Young's method of estimating the total profile drag of a body of revolution (1939) assumes a boundary layer of mixed laminar and turbulent flow, the transition occurring at a plane across which the momentum thickness remains continuous; the laminar boundary layer is investigated using the momentum equation method of Tomatika, and the state of the turbulent layer is found by assuming von Karman's logarithmic law for the velocity distribution, as noted earlier. Finally the conditions of flow in the wake are found by solving the relevant form of the momentum equation (53), which is

$$\frac{1}{\sigma_2}\frac{d\sigma_2}{dx} + (H+2)\frac{1}{U}\frac{dU}{dx} = 0$$

where σ_2, the momentum area of the wake, replaces $2\pi r_w \delta_{2x}$. In integrating this equation, Young uses the approximation that, in the wake, the value of $(H-1)$ varies linearly with $\log \frac{U}{V_\infty}$, where U is the velocity just outside the wake, (Squire and Young, 1937). It follows then that, if the subscript 'l' denotes conditions at the tail of the body, the ultimate momentum area of the wake, σ_{2_∞}, (say), is given by

$$\frac{\sigma_{2\infty}}{\sigma_{2l}} = \left(\frac{U_l}{V_\infty}\right)^{3.2} \qquad \text{.....(55)}$$

The value of σ_{2l}, the momentum area of the boundary layer at the tail, is known as the limiting value of $2\pi r_w \delta_{2x}$ on the body surface at the tail (which remains finite, although r_w vanishes). The total profile drag of the body is obtained from the expression

$$D = 2\pi\rho \int_0^\infty u\,(V_\infty - u)y\,dy = \sigma_{2\infty}\rho V_\infty^2$$

where u is the velocity in the wake parallel to the main stream, and y is measured normal to the centre line of the wake infinitely far downstream of the body. The results (using

experimental determinations of U_l) show that over the Reynolds number range from 10^6 to 10^8, the proportion of the total profile drag due to the form drag is practically constant, depending mainly on the fineness ratio of the body, and to a small extent, also, on transition position, as is illustrated in figure 14.

A very similar method of estimating profile drag is due to Grenville (1953); the main differences being in his use of a power law velocity distribution for the turbulent boundary layer, with a special modification of the momentum equation to compute conditions near the tail of the body, and the assumption that the parameter (H-1) varies (in the wake) as the seventh root of $\log(U/\nu_{lo})$. The last mentioned difference might seem an important one, but in fact it has little effect; it merely implies that in the relation (55) the power index is 3.38, instead of 3.2. Both methods require the assumption of a certain transition plane, and Grenville adapts certain criteria which have been developed for the prediction of its position in two-dimensional flow to the axi-symmetric boundary layer, by the use of the Mangler transformation; the accuracy of the resulting procedures for transition prediction are not known, however.

23. Conditions of Flow in the Laminar Boundary Layer at Low Incidence

The evaluation of the boundary layer over a body of revolution moving at incidence to the direction of motion presents a difficult and involved theoretical problem which has as yet received but little attention. It is no longer generally possible, owing to the non-linearity of the boundary layer equations, to express the effects of the lateral flow by superposition, as in the study of potential flow. Boundary layer phenomena, as revealed for instance in the variation of lift with incidence, are strongly non-linear in character. Superposition is only possible if the incidence is assumed to be

very small, although the results thus obtained are, naturally, of limited significance.

Such a solution has been given by Nonweiler (1955 a) for laminar flow about slender bodies of revolution. The assumptions of slenderness and low incidence are in this connection a great simplification but to a certain extent in conflict, as it can be shown that the magnitude of the velocity perturbations within the boundary layer due to incidence depends on the ratio

$$\frac{2al}{d} = \text{incidence} \times \frac{\text{length}}{\text{diameter}}$$

which must be small for the theory to apply. These incremental velocity components are all found to vary sinusoidally round the body, but their downstream variation, however, is much more difficult to describe and depends to some extent at least on the actual shape of the meridian section.

It can best be illustrated by a study of the flow pattern in planes perpendicular to the body axis, as shown diagrammatically in figure 15.

Over the fore-part of the body the boundary layer motion consists of a radial outflow - due to the axi-symmetric displacement effect - together with a deceleration of the circumferential flow (figure 15a). Further downstream where the body cross-section starts to contract, this deceleration becomes more marked, ultimately causing the circumferential velocity component to reverse near the surface (figure 16). This, at first, produces the streamline pattern show in figure 15(b), but as the extent of the reversal increases, the radial velocity also becomes significantly modified, due to the increased mass flow defect of the circumferential flow. The modification takes the form of an induced outflow due to incidence, in the outer strata of the boundary layer over the bottom surface, (where the mass defect of the circumferential flow increases in its direction of

motion), but an incremental inflow occurs over the lee-side of the body. Ultimately this induced inflow is sufficient to reverse the radial velocity over the top surface, and the resulting streamline pattern shows that two vortex lobes are then formed in the boundary layer on either side of the body (figures 15(c) and (d).)

The reversal of the circumferential flow, shown in figure 16 from calculations for the airship 'Akron', is an important effect which can be accounted for by noticing that, over the rear of a body at low incidence, there is a suction on the bottom surface and a positive pressure over the top surface, (together combining to yield a local negative lateral force). The boundary layer flow near the surface would tend to move from the high to the low pressure region, which is therefore in a direction opposed to the external flow.

24. The Lateral Force on Bodies at Low Incidence

The properties of the boundary layer flow discussed in the previous section immediately suggest one reason for the overall lift or lateral force which we have earlier noticed exists on a body at incidence. The pair of vortices formed over the rear of the body would induce a downwash, tending to alleviate the negative lateral force which exists in that region in potential flow. An analogy to this effect comes to mind in relation to conditions on a slender plane wing, such as is sketched in figure 17 . That part of its surface behind the maximum span is immersed in the vortex layer - or boundary layer - coming off the front part of the wing: this induces over the rear part a downwash, exactly cancelling the free-stream normal component of velocity, with the result that no bound vorticity, and so no lift, is developed in this region. This can of course be found without knowledge of the state of flow of the boundary layer, merely as a result of applying the Joukowski condition at the trailing-edge of such a wing. This

condition in itself is an expression of a viscous flow effect, and in fact enables one to select the unique potential flow solution of the infinite number which could exist merely satisfying the boundary condition on the normal velocity at the surface.

However, the motion of a solid (as distinct from a plane body) produces a potential flow in a simply connected space, for which a unique solution exists. Viscosity effects, as manifested by the presence of the boundary layer, may only be simulated by modifying the boundary condition to be applied at the surface so that the normal component of fluid velocity in the external potential flow is not zero, but is continuous with that produced by the boundary layer at its outer edge. Now, in the flow over the rear of a body of revolution at low incidence, we have seen that it is an adequate approximation to suppose that the incremental normal velocity in the boundary layer varies sinusoidally round the body, producing an inflow over the top, and an outflow over the bottom surface. On the basis of slender-body theory, for instance, we could simulate this in potential flow by an additional axial doublet (or vortex pair) distribution. But as the lateral force per unit length is proportional to the downstream rate of increase of doublet intensity, the effect of the boundary layer flow is, therefore, to supply a lift.

Again, the concept of a 'displacement surface', or 'equivalent body', can be used to illustrate this effect. The displacement effect in longitudinal motion merely indicates a progressive fattening of the body towards the tail (figure 18(a)), in proportion to the total volume outflow from the boundary layer. This is unaltered at low incidences, the only effect of the additional, sinusoidal variation of normal velocity, at the outside of the boundary layer, being to deflect the displacement surface downwards near the tail, and maybe to distort its shape (figure 18(b)). It will be readily appreciated that the

'equivalent body' thus formed would experience a lift force, and the vortex-pair within the wake will continue indefinitely downstream, like the trailing vortex system of a wing (figure 18(c)).

The theoretical solution for low incidence permits the calculation of the effect of the boundary layer on the lateral force distribution, and results for the 'Akron' body are shown in figure 19. It will be noted first of all that the incremental lateral force decreases with increasing Reynolds number, - as the displacement area of the boundary layer becomes smaller. The theory will also be seen to indicate an ultimate reversal of the lateral force, but this is plainly unrealistic. For it is the pressure distribution associated with the existence of a local negative side-force which causes the reversal of the boundary layer flow, which in turn is the reason for the large increment in side force. The latter effect could never be so large as completely to remove its cause, although it will certainly go some way towards this, as appears from the experimental measurements. There are, of course, many other examples of reversal of flow acting in such a way as to remove its cause, - the formation of the starting vortex on a wing being a particularly important one.

In the theory quoted, this interaction between cause and effect is neglected; and so it overestimates the force developed. Consequently, the value it indicates for the total lateral force, existing on the body ahead of the plane of theoretical lift reversal, should provide an upper limit to the overall lateral force actually developed, (figure 20). This theoretical force is proportional to σ_1, the displacement area of the boundary layer, and to the effective local incidence of the displacement surface, which in turn is proportional to the body incidence, α. The local incidence appears to be also dependent on the parameter (σ_1/S_{max}), where S_{max} is the body frontal area, - at least for bodies with similar

meridian sections, but of arbitrary fineness ratio. Thus the theoretical upper limit to the total lateral force can be written as

$$\frac{dF}{d\alpha} = \tfrac{1}{2}\rho V_\infty^2 \, S_{max} \, f\left(\frac{\sigma_1}{S_{max}}\right)$$

Fortuitously, perhaps, as shown in figure 21(a), such an expression also provides an excellent means of collapsing the measured data of tests on the actual first-order variation of side force with incidence, as revealed by tests on a variety of airship hulls.

This is all the more surprising when it is noted that σ_1 is taken here as the laminar-flow displacement area, whereas in the tests the boundary layer was to a greater or less extent turbulent. On the other hand, taking σ_1 as the turbulent-flow displacement area provides almost as good a means of collapsing the data, and further suggests that the lateral force varies in direct proportion to σ_1 in this case (figure 21(b)). A good fit is obtained by putting

$$\left.\frac{dF}{d\alpha}\right|_{\alpha=0} = 6\rho V_\infty^2 \, \sigma_1 = 1.75 \frac{A}{R_l^{0.2}} \cdot \tfrac{1}{2}\rho V_\infty^2$$

In this equation, A is the side area of the body, and R_l the Reynolds number based on body length.

It seems then that the state of the flow has no effect (upon the magnitude of the lift developed) that we can isolate from the available data which cover a Reynolds number range from 0.3 to 18 millions. What is better established is that, for a body of given side area, the lift decreases either as the (length/diameter) ratio is increased, or as the Reynolds number is increased. However, all the numerical data quoted so far refer to airship hulls, and other body shapes might well yield different results. Indeed, some tests by Lange (1949) on a family of bodies with bluff, spherical noses, although displaying similar trends, show the side force to be about twice that given above.

25. Conditions over a Body at High Incidence

At low incidences we have noted that a reversal of the cross-flow occurs where the circumferential pressure gradient reverses. This result follows from a study in which the effects of incidence are small perturbations, linear with the incidence a, to which approximation the pressure coefficient about slender bodies may be quoted from equation (44) as

$$C_p = -4 \cos\theta \, r_w'(x) a \left[1 + \mathcal{O}\left(\frac{al}{d}\right)\right]$$

Thus the pressure gradients are reversed behind the plane of maximum diameter (where $r_w' < 0$). In the general case, such an approximation is inadequate, except in an incidence range so small as to be insignificant, and a better one is obtained for slender bodies by including the second-order term in a^2. This has the effect of adding a pressure distribution similar in form to that on a circular cylinder in two-dimensional motion, as illustrated in figure 10. The pressure gradient reverses - not at the plane of maximum diameter (as is true only of vanishingly small incidence) - but along a line which tends towards the meridians $\theta = \pm \frac{\pi}{2}$ as the incidence is increased. This is shown in figure 22, for the Akron hull. In the limiting condition of high incidence, the maximum suction occurs at the maximum diameter of the body viewed in the lateral planes, as it would do of course on an infinite circular cylinder in potential flow.

Allen and Perkins (1951) have conjectured that the circumferential flow will reverse along a line which would be roughly parallel to the position of minimum pressure on the hull. This we see is entirely compatible with the results quoted earlier, relevent to conditions at low incidence. Thus, as the incidence is increased, more and more of the flow over the top surface will reverse.

Furthermore, they have noticed that there would exist

a certain analogy between the cross flow at various stations along the body and the development with time of the flow about a circular cylinder starting from rest. For, considering conditions in a plane perpendicular to the body axis, and moving with the free-stream velocity component $V_\infty \cos \alpha$, the trace of the body will be a circle, whose size will expand and contract as the plane moves along the body. Ignoring this rate of change of cross-sectional area, we see that the development of the cross flow, as viewed in this moving plane, would appear at least similar to that observed with passage of time for a cylinder suddenly introduced into a stream of velocity $V_\infty \sin \alpha$. The potential flow pattern about the cylinder would at first be modified by a reversal of flow over its lee side, leading to the formation of a pair of standing vortices; ultimately these might elongate and break up into a Karman vortex-sheet, if the scale were sufficiently high. Thus, in the flow over a body of revolution we would be led to expect the circumferential flow to reverse (as already suggested), and a pair of vortices to be formed as a consequence. This again has been observed to be theoretically justified at low incidences, and certainly it would be true of a slender body at high incidence, where the flow will resemble that about a yawed infinite circular cylinder (except, perhaps, near its end points). In other words the cross-flow appears two-dimensional in character over a slender body at high incidence, in much the same way as it does if the flow is inviscid and potential. This can, in fact, be demonstrated to be true in theory, provided that the parameter $(\alpha l/d)$ is large, using the method of analysis of Moore (1951).

The analogy is particularly useful in that it allows us to infer that, in certain conditions, the pair of vortices might each in turn discharge from the body, being carried away downstream on its lee side; also, that a new pair will form and these break away, and so on, going to form a vortex-street.

Relative to the body these shed vortices would appear fixed, but relative to a transverse plane moving with the fluid, the cylinder would appear to leave them behind in its lee-side wake (figure 23). The length of body over which the vortex pair could remain attached would presumably become shorter as the incidence grows, because the trace of the body in the transverse plane would then move further. On the other hand, if the Reynolds number of the cross-flow were small enough - due to a small radius of the body, or its low incidence, say - the standing vortices might well remain stable.

26. The Separation of the Flow

The shedding of the vortices from the body surface would seem inevitably to imply a separation of the boundary layer. Whilst this is no doubt true, the meaning of separation, and the indication of its presence in three dimensional boundary layer flow, needs careful consideration. In plane flow, no ambiguity exists if we take the separation point as the position where the boundary layer velocity profile reverses at the surface. Moore (1953) generalises this to three dimensions by postulating that, at a separation line, the wall stream surface bifocates, and further if there is a point of reattachment, the separated stream surface joins again with the wall. Thus there would be a distinct bubble embedded in the boundary layer which does not exchange fluid with the rest of the flow (figure 24).

Within this bubble would be sheet pattern of vorticity, whose nature would of course depend on the particular problem; Moore shows, however, that such a vortex sheet tends to coalesce into strong discreet vortices, with the result that the external flow becomes greatly disturbed. In this way, the formation of a bubble of separation might often presage a complete breakaway of the flow from the surface. It will be evident that this kind of breakaway could not be predicted by a theory which assumes the existence of a finite, thin boundary layer, whereas the

occurrence merely of a bubble of separation is not incompatible with the assumptions of that theory. It is difficult to envisage how one could determine by experiment the position of such a complete breakaway, simply because it is a phenomenon so loosely defined.

One must be content, therefore, to look for the symptoms of its origin, such as the existence of a separation bubble, although here again difficulties of interpretation arise, since this type of flow never seems to occur in the boundary layer of a body of revolution. It is most appropriate in this connection to examine the streamlines of the boundary layer flow close to the surface, which are tangential to the local direction of shear stress on the body, and can be revealed by the well-known surface flow visualisation techniques.

At low incidences, such that $a \ll (d/l)$, these surface streamlines are - according to theory (Nonweiler 1955a) - as shown in figure 25(a). First the circumferential component of flow reverses over the rear of the body, where a vortex pair is formed in the cross flow (figure 15), and ultimately the longitudinal component also tends to reverse, on the windward side of the body in the plane of symmetry. If indeed it did so, then a nodal, or 'stagnation', point of the surface streamlines would be formed on the underside, where the local shear stress intensity vanishes, and near where the flow is being radiated outwards and downwards. As is shown in figure 25(b) , a degenerate form of bubble would thereby be produced, (in the plane of symmetry), containing a vortex which effectively serves to join the two lobes on either side of the body (figure 25(c)). However, as mentioned earlier the theory breaks down very near the tail, where in any case it predicts infinitely large disturbances in the boundary layer, and this suggests that a thin layer cannot exist in this region. In turn, this lends substance to the belief that a complete breakaway of the flow would occur, carrying this connecting

vortex downstream from the undersurface, like the starting vortex from a wing (figure 25(d)). If this were so, the theoretical reversal of the longitudinal flow on the underside would not be observable in the steady state, but the two vortex lobes would trail downstream in the wake, as shown in figure 18 .

At higher incidences (where al/d is say, about unity), experimental evidence suggests that a reversal of the longitudinal flow occurs over the sides of the body. This, like the theoretical reversal over the rear, is presumably due to the accumulation of the boundary layer flow, in a low pressure region. The position of the line of minimum pressure is illustrated in figure 26 and the circumferential flow is generally reversed on the lee side of this line, tending to move downward, away from the upper meridian and towards this line. As verified by experiment, the line of minimum pressure thus marks closely the edge of the vortex lobes in the circumferential flow, and to judge from surface flow studies using the lampblack technique, (Plate 1(b)) a region of de-energised air exists close to, and just to the leeward side of this line. In the photograph this shows itself as a dark region where the lampblack has collected, and where it is not easy to see the precise shape of the surface streamlines. Likewise, velocity explorations (figure 26) have verified that the axial component is locally considerably reduced at least in the outer strata of the boundary layer, without so far being able to penetrate sufficiently close to the surface to show positive evidence of a reversal. The presumed state of the surface flow is suggested in figure 27(a).

As seen in figure 26 and in the streamline patterns of Figure 27, there are usually two distinct pairs of vortex lobes in the cross-flow; one just to the leeward side of the stagnant region (and the minimum pressure line), and another pair - often separated from it by a region of unreversed circumferential flow - whose core lies close to the upper meridian. (It is of interest to note that a similar formation of two pairs of vortices is observable in the two-dimensional flow, at low Reynolds numbers, about a circular cylinder). The upper pair of vortices is generally of weaker intensity, and rarely produces any observable retardation of the longitudinal flow except perhaps near the tail. (see Plate 1a).

These regions of retarded flow have often been termed 'separation fronts', but it seems doubtful at least whether any separation of the kind defined by Moore exists, as it appears there is an exchange of air between those regions and the rest of the boundary layer. Moreover velocity explorations show that (at least up to a length within 20% of the body length from the tail) the vortex lobes remain attached to the surface.

Admittedly at much higher incidences, they do in fact shed from the surface to form a 'vortex street' above the body in the manner shown in figure 23. Surface flow studies then reveal the oscillatory character of the flow in this condition, by their marked assymmetrical patterns. It is difficult to suggest the incidence at which this change in the character of the cross-flow occurs, but it would seem safe to infer that it is well outside the range of practical aeronautical interest.

27. Forces on a Body at High Incidence

We have noted earlier that the viscous cross flow about a slender body is the same as that about an infinite circular cylinder of the same local radius, provided that the parameter $(a\bar{l}/d)$ is sufficiently large. It follows that the viscous drag force associated with the flow about a circular cylinder will occur as a local side-force on the body. In other words, the circumferential pressure will be constant over the lee-side surface, as it is in the separated flow

about the cylinder, instead of recompressing in the way indicated by potential theory. Except near the nose, this deduction is verified by experimental evidence (figure 10). If c_d is the drag coefficient of a circular cylinder, based on its diameter, then the local side force will be simply $(c_d \frac{1}{2}\rho V_\infty^2 \sin^2\alpha . 2r_w)$ per unit length. This drag coefficient appears to be virtually insensitive to changes of the cross-flow Reynolds number, except in so far as this determines the state of the boundary layer flow, - whether it is laminar or turbulent, - so that a strict interpretation of the theory would indicate the addition of a side force on a body given by

$$\Delta F = \bar{c}_d \tfrac{1}{2} \rho V^2 A \sin^2\alpha \qquad \text{.....(56)}$$

where A is the body side area.

Figure 28 shows the variation of the side force at high angles of attack on a number of airship hulls, from which it will be seen that above an incidence of about 6°, some such force - as given by the above expression (56) - provides an increasingly important contribution to the total side force variation. The value of the cross-flow drag coefficient, $\bar{c}_d$, inferred from these results appears to vary with the parameter $\left(\frac{V_\infty d}{\nu}\right)$, - which determines, at each incidence, the cross-flow Reynolds number. In this connection we recall that for a two-dimensional circular cylinder, a value of $c_d = 1.2$ would be appropriate for laminar flow, and $c_d = 0.4$ for turbulent flow.

For purposes of prediction, it would be convenient to find some way of reconciling these figures with the values of $\bar{c}_d$ inferred from the side force measurements. Allen and Perkins (1951) have suggested, for instance, that an allowance ought to be included for the end effects on the body by comparing the measured value of $\bar{c}_d$ with that for a circular cylinder of corresponding (length/diameter) ratio: with laminar flow, experimental evidence indicates a value of $\bar{c}_d = 0.8$ for a

circular cylinder whose span is 5 to 10 times its diameter. Again, by analogy of the development of the cross-flow along the body with that about a circular cylinder started impulsively from rest, we note that the reduced drag of the latter in the first few diameters of its travel would account for a lower value of the side force on a body, depending on the parameter (al/d), which describes the distance moved by the trace of the body relative to the cross-stream in terms of the body diameter. However, in view of the complexity of the problem we are attempting to rationalise, it could hardly be anticipated that a simplified theory could give any more than qualitative agreement, and these comparisons will be pursued no further.

28. Side Force on Bodies with Flat Bases

Allen and Perkins (1951), and also Kelly (1954), have attempted to apply the concepts outlined in the previous section to the prediction of the side force on projectile bodies (with flat bases), and have thereby discovered that slender-body theory provides an adequate means of estimating the side force at low incidences. The result is, from equation (45) that the side force

$$F \triangleq \rho V_\infty^2 \, S(l) a$$

where $S(l)$ is the base area. This seems to be fortuitous, as of course no form of potential theory is strictly applicable to such shapes, owing to the inevitable flow separation at the base section. It appears therefore, that such a separation precludes the existence of any violent change of flow velocity or direction at the base, which would render slender body theory inapplicable; consequently, the separation has little or no influence on the cross-flow upstream.

29. Pitching Moment and Drag of Bodies of Revolution

We have earlier seen that potential theory accounts for a destabilising pitching moment given from equation (50) by

$$C_m = (k_2 - k_1) \sin 2\alpha$$

and slender body theory suggests from equation (51) that we may take $k_2 = 1$, $k_1 = 0$ to find an approximate value. In fact, in most applications there seems little point in attempting any more refined assessment, as in practice the pitching moment is considerably modified by viscosity effects. In the first place, the shear stresses on the body contribute to a destabilising moment, owing to the reversal of the cross-flow; and secondly, the modification to the normal pressure distribution, which results in the side force, produces appreciable effects, - the centre-of-pressure of this side force apparently moving upstream from the tail as the incidence is increased, and as the cross-flow pattern becomes similar over the entire body length. However, the phenomena appear to depend on too many factors to allow any quantitative deductions to be made from the experimental measurements.

This is equally true of the estimation of the longitudinal force on a body of revolution. This force at low incidences consists of the form and friction drag, which can be assessed by the methods described earlier; but as the incidence is increased, an appreciable suction or thrust force is also developed. This arises from the typical 'circular cylinder' type of circumferential pressure distribution which exists at low incidences over the front part of the body surface, but not over the rear part where the effects of flow separation are more pronounced. Using the results of Slender Body theory, from equation (44), we can work out that the pressure on the body surface upstream of the maximum diameter contributes to a longitudinal (thrust) force of amount

$$\tfrac{1}{2} \rho V_\infty^2 \sin^2\alpha \, S_{max}$$

This should theoretically be cancelled out by an equal force over the rear of the body, but as we have noted this is not so, owing to the flow separation. However, when the separation front moves forward on to the nose of the body at higher angles of attack, then in turn this suction force also become reduced. No doubt the separation of the flow has other important effects on the friction and form drag. Nevertheless, a reduction in the resultant longitudinal force is invariably observed with increase of incidence. Typical results are shown in figure 29.

30. Flow about Rotating Bodies

Little reliable experimental information is available concerning the conditions over rotating bodies. Thus we have to rely in the main upon the results of potential theory, and in this connection we note that all the methods available for the analysis of the potential flow about bodies at incidence are easily applied to the problem of the flow about rotating bodies. The only difference of course lies in the change of the boundary condition to be applied to the normal velocity at the body surface: this affects the details but not the principles of the methods which we have discussed earlier.

For instance, in Slender Body theory, if the body is rotating with angular velocity Ω about an axis $\theta = \theta_o$ in the plane $x = x_o$, we can easily calculate that the perturbation potential on or near the body surface is given, by analogy with equation (41), as

$$\phi' = \frac{\Omega(x-x_o)S(x)}{\pi r} \sin(\theta-\theta_o) \left[1 + \mathcal{O}(r^2 \log r)\right]$$

referred to a system of coordinates fixed in the body. This solution may of course be superposed on that due to the longitudinal and lateral translational velocities, to give the general expression for the perturbation potential, relevant to an arbitrary motion of a body of revolution.

With a frame of axes moving with the body - the motion being specified by a translational velocity $\underset{\sim}{V}$, relative to the undisturbed fluid, and by an angular velocity $\underset{\sim}{\Omega}$ about the origin, referred in both instances to the instantaneous positions of the axes, - the relevant form of Bernouilli's equation can be found as

$$\frac{p-p_\infty}{\rho} = (\underset{\sim}{V} + \underset{\sim}{\Omega}\wedge\underset{\sim}{r}).\ \nabla\phi' - \tfrac{1}{2}(\nabla\phi')^2 - \frac{\partial\phi'}{\partial t} \qquad (57)$$

where $\underset{\sim}{r}$ is the position vector of any point referred to the moving axes. Of the various kinds of quasi-steady flow, for which $\frac{\partial\phi'}{\partial t} \equiv 0$, the one of greatest interest here is that due to the motion of the body in a circular path, so that $\underset{\sim}{V}.\underset{\sim}{\Omega} = 0$. Using Slender Body theory we may then calculate from equation (57) that, if the axis of rotation is taken as the y-axis and the body incidence is α, the surface pressure coefficient is given by

$$C_p = \frac{p-p_\infty}{\frac{1}{2}\rho V_\infty^2} = \left(\frac{\Omega x}{V_\infty} + \sin\alpha\right)^2 (1-4\sin^2\theta)$$

$$- \frac{2\cos\alpha\cos\theta}{\pi r_w(x)}\frac{d}{dx}\left[\left(\frac{\Omega x}{V_\infty} + \sin\alpha\right) S(x)\right] + \mathcal{O}(\bar{r}_w^2 \log \bar{r}_w) \qquad \ldots\ldots\ldots\ldots(58)$$

This reduces of course to the result for translational motion, in equation (44), if $\Omega = 0$.

Jones (1925) has derived the exact surface pressure distribution for a spheroid, based on the potential flow solution outlined in section 2 , and figure 30 gives a comparison of these results with those derived from Slender Body theory.

The latter shows from equation (58) that the curvature of the path introduces an incremental side force per unit length (ΔF) given by

$$\frac{d}{dx}(\Delta F) = \rho V_\infty \Omega \cos\alpha \frac{d}{dx}\left[x\, S(x)\right]$$

from which it follows that, to this order of approximation, the resultant incremental side force is zero; moreover, if

the axis of rotation passes through the centre of volume, the incremental pitching moment also vanishes. On the other hand, the exact theory for a spheroid predicts a finite resultant side force, but the reason for this apparent disparity may easily be ascertained.

Using arguments similar to those of section 17 , we can show that if $\underset{\sim}{M}$ is the momentum of the undisturbed flow relative to axes fixed in the body, which has a translational velocity $\underset{\sim}{V}$, and angular velocity $\underset{\sim}{\Omega}$ about the origin, then there must be an external force acting on the body necessary to maintain the fluid motion, which (with respect to the same reference system) is equal to

$$\underset{\sim}{F} = \frac{\partial \underset{\sim}{M}}{\partial t} + \underset{\sim}{\Omega} \wedge \underset{\sim}{M}$$

We may, as before, relate $\underset{\sim}{M}$ to the virtual mass components m_1 and m_2, by introducing the expression for the total kinetic energy of the disturbed flow in the form

$$T = \tfrac{1}{2} m_1 u_\infty^2 + \tfrac{1}{2} m_2 (v_\infty^2 + w_\infty^2) + \tfrac{1}{2} I(\Omega_y^2 + \Omega_z^2)$$

where $(-u_\infty , -v_\infty , -w_\infty)$ and $(\Omega_x, \Omega_y, \Omega_z)$ are the components of $\underset{\sim}{V}$ and $\underset{\sim}{\Omega}$ respectively. We can always express T in this way, by suitably choosing the origin of the axes of reference; then m_1 and m_2, - and so also the virtual mass coefficients k_1 and k_2, - depend only on the fluid motion engendered by the translation. Accordingly, if $\Omega_y = \Omega$, and $\Omega_x = \Omega_y = 0$, we can calculate that the fluid exerts a 'centrifugal' side force on the body of magnitude

$$F = - k_1 \rho V_\infty \Omega \cos \alpha \ (\text{Vol})$$

and a retarding longitudinal force

$$X = k_2 \rho V_\infty \Omega \sin \alpha \ (\text{Vol})$$

The first of these equations is compatible with the result of Slender Body theory, as the latter merely implies that k_1 may be ignored for a slender body; also, by integrating the surface pressure distribution, given in equation (58), we can find (as before) that to the same order of accuracy we may take $k_2 = 1$,

assuming that the body rotates about its centre of volume. A longitudinal retardation is thus the chief effect of what may be recognised as a kind of Coriolis force exerted by the fluid on a slender body.

We would expect these potential flow results to be modified in reality by viscous effects, in much the same way as those relevant to a purely translational motion, but it is very difficult to form any firm conclusions from the meagre experimental data. Some comparisons of the exact side force distribution about a spheroid with measurements taken on a whirling arm (Jones 1925) are shown in figure 31. From these it appears that theory gives no agreement whatsoever with experiment, even over the nose of the body; furthermore, increments due to rotation for positive and negative incidences differ considerably, in contrast with the result of potential theory. The total side-force measurements are also shown in figure 31, from which it will be seen that as a consequence, the extra force introduced by rotation changes sign with the incidence, α. These are unexpected and unexplained effects.

31. The Application of Potential Flow Theory to Ducted Bodies

The exact theory of potential flow about ducted bodies has only been developed to deal with the flow about toroidal boundaries of circular, or nearly circular cross-section, and consequently the results have only a limited significance in practical aerodynamics. There are, however, various approximate methods available which are applicable to the design of useful shapes of ducted bodies and these will be described in the sections which follow.

Before proceeding with this, it is desirable to draw attention to the methods used in simulating, within the framework of potential theory, the effect on the external stream of external forces applied upon the fluid within the duct. For the purposes

of the present argument we shall suppose that the perturbation potential for a duct of finite length is represented by a vorticity distribution merely over its surface; then it transpires that it is possible to adjust this distribution in such a way as to leave the duct a stream surface, but to alter the internal rate of volume flow through it. In general, any such solution will imply a certain flow round the trailing-edge of the duct, and in practice, if there were no external forces applied upon the fluid, the action of viscosity would inhibit this process; thus there would be one unique vorticity distribution, which would satisfy this physical condition on the flow around the trailing-edge, and which would most closely describe the actual flow of a viscous fluid. In other words, we are concerned with a flow in a doubly-connected space, and (as in two-dimensional aerofoil theory) the Joukowski hypothesis must be invoked to obtain a unique solution.

However most problems of practical interest arise where the internal flow through the duct suffers some form of external constraint - due, say, to the action of a fan, - which will induce a greater (or smaller) internal rate of volume flow than in its absence. Many investigators attempt to simulate the effect on the external stream by relaxing the trailing-edge condition, and allowing the fluid to move round it, so that the appropriate rate of volume flow through the duct is reproduced. This has perhaps little physical reality, but nevertheless provides a solution which has some relevance to the flow near the leading-edge, or lip, of the duct, where the effect of the unreal condition at the trailing-edge is more remote.

In particular, if the duct has head and tail portions (of varying cross-section) each mounted on a long centre portion of constant radius, - say, of three or more diameters in length, - then experimental evidence suggests that variations in the shape of the head portion produce changes in the surface

pressure distribution which have negligible magnitude over the tail portion, and vice versa. The pressure over the centre is, in fact, roughly that of the free-stream. In this event, the flow over the head (or tail) portion may effectively be considered by supposing it mounted on a cylinder extending indefinitely downstream (or upstream).

In a number of problems it is possible to construct a more satisfactory representation of the flow, by extending the vorticity distribution over the surface of a duct of finite length downstream into the wake; even so, the basic assumptions - that the flow is incompressible, irrotational and inviscid, - limit the applicability of the results, and a greatly simplified notion is required of the form of the external action on the flow. Because the flow is irrotational and incompressible, we must assume that the external forces applied are conservative. But as we are not concerned here with the precise pressure distribution within the duct we have no need to stipulate the actual process by which these forces are produced, other than to suppose that they are confined at least to the flow within the duct, so that the issuing jet will have a different (but constant) value of the total head from that of the external stream. Accordingly, the jet boundary must form a free vortex sheet, whose shape and intensity will be determined by the condition that it lies on a stream surface of the flow, and that the pressure on either side of the sheet is identical. Because of the change in total head, this latter condition implies that the difference in the kinetic energy of the fluid on either side of the vortex sheet is a constant: if the disturbance to the flow, and the external forces, are sufficiently small, this approximates to the condition that the intensity of surface vorticity on the jet boundary is a constant. It will be appreciated that this free vortex sheet will in fact be unstable and break up into a growing turbulent 'mixing zone', but the consideration of this is

outside the scope of potential theory, and of the present discussion.

32. Quasi-Cylinder Theory of Thin Ducts with Prescribed Pressure Difference

By a thin duct we mean to imply one with a thickness so small that it can be represented with sufficient accuracy by a plane surface. Further, the assumption of the 'Quasi-cylinder' theory is that the change in local radius (r_w) of the duct is small compared with its mean radius ($\bar{r}_w$, say), in other words a length $\bar{r}_w$ exists such that

$$\left| \frac{r_w - \bar{r}_w}{\bar{r}_w} \right| << 1$$

Provided that external forces are either absent, or at most of small magnitude, then it follows that the disturbance to the stream due to the duct will also be small. Accordingly, if we represent its effect on the flow by a vortex sheet over its surface, the surface intensity of this sheet will be proportional to the (small) velocity difference on either side of the duct, and so also it will be proportional (to a first approximation) to the (small) pressure difference across the duct surface. Thus, if this pressure difference is prescribed the surface vorticity distribution is known; further, if we are then to find the shape of the duct, we may assume (to a consistent order of approximation) that this vorticity is distributed over the mean cylindrical surface of radius $\bar{r}_w$, which of course only corresponds to the duct surface in the limiting condition of vanishing disturbances. The approach to this problem will be seen to be analogous to that used in the theory of two-dimensional flow over slightly cambered aerofoils.

The Stokes Stream function for a vortex ring of radius a about the axis $r = 0$ in the plane $x = \text{constant}$, may

be expressed as

$$\frac{\Gamma}{2\pi}\left[x^2+(r+a)^2\right]^{\frac{1}{2}}\left\{\left[\frac{x^2+r^2+a^2}{x^2+(r+a)^2}\right]K-E\right\}$$

where K and E are respectively the complete elliptic integrals of the first and second kinds with modulus k equal to

$$\sqrt{\left\{4ar\Big/\left[x^2+(r+a)^2\right]\right\}}$$

A distribution of such vortex rings over the cylinder $r=\bar{r}_w$ for $|x|\leq l$, say, in an axial uniform stream of speed u_∞ yields a flow described by the stream function

$$\Psi=\tfrac{1}{2}u_\infty r^2+\frac{1}{2\pi}\int_{-l}^{+l}\left[(x-t)^2+(\bar{r}_w+r)^2\right]^{\frac{1}{2}}\left\{\left[\frac{x^2+r^2+\bar{r}_w^2}{x^2+(r+\bar{r}_w)^2}\right]K-E\right\}\Gamma'(t)dt \qquad \text{.....(59)}$$

where

$$k^2=4r\,\bar{r}_w\Big/\left[(x-t)^2+(r+\bar{r}_w)^2\right]$$

We can accordingly deduce the shape of the duct, knowing $\Gamma'(t)$, by evaluating the magnitude of the integral (which will be small) on the mean surface $r=\bar{r}_w$, and finding the value of $r=r_w$ in the free-stream term $\tfrac{1}{2}u_\infty r^2$ which will make Ψ a constant, as required, on the duct surface.

This approach is easily extended to an iterative method of finding the exact shape of the surface corresponding to a prescribed vortex distribution; the value so found for the duct radius is used as a first approximation $r_{w1}(x)$, say, and then by replacing r and $\bar{r}_w$ in the integrand of equation (59) by $r_{w1}(x)$ and $r_{w1}(t)$, we can find a second approximation $r_{w2}(x)$, and so forth. The process is laborious, but convergent; plainly, the surface of the vortex distribution is made in the end to coincide with that of the duct, as required. A typical example is given in figure 32, where the shape of the duct surface, corresponding to a uniform vorticity distribution, is shown as calculated by quasi-cylinder theory, and as more

accurately determined by successive approximations (Kuchemann and Weber, 1948). Although the iterative technique provides an exact method, it is still of limited value, in relation to the problem originally posed, as the vortex distribution is only known approximately from the prescribed pressure difference; but no doubt this approximation could be improved at each step of the iterative process if necessary, by finding the surface velocity.

Some examples of the application of quasi-cylinder theory have been given by Warren (1945) with a specified vortex distribution over a duct of finite length; the results may be readily generalised to include the effects of the vortex wake on the jet boundary, where the internal flow has a different total head, merely by addition of the flow due to uniform distribution of vorticity over a semi-infinite cylinder downstream, the vorticity being of course continuous across the trailing-edge with that on the surface.

33. Thin Ducts of Prescribed Shape

The problem of finding the pressure distribution about thin ducts with a given variation of radius is again amenable to approximate treatment in a few particular cases. For short ducts (i.e. those with small fineness ratios of the duct length to its maximum diameter), the method of Dickmann (1940) is most appropriate: this is based on the 'quasi-cylinder' approximation. The integral in (59) is evaluated for $r = \bar{r}_w$, with the vortex distribution expressed as a Fourier series in terms of the angle whose cosine is (x/l), and with the kernal of the integral expanded in ascending powers of $(x-t)/\bar{r}_w$. Provided the duct is sufficiently short, so that $l/\bar{r}_w$ is small, this latter expansion need be taken only to the first few terms; use of simply the first term yields the same result as would be obtained by

treating the flow about the duct section as two-dimensional. To evaluate the vorticity distribution corresponding to a given shape, Dickmann also suggests including only the first few terms of the Fourier series describing its shape, whose coeffficients can then be evaluated by comparing with the known radius or slope of the duct at an appropriate number of stations.

On the other hand, if the duct is long compared with its diameter, it is possible to relax the assumptions of 'quasi-cylinder' theory, and to deal with a duct whose radius varies by large factors, and the internal flow through which is subjected to large forces. The method of approach to be used in this case is an extension of Slender Body Theory; with the effects of the vorticity on the jet boundary included, it is shown by Nonweiler (1955 b) that the pressure distribution over the exterior of the duct is identical in form with that found for closed bodies, but with the addition of a term which behaves, sufficiently far downstream of the nose, as

$$\Delta p = \left[\frac{\dot{Q} - V_\infty S(0)}{2\pi V_\infty x^2}\right] \tfrac{1}{2}\rho V_\infty^2$$

Here $\dot{Q}$ is the rate of volume flow through the duct, V_∞ is the free-stream speed, and $S(x)$ is the cross-sectional area of the duct at a distance x from the nose. Additionally, the theory shows that the internal flow is given to a first approximation by the one-dimensional continuity law, that the longitudinal velocity

$$u = \dot{Q}/S(x) \qquad \text{.....(60)}$$

It will be seen that the pressure induced on the external surface by the flow through the duct, as given above, vanishes only if the intake velocity equals the free stream speed; on the other hand, if it is smaller, a suction is induced which attains a large magnitude near the nose (figure 33). In fact there will be, in general, a finite

longitudinal force on the nose due to the local singularity in the pressure distribution, which is analogous to the suction force at the leading-edge of a flat plate.

According to Slender Body Theory, the jet leaves the duct with a speed which is, to a first approximation, equal to that of the free stream if no external forces act on the body: if such forces do exist, however, the jet will be bounded by a vortex sheet of approximately constant intensity, and of constant radius, so that from equation (60) above, the jet velocity is constant, - again, of course, to a first approximation.

34. The Theoretical Representation of the Effects of Duct Thickness

We have so far considered the duct as a thin shell, without thickness. No exact treatment has been so far suggested by which potential theory may be applied to derive the effects of the actual thickness of the duct on the flow. However, an approximate treatment, is, at least, well known in principle. Provided that the thickness is everywhere sufficiently small to justify the assumption that the disturbance to the flow it engenders is likewise small, then the direct effects of thickness may be simulated by a distribution of sources or source-rings on, say, the mean surface of the duct, whose intensity is proportional to the change in area of the solid annular cross-section of the duct. Thus it is possible to construct, on the basis of quasi-cylinder theory, the shape of duct having a prescribed thickness and vorticity distribution, and one such example is shown in figure 34 . The method of derivation follows along precisely similar lines to that stated in section 32, except of course that an expression for the increment in the Stokes Stream function due to a distribution of source rings must be added.

However, in relation to the direct problem of finding the flow due to a duct whose shape is prescribed, it will be seen from the figure that a source distribution (alone) induces a distortion or camber of the mean duct surface, which can of course be corrected by an additional vortex ring distribution: to determine its intensity it would be necessary to apply one of the two methods discussed in the preceding section - depending on whether the duct can be adequately described as short, or long (and slender).

On the basis of Slender Body Theory (Nonweiler, 1955 b) it can be demonstrated that the expressions for the pressure over the external surface stated earlier are still applicable provided that the duct cross-sectional area, $S(x)$, is taken to include that of the solid annular cowling as well. Thus the external flow can be said, to this approximation, to be independent of the shape of the internal ducting. The addition of a centre-body, within the duct, has likewise no important effect on the external flow (figure 35), and this general conclusion is supported by experimental evidence.

35. Thick Fairings with Uniform Pressure

An ingenious experimental technique of obtaining the shape of ducts having a uniform pressure over their external surface is due to Riechardt (1944). If a cylindrical tube is inserted in a stream of liquid and the flow through it is adjusted by a porous screen, or some such device, some of the liquid will spill round the nose of the tube, and having its pressure sufficiently depressed, it will form a cavitation bubble, extending downstream from the inlet (figure 36). The boundary of this bubble will be a constant pressure surface and also a streamline: hence it satisfies the requirements for the outside fairing of duct, over which the pressure is constant. The method is obviously

limited to this particular problem, and even in relation to this it has its limitations owing to the collapse of the bubble downstream.

Application of the momentum theorem to the flow about a semi-infinite duct with a cylindrical inner surface (figure 37) shows that the longitudinal forward force on the curved outer face equals

$$(-X) = -\int_{S_n} (p_w - p_\infty)\, d\, S_n$$

$$= \rho v_i\, S_i (v_\infty - v_i) - (p_i - p_\infty) S_i = \tfrac{1}{2}\rho v_\infty^2\, S_i \left(1 - \frac{v_i}{v_\infty}\right)^2$$

where v_i is the 'intake velocity'. If this force is due to the action of a uniform suction over the duct outer surface, we may easily calculate that the external velocity (v_w) is related to the annular frontal area of the duct (S_n) and the intake area, S_i, by the expression

$$\frac{v_w^2}{v_\infty^2} = 1 + \left(1 - \frac{v_i}{v_\infty}\right)^2 \frac{S_i}{S_n}$$

The experimental observations (figure 38) on fairings deduced from this cavitation method are seen to be in good agreement with this law.

36. Experimental Measurements of the Flow about Ducts

Most of the experimental work has concerned itself with conditions existing over intake or exit portions of ducts, mounted on what may be assumed to be, effectively, a semi-infinite cylinder. Only a few isolated results are available for ducts of finite length. The work on intakes has been largely concerned with the deduction of shapes having a roughly constant external pressure distribution. In practice, however, the results given by the quasi-cylinder theory, or the cavitation technique just described, which are of application to such a problem, are of limited significance for it

is evident that the duct has to operate under not one, but a variety of conditions of intake velocity ratio, and incidence, and the duct lip has to be designed primarily to avoid flow separation. Nevertheless, although it is not capable of describing conditions over a duct at incidence, theory does show reasonable agreement in axial flow (figure 39).

On the other hand, the theory of the flow over the curved after-bodies of ducts in the presence of an emerging jet could hardly be expected to show complete agreement with experimental results (figure 40) as viscous effects will modify to an important extent both the state of the flow near the surface, and over the jet boundary, which is represented in theory as a vortex sheet. The disparity between theory and experiment, of course, becomes more apparent as the intensity of this free vorticity increases. Turbulent mixing between the jet and the surrounding air causes an additional inflow towards the jet, due to much the same causes as the 'sink-effect', or the decrease in displacement thickness of a wake. The modification to the airflow brings about a change in the surface pressure distribution, particularly near the exit plane. The results of figure 40 suggest that the effect is relatively slight, causing a pressure change at the exit which varies linearly with the jet exit velocity V_e, i.e.

$$\Delta C_p = - 0.01 \left(\frac{V_e}{V_\infty} - 1 \right)$$

In other words, with $V_e > V_\infty$, the 'sink effect' tends to accelerate the flow over the rear of the duct.

Acknowledgement

The author acknowledges with gratitude the advice and criticism of Professor A.D. Young, M.A., F.R.Ae.S., of Queen Mary College, London, which were of considerable help in the preparation of this chapter.

LIST OF NOTATION

a, $a(x)$	radius of source or vortex ring (in plane x = constant)
a, b	limiting x-coordinates of doublet distribution
c_d	two-dimensional drag coefficient of circular cylinder
$\bar{c}_d$	mean cross-flow drag coefficient
d	maximum diameter of body
h_1, h_2, h_3	coefficients of metric
k	argument of elliptic functions
k_1, k_2	coefficients of longitudinal and lateral virtual mass
l	half length of body
l_f	half distance between foci of spheroid
m	point source intensity
$m(x)$	total source intensity upstream of plane x = constant
m_1, m_2	longitudinal and lateral virtual mass
n	distance measured along outward normal to body
$\underset{\sim}{n}$	unit outward normal
p	pressure
$q(x)$	source intensity per unit length in plane x = constant
r	radial coordinate in cylindrical polars measured perpendicular to body axis
$\underset{\sim}{r}$	position vector
$\bar{r}_w$	mean radius of body
s	distance (general)
t	parameter of integration
u	fluid velocity component along x-axis
u'	perturbation velocity component along x-axis
v	fluid velocity component along y-axis
v_r	fluid radial velocity component
$\underset{\sim}{v}$	speed of fluid relative to body
v_i	intake speed

w	fluid velocity component along z-axis
x	(potential flow) longitudinal coordinate in cartesians and cylindrical polars measured downstream along body axis, with origin half way between nose and tail
x	(boundary layer flow) coordinate measured along surface downstream from nose in meridian plane
$\bar{x} = \frac{1}{l^2}\int_0^x r_w^2\,dx$,	in Mangler's Transformation of boundary layer equations
y,z	(potential flow) cartesian coordinates in plane perpendicular to body axis, z being taken to lie in plane of (translational) motion and positive in direction of free-stream component
y,z	(boundary layer flow) coordinate system with z measured normal to surface and y in surface
A	side area of body
$C_m = (\text{moment})/\frac{1}{2}\rho V_\infty^2(\text{Vol})$,	pitching moment coefficient positive if nose-up
$C_p = \frac{p-p_\infty}{\frac{1}{2}\rho V_\infty^2}$	pressure coefficient
D	drag
E, $E(k^2)$	complete elliptic integral of second kind with modulus k
F	side force, taken by convention in direction of z-axis
$\underset{\sim}{F}$	external force exerted on body to sustain motion through fluid
G	'growth parameter' in boundary layer momentum equation
$\underset{\sim}{G}$	external couple exerted on body to sustain motion through fluid
$H = (\delta_{1x}/\delta_{2x})$	
I	virtual moment of inertia
K,$K(k^2)$	complete elliptic integral of first kind with modulus k
$K_n^m(t)$	Legendre associated function of first or second kind
M	point doublet intensity
$\underset{\sim}{M}$	momentum of perturbed fluid flow
$\underset{\sim}{N}$	moment of momentum of perturbed fluid flow
$P_n^m(t)$	Legendre associated function of the first kind
Q	volume occupied by fluid (general)

$Q_n^m(t)$ Legendre associated function of the second kind

$\dot{Q}$ rate of volume flow through duct

$R_v = V_\infty (Vol)^{1/3}/\nu$, Reynolds number

$R_l = V_\infty (2l)/\nu$, Reynolds number based on body length

S area (general)

$S(x)$ cross-sectional area of body in plane x = constant

S_{max} maximum cross-sectional area of body

S_i intake area of duct

T total kinetic energy of perturbed fluid flow

$U, U(x)$ velocity component at, and parallel to, outside of boundary layer

$V, V(x)$ body volume contained upstream of plane x = constant

$\underset{\sim}{V}_\infty$ velocity vector of body relative to undisturbed fluid

(Vol) total volume of body

$V_\wedge, V_\wedge(x)$ velocity component at, and parallel to, body surface

X longitudinal force in direction of x-axis

α incidence of body, taken by convention as a positive rotation about y-axis

$\beta = \tan^{-1}\left(\frac{dr_w}{dx}\right)$ slope of body surface relative to body axis

γ strength of infinitesimal horseshoe vortex

δ_{2x} momentum thickness of body in axial flow

ζ semi-elliptic coordinate defined in equation (1) of text

$\theta = \tan^{-1}\left(-\frac{Y}{z}\right)$, cylindrical polar coordinate (measured from z-axis as datum) in positive sense about x-axis

θ_o value of θ on axis of rotation of body

μ viscosity

μ semi-elliptic coordinate defined in equation (1) of text

ν kinematic viscosity

ρ density of fluid

σ_1 displacement area of boundary layer or wake $(= \oint \delta_{1x}\, dy)$

σ_2 momentum area of boundary layer or wake $(= \oint \delta_{2x}\, dy)$

τ_w	shear stress at wall
ϕ	velocity potential
ϕ'	perturbation velocity potential
ϕ_n, ϕ_{nm}	coefficients in expansion of potential function
Γ	circulation
$\Gamma'( )$	circulation per unit length in plane x = constant
Ψ	Stokes stream function defined in equation (10) of text
Ω	angular speed of rotation of body relative to undisturbed stream
$\underset{\sim}{\Omega}$	angular velocity vector of body relative to undisturbed stream.

LIST OF REFERENCES

Adams, Mac.C., and Sears, W.R. (1953) Slender Body Theory - Review and Extension. J.Ae.Sc. 20, p.85.

Allen, H.J., and Perkins, E.W. (1951) A Study of the Effects of Viscosity on Flow over Slender Inclined Bodies of Revolution. N.A.C.A. Rep. No. 1048.

Bilharz, H., and Hölder, E. (1947) Calculation of the Pressure Distribution of Bodies of Revolution in the Subsonic Flow of a Gas Part I: Axi-symmetric Flow. N.A.C.A. Tech. Memo. No. 1153.

Dickmann, H.E. (1940) Fundamental Theory of the Ring Aerofoil. Ing. Arch. Vol. 11, p.36.

Freeman, H.B. (1932a) Pressure Distribution Measurements on the Hull and Fins of a 1/40 scale model of the U.S. airship Akron. N.A.C.A. Rep. No. 443.

Freeman, H.B. (1932b) Measurements of Flow in the Boundary Layer of a 1/40 scale model of the U.S. airship Akron. N.A.C.A. Rep. No. 430.

Fuhrmann, G. (1911) Theoretical and Experimental Investigations on Balloon Models. Zeitschrift fur Flugtechnik und Motorluftschiffart, 11.

Goldstein, S. (1938) Modern Developments in Fluid Mechanics. O.U.P. Oxford 1st Edn. 1938.

Grenville, P.S. (1953) The Calculation of the Viscous Drag of Bodies of Revolution. U.S. Navy Dept. D.W. Taylor Model Basin Rep. No. 849.

Jones, R. (1925) Distribution of Normal Pressures on a Prolate Spheroid. A.R.C. R. and M. 1061.

Kaplan, C. (1934) Potential Flow about Elongated Bodies of Revolution. N.A.C.A. Rep. No. 516.

Kaplan, C. (1943) On a New Method of Calculating the Potential Flow past a Body of Revolution. N.A.C.A. Rep. No. 752.

Karman, Th. von, (1927) Calculation of Pressure Distribution on Airship Hulls. N.A.C.A. Tech. Memo. 574.

Kelly, H.R., (1954) The Estimation of the Normal Force, Drag and Pitching Moment Coefficients for Blunt-nosed Bodies of Revolution at High angles of attack. J.Ae.Sci. 21, pp.549-555.

Kuchemann, D., and Weber, J. (1948) Power Unit Ducts. A.V.A. Monograph, M.A.P. Volkenrode Trans. No. 984.

Kuchemann, D., and Weber, J. (1953) Aerodynamics of Propulsion. McGraw Hill Publishing Co. London, 1st Edn. 1953.

Laitone, E.V. (1947) The Subsonic Flow about a Body of Revolution. Q.App.Maths. 5. p.227.

Lamb, H. (1879) Hydrodynamics. C.U.P., Cambridge 6th Edn. 1932.

Landweber, L. (1951) The Axially Symmetric Potential Flow about elongated Bodies of Revolution. U.S. Navy Dept. D.W. Taylor Model Basin Rep. No. 761.

Lange, G. (1941) Force- and Pressure-Distribution Measurements on eight fuselages. N.A.C.A. Tech. Memo. No. 1194.

Lotz, I. (1931) The Calculation of the Potential Flow past airship Bodies in Yaw. N.A.C.A. Tech. Memo. No. 675..

Lyon, H.M. (1934) A Study of the Flow in the Boundary Layer of Streamline Bodies. A.R.C. R. and M. 1622.

Mangler, W. (1946) Compressible Boundary Layers on Bodies of Revolution. A.R.C. Rep. No. 9740.

Millikan, C.B. (1932) The Boundary Layer and Skin Friction for a Figure of Revolution. Trans. A.S.M.E. APM-54-3.

Moore, F.K. (1951) Three-Dimensional Compressible Laminar Boundary Layer Flow. N.A.C.A. Tech. Note No. 2279.

Moore, F.K. (1953) Three Dimensional Laminar Boundary Layer Flow. J.Ae.Sci. 20, pp.525-534.

Munk, M.M. (1934) Aerodynamic Theory (ed. Durrand) Vol. I. Div.C. Julius Springer, Berlin, 1st. Edn. 1934.

Munzer, H., and Reichardt, H. (1944) Rotationally Symmetric Source-sink Bodies with predominantly constant Pressure Distributions. M. of S. A.R.E. Trans. No.1/50.

Neumark, S. (1950) Velocity Distribution on Thin Bodies of Revolution at Zero Incidence in Incompressible Flow. A.R.C. Rep. No. 13756.

Nonweiler, T. (1955a) A Theoretical Study of the Boundary Layer Flow and Side force on inclined slender bodies. Coll. of Aeronautics Rep. (unpublished).

Nonweiler T.	(1955b)	Potential Flow about slender Ducted bodies of revolution. Coll. of Aeronautics Rep. (unpublished)
Rankine, W.J.M.	(1871)	On the Mathematical Theory of Streamlines, especially those with four foci and upwards. Phil. Trans. 1871, p.267.
Riechardt, H.	(1944)	Cavitation-model method for construction of constant pressure surfaces of revolution. Deutsche Luftfahrforschung U.M. Bericht 6606.
Riegels, F. and Brandt, M.	(1944)	Stream Functions and Velocity Fields of Space Distributions of Sources, and their use in determining the profile and pressure distribution of axially symmetric bodies, with examples. Deutsche Luftfahrforschung U.M. Bericht 3106.
Rott, N., and Crabtree, L.F.	(1952)	Simplified Laminar Boundary Layer Calculations for Bodies of Revolution and for Yawed Wings. J.Ae.Sci. 19, pp.553-566.
Sadowsky, M., and Sternberg, E.	(1950)	Elliptic Integral Representation of Axially Symmetric Flows. Q.App.Maths. 8, pp.113-126.
Sampson	(1891)	On Stokes' Current Function. Phil. Trans. A. clxxxii
Schlichting, H.	(1951)	Grenzchichte-Theorie Verl.G. Braun, Karlsruhe.
Smith, R.H.	(1935)	Longitudinal Potential Flow about an arbitrary body of revolution with application to the airship 'Akron'. J.Ae.Sci. 3, p.26-31.
Squire, H.B., and Young, A.D.	(1937)	The Calculation of the Profile Drag of Aerofoils. A.R.C. R. and M. 1838.
Stokes	(1842)	On the Steady Motion of Incompressible Fluids Papers (i) 1
Taylor D.W.	(1894)	On Ship-Shape Forms Trans. Inst. Naval Arch. 35
Thwaites, B.	(1949)	Approximate Calculation of the Laminar Boundary Layer. Aero. Quart. 1, p.245.
Tomatika, S.	(1935)	The Laminar Boundary Layer on the Surface of a Sphere in a Uniform Stream. A.R.C. R. and M. 1678.
Tuyl, A. van.	(1950)	Axially Symmetric Flow around a new family of half-bodies. Q.App. Maths. 7, p.399.

Upson, R.H., and Klikoff, W.A. (1931) Application of Practical Hydrodynamics to Airship Design. N.A.C.A. Rep. No. 405.

Vandrey, F. (1953) Method for Calculating the Pressure Distribution of a Body of Revolution moving in a circular path through a perfect fluid. A.R.C. Rep. No. 16,655.

Ward, G. (1949) Supersonic Flow past Slender Pointed Bodies. Q.J.M.A.M. 2 , p.75.

Ward, G. (1955) The Drag of Source Distributions in Linearised Supersonic Flow. Coll. of Aeronautics Rep. No. 88.

Warren, C.H.E. (1945) Theory of Thin Sections applied to derive the surfaces of revolution having specified distributions of pressure differences between the inside and outside. R.A.E. Tech. Note No. Aero. 1636.

Weinstein, A. (1948) On Axially Symmetric Flows. Q.App. Maths. 5, p.429.

Wijngaarden, A.von (1948) Potential Flow about a Body of Revolution. Colloques Internationaux du Centre National de la Recherche Scientifique, XIV. Methods de Calcul dans les Problemes de Mecanique, Paris.

Young, A.D. (1939) The Calculation of the Total and Skin Friction Drags of Bodies of Revolution at zero Incidence. A.R.C. R. and M. 1874.

Young, A.D. and Owen, P.R. (1943) Simplified Theory for Streamlined Bodies of Revolution, and its application to the development of High Speed Low Drag Shapes. A.R.C. R. and M. 2071.

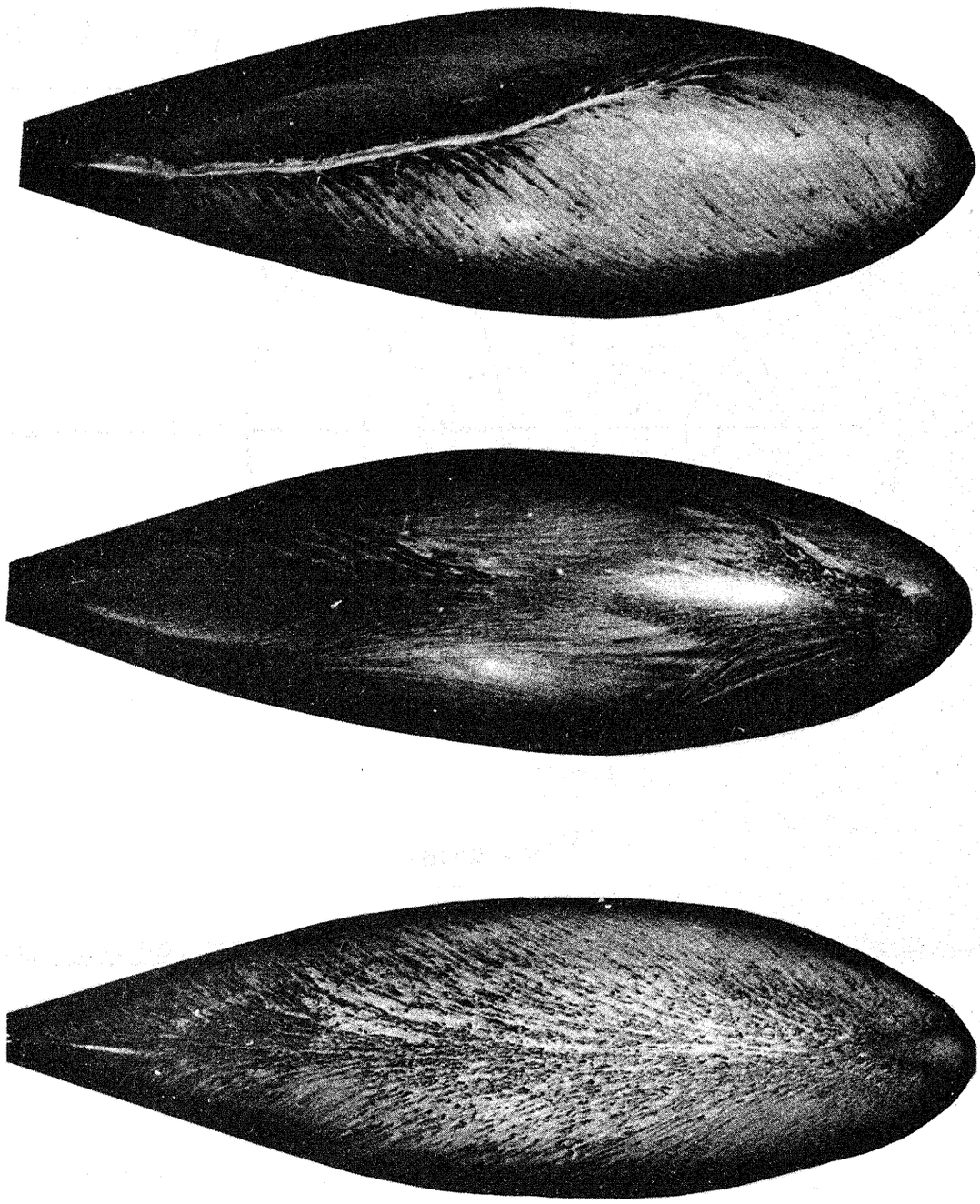

PLATE 1.

17,619.
FIGS. 1 & 2.

FIG. 1.

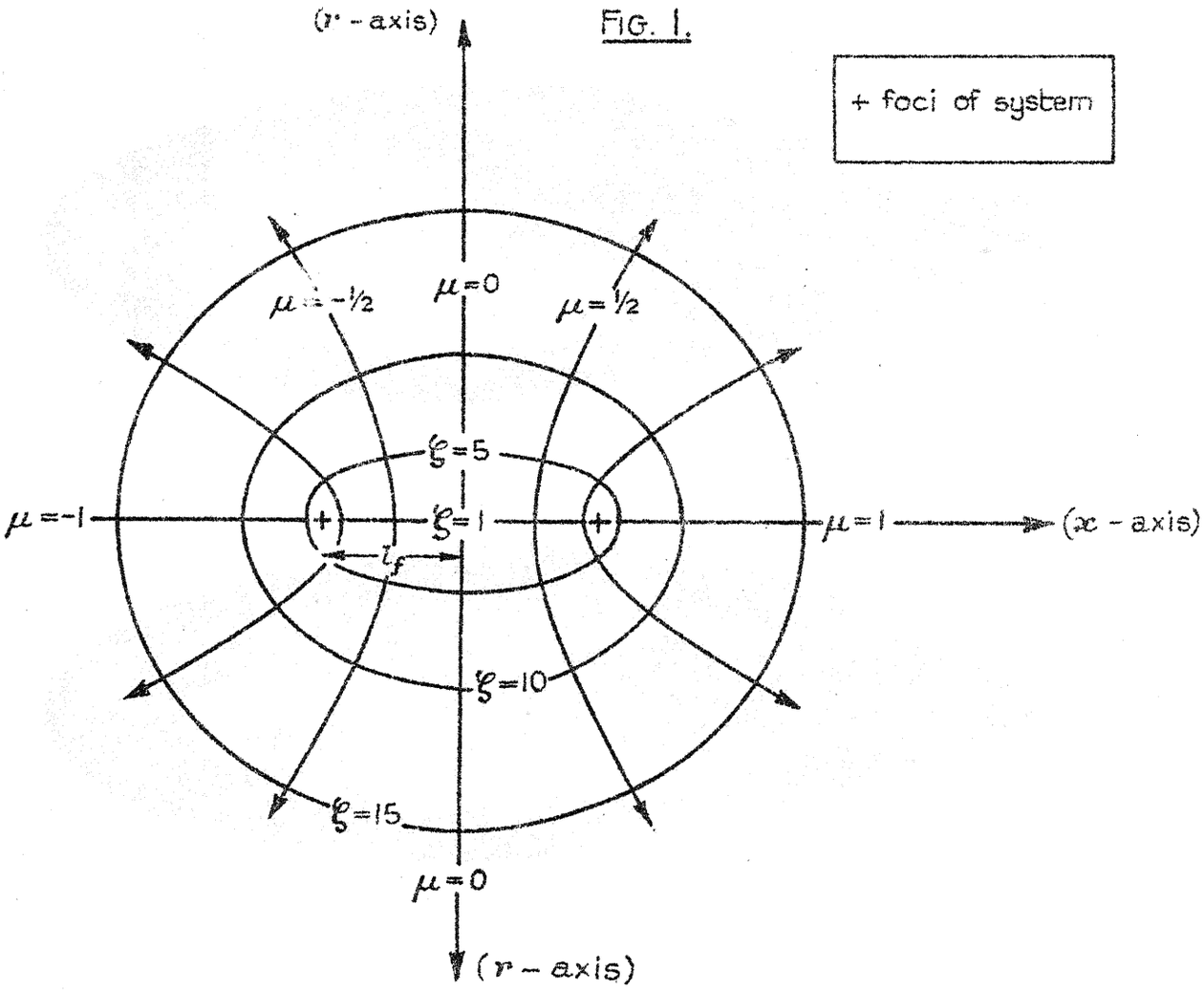

Diagram showing interpretation of system of semi-elliptic coordinates.

FIG. 2.

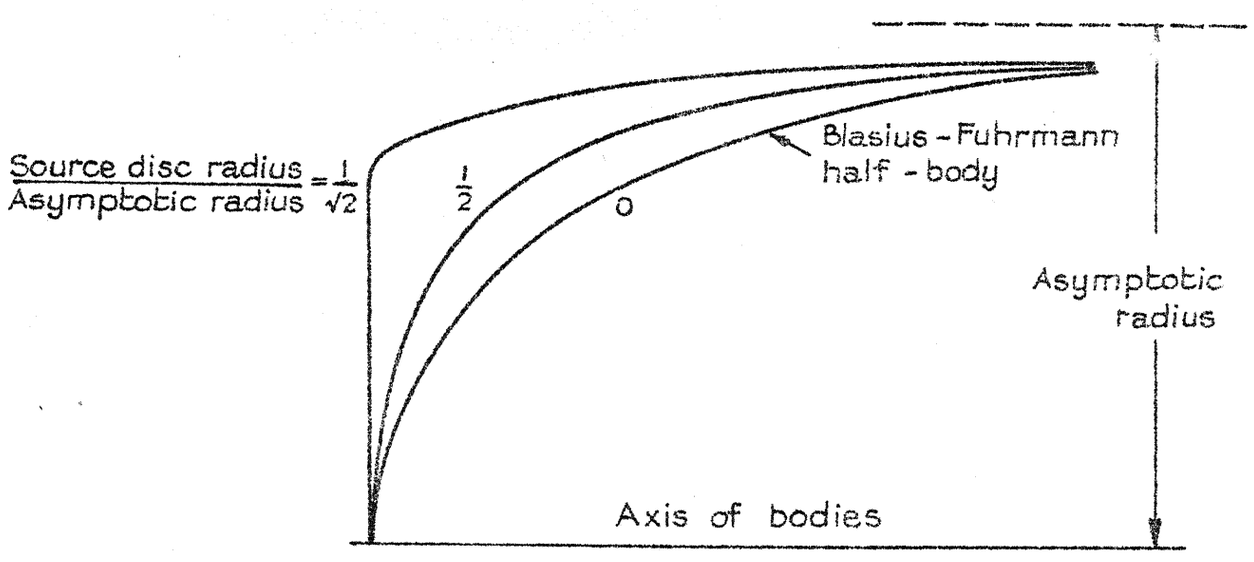

Shapes of half-body simulated by placing a source disc perpendicular to a free-stream.

FIG. 3.

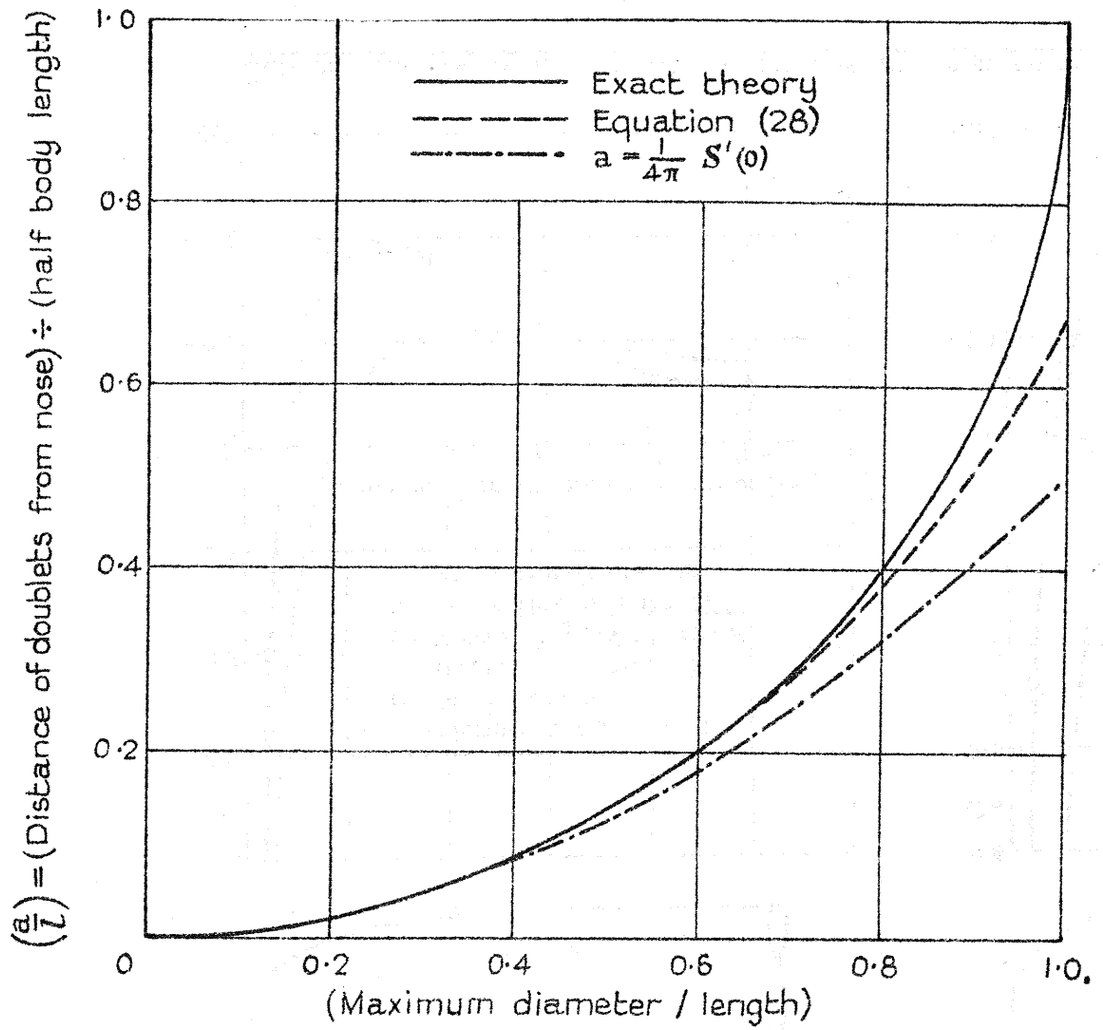

The distance between the nose of a spheroid and the upstream end of the axial doublet distribution representing its effect in axi-symmetric flow.

FIG. 4.

Body shape given by: $S(x) = \frac{27\pi}{800}(l-x)(l+x)^2$

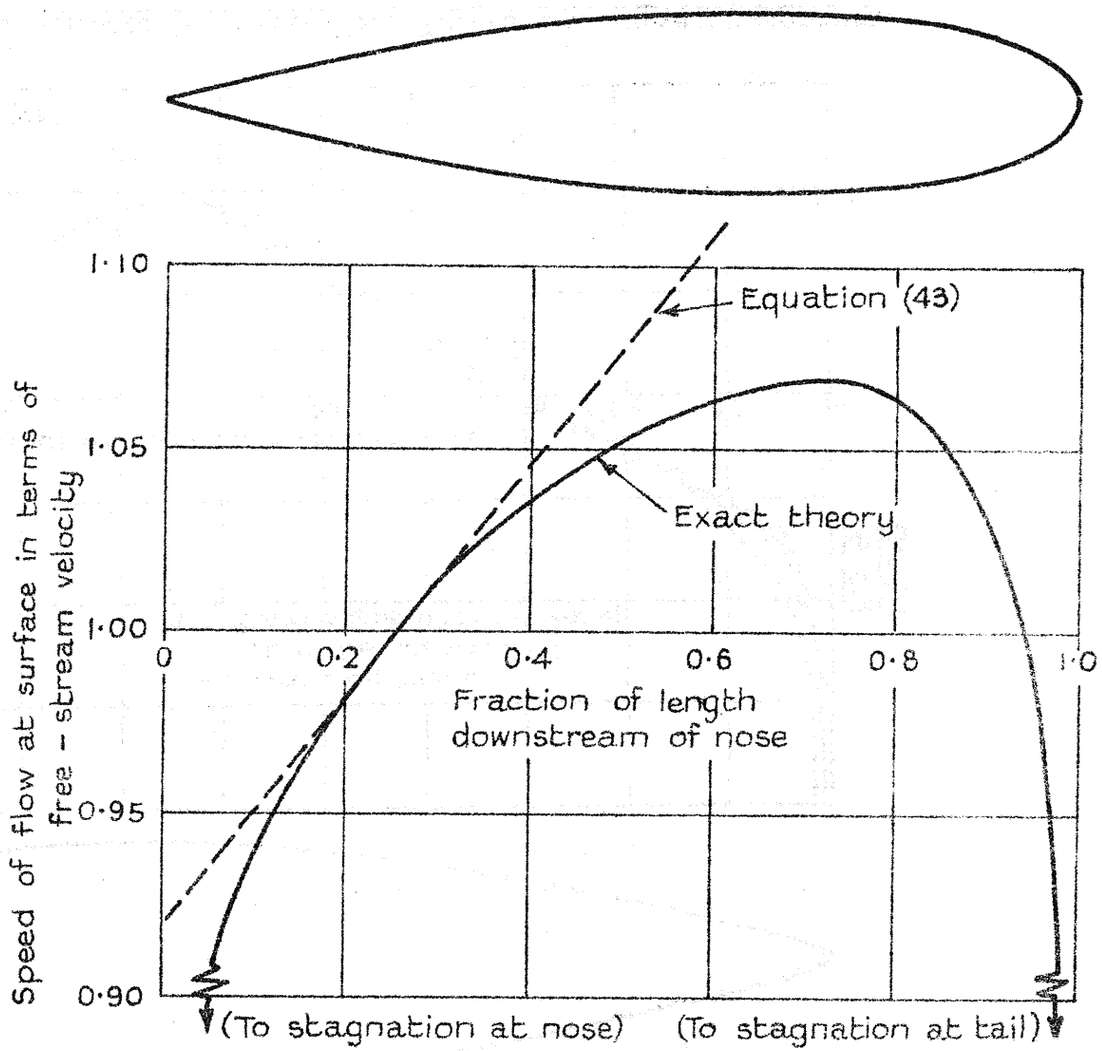

Surface velocity distribution of body of fineness ratio 5 designed by the method of Young and Owen to provide a uniform favourable velocity gradient.

Body shape given by $r_w = 0{\cdot}2\sqrt{l^2 - \frac{x^4}{l^2}}$;
(Length/diameter = 5)

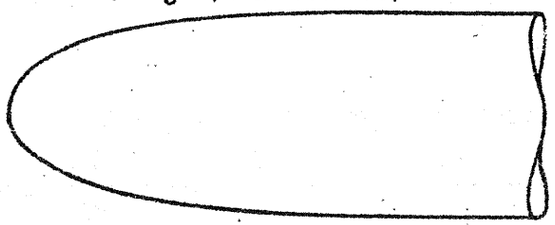

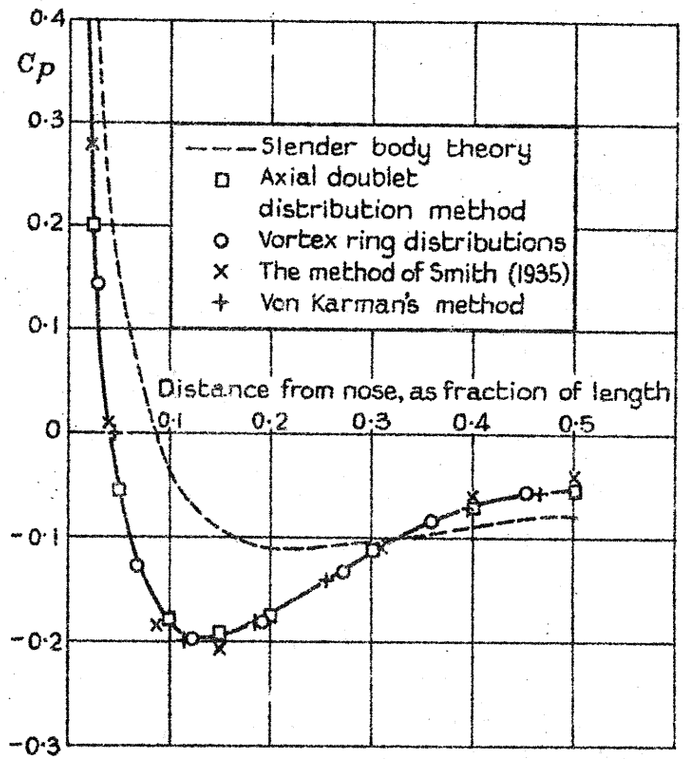

Body shape derived from Joukowski profile (Length/diameter = 4·2)

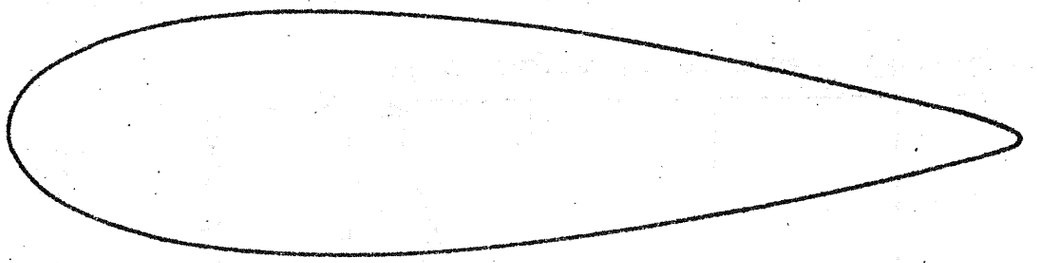

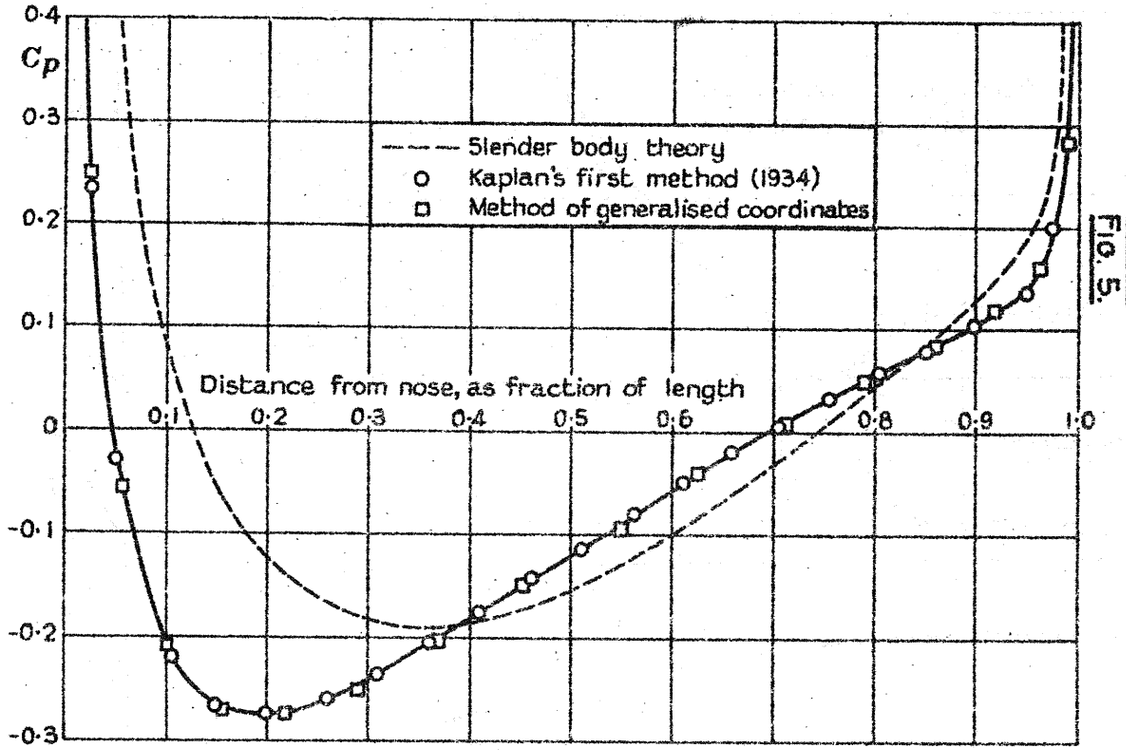

17.619
Fig. 5.

Comparison of pressure distribution in axi-symmetric flow as deduced by slender Body Theory, and by exact techniques.

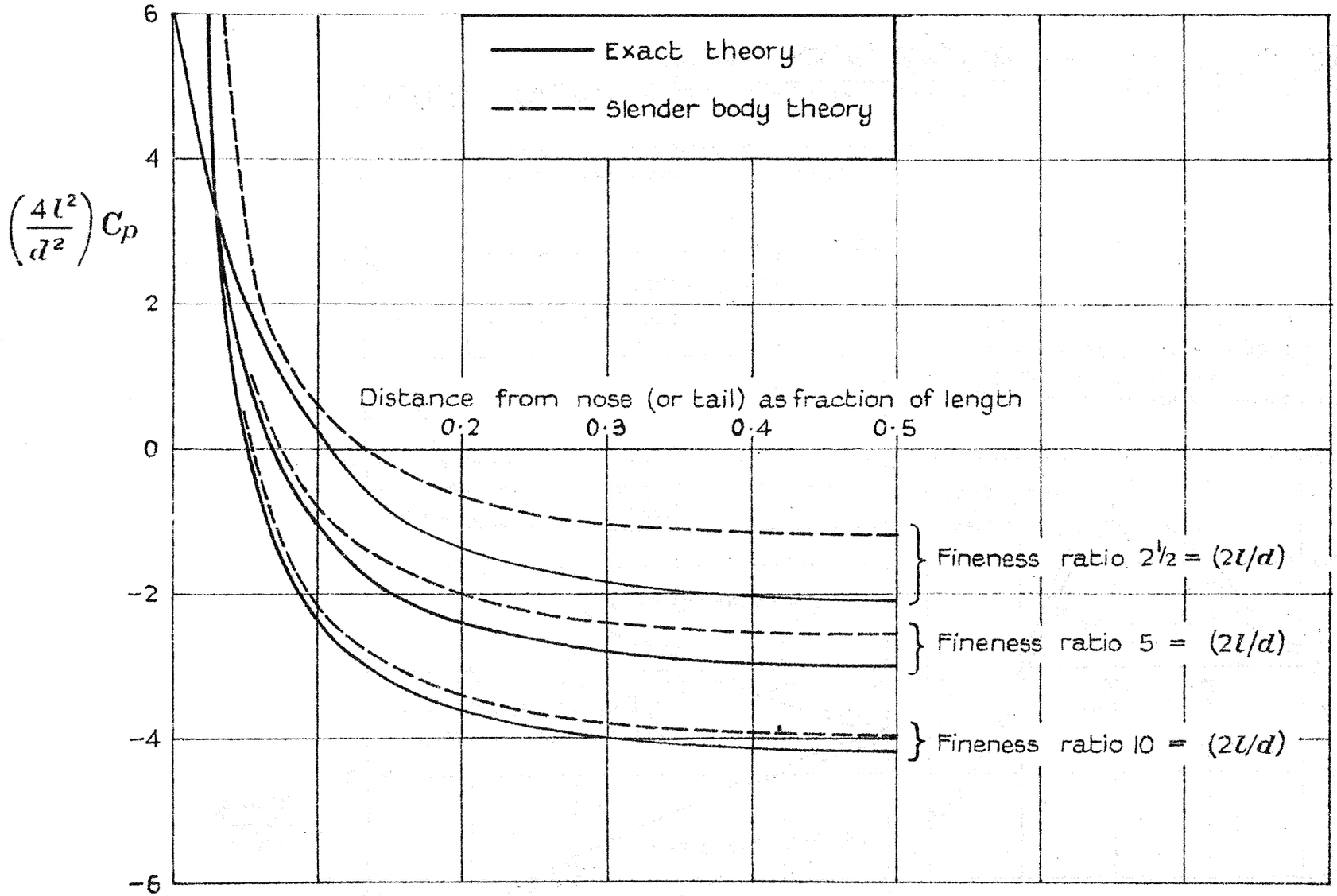

A comparison of exact and slender body theory results for the surface pressure distribution on spheroids in axi-symmetric flow.

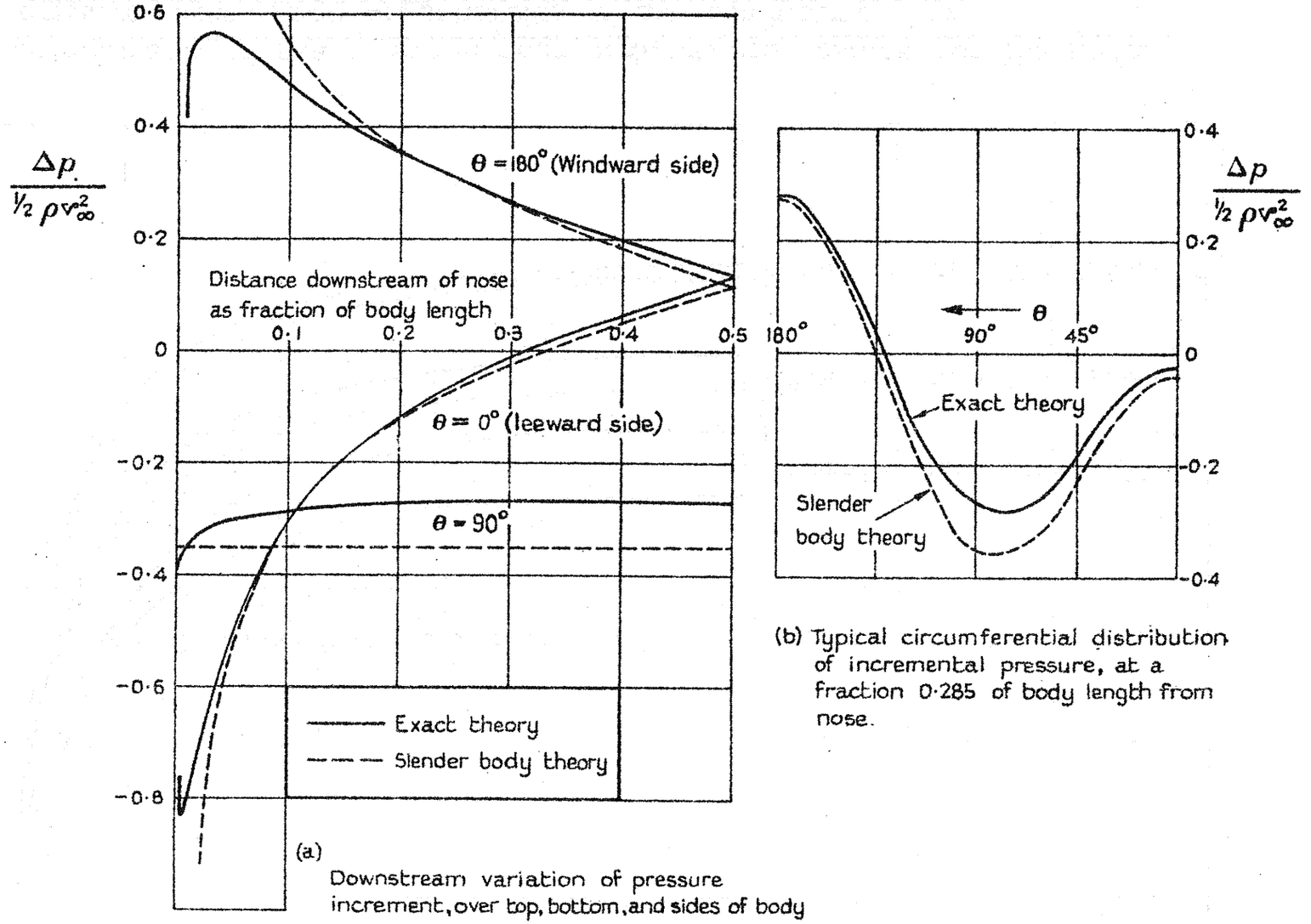

17,619.
FIG. 7.

The incremental pressure Δp induced by incidence on a spheroid (Incidence 20° fineness ratio of spheroid 4)

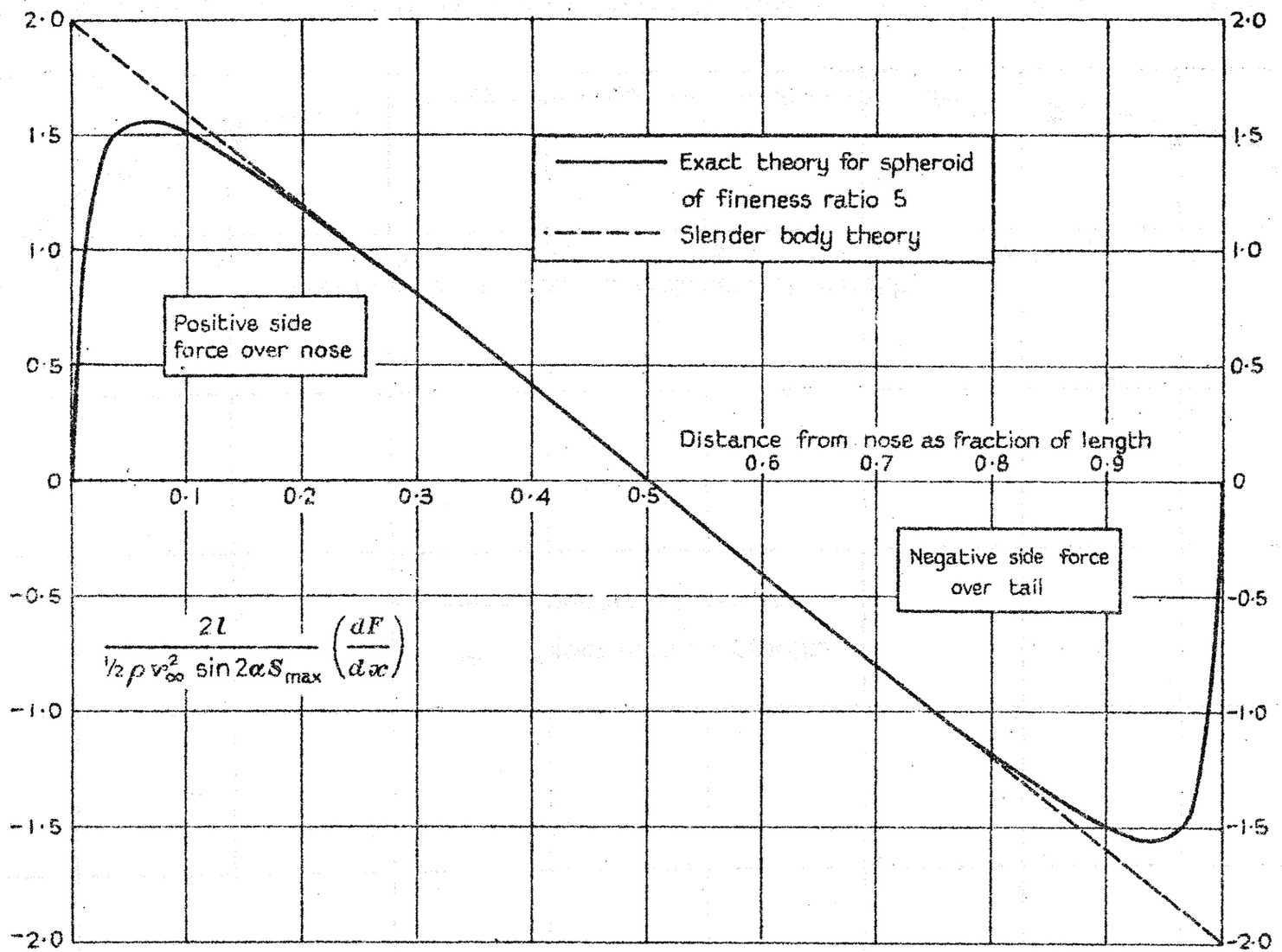

Side force distribution on spheroids

17.619.
FIG. 8

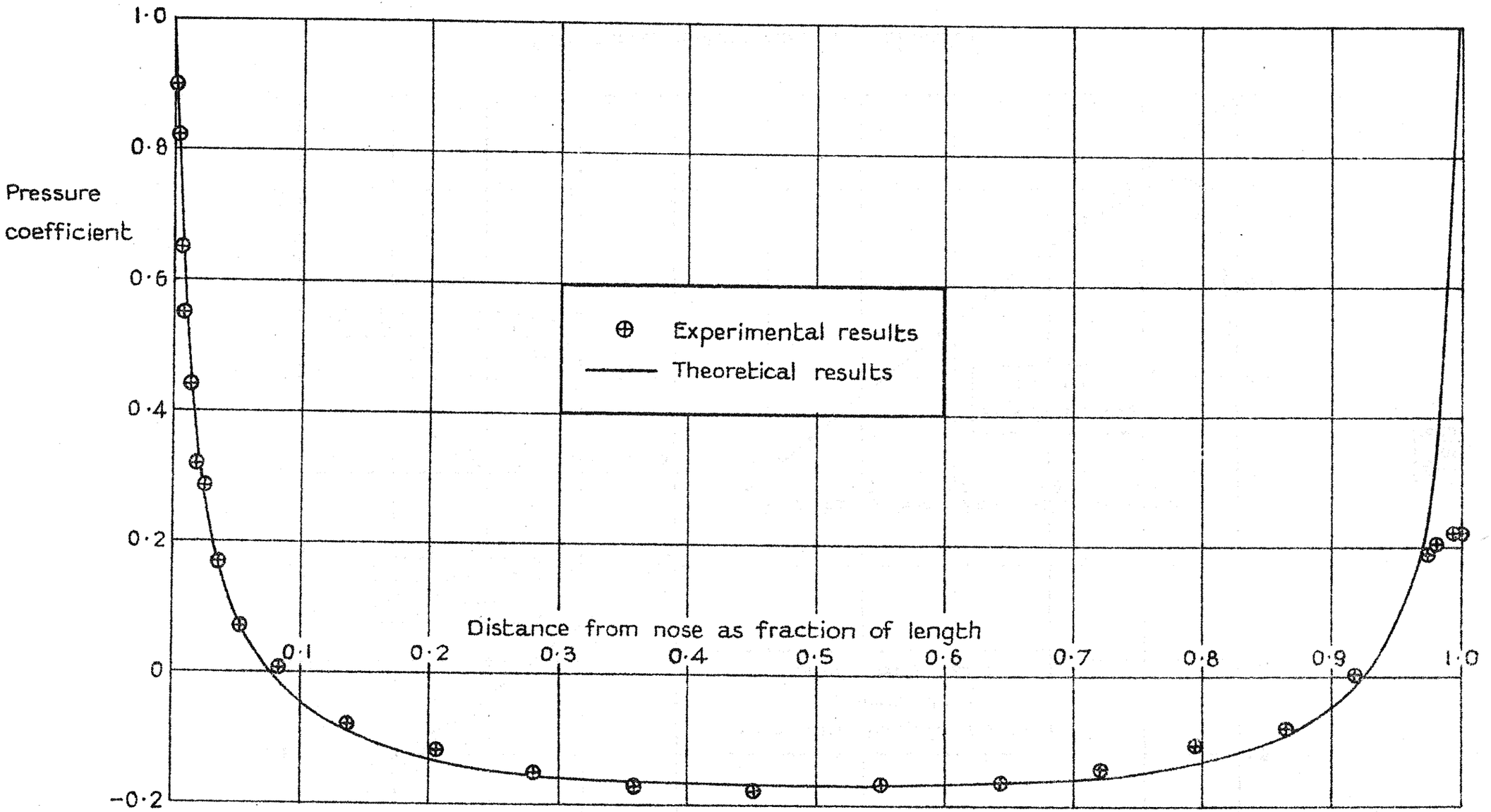

17.619.
FIG. 9.

Theoretical and experimental pressure distributions on a spheroid of fineness ratio 5 in axi-symmetric flow.

17,619.
FIG. 10.

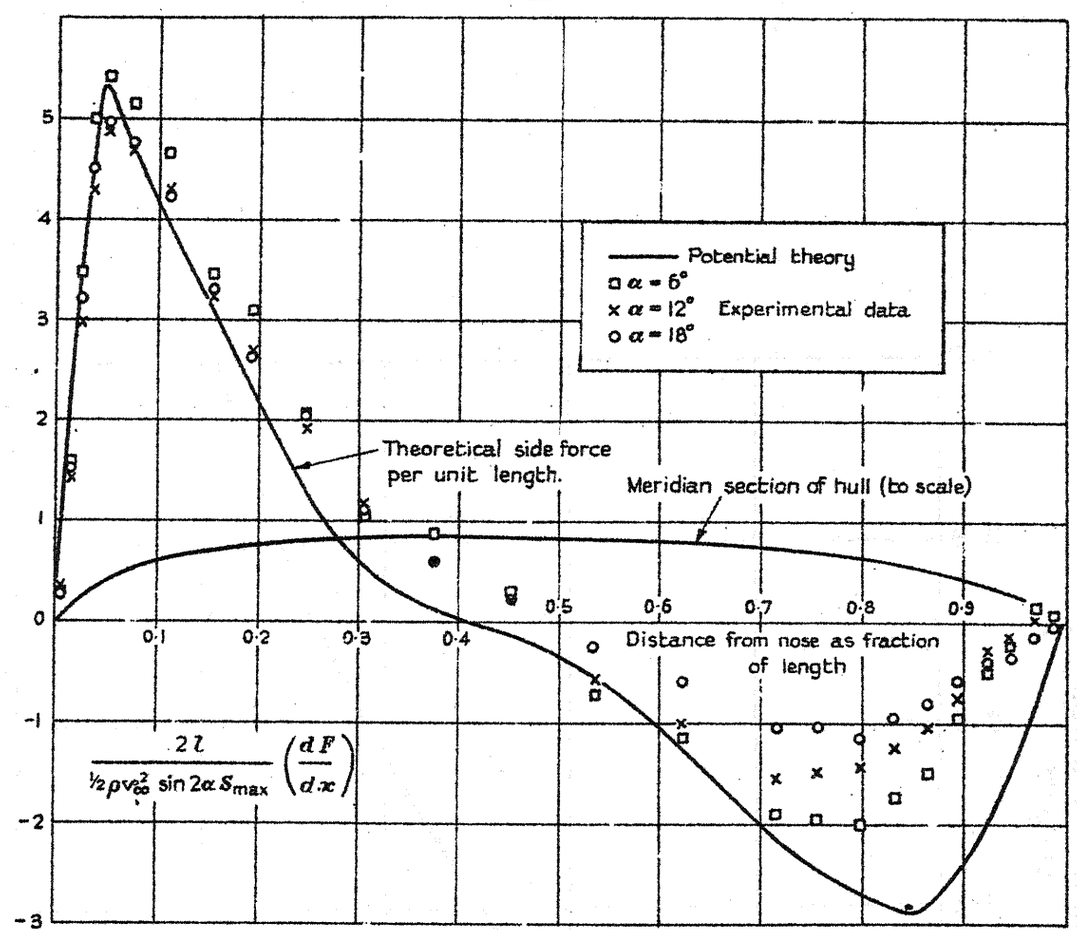

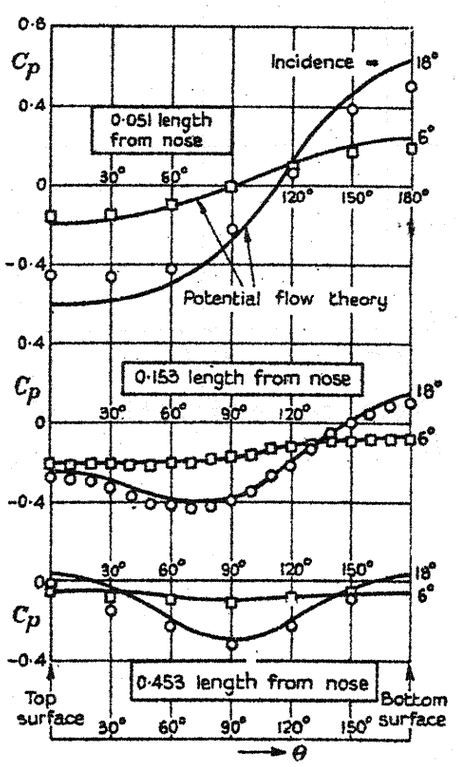

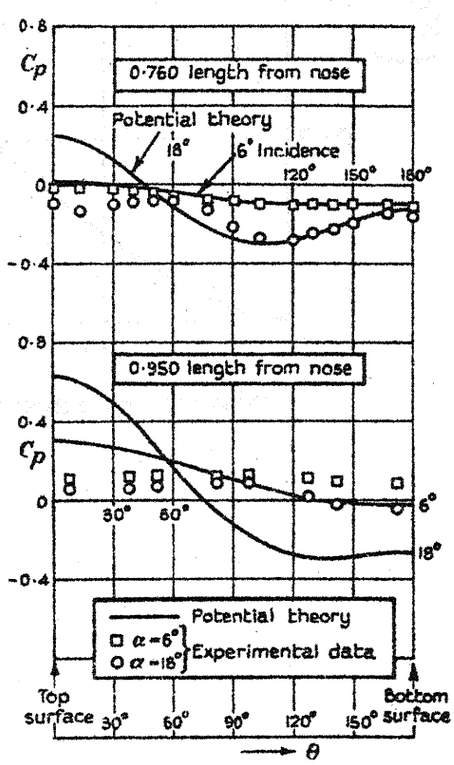

Side force distribution and some circumferential pressure distributions on model of the airship "Akron". (Reynolds number, R_l = 18 million)

17, 619.
FIG. 11.

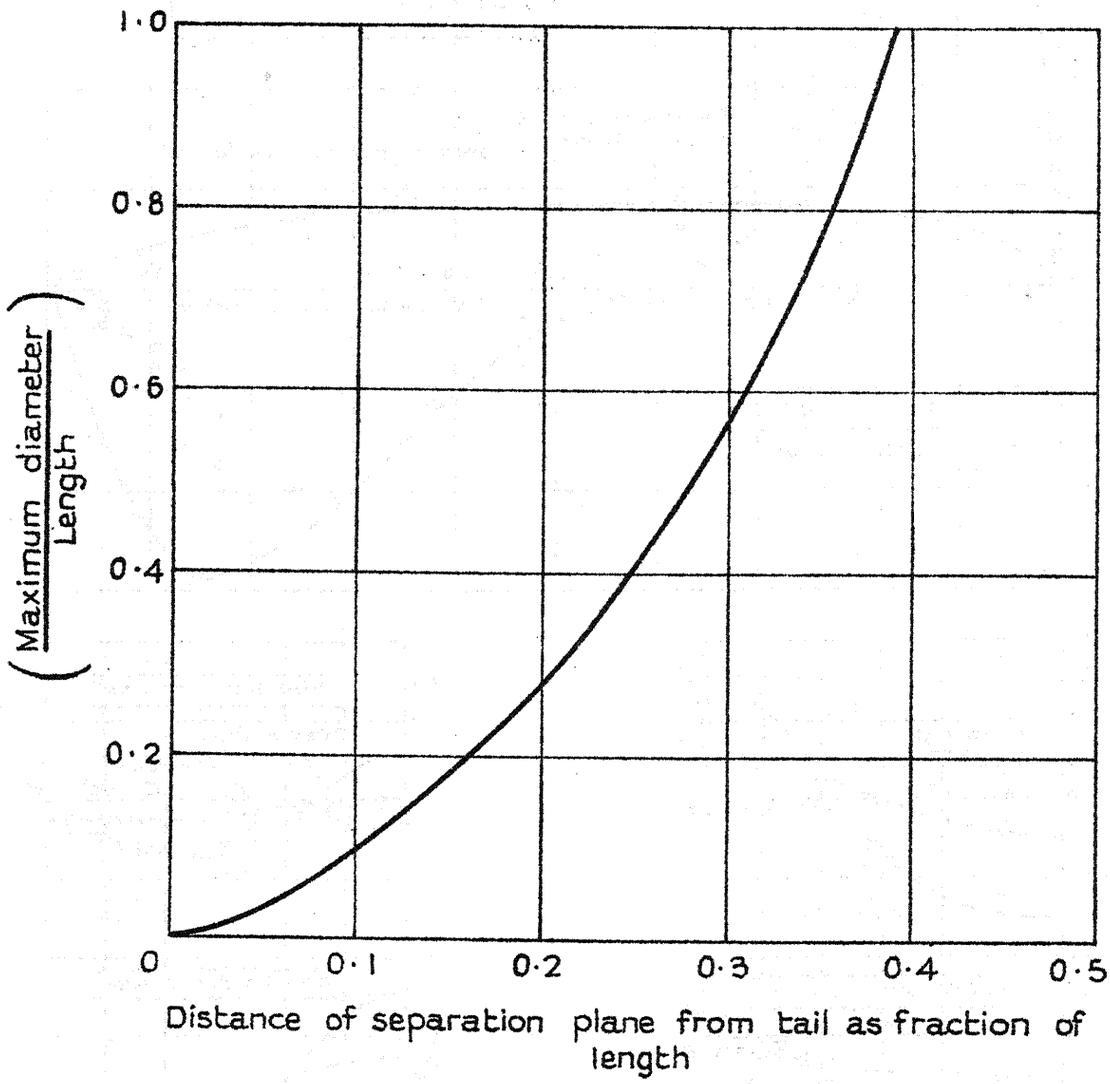

Plane of laminar separation of spheroids

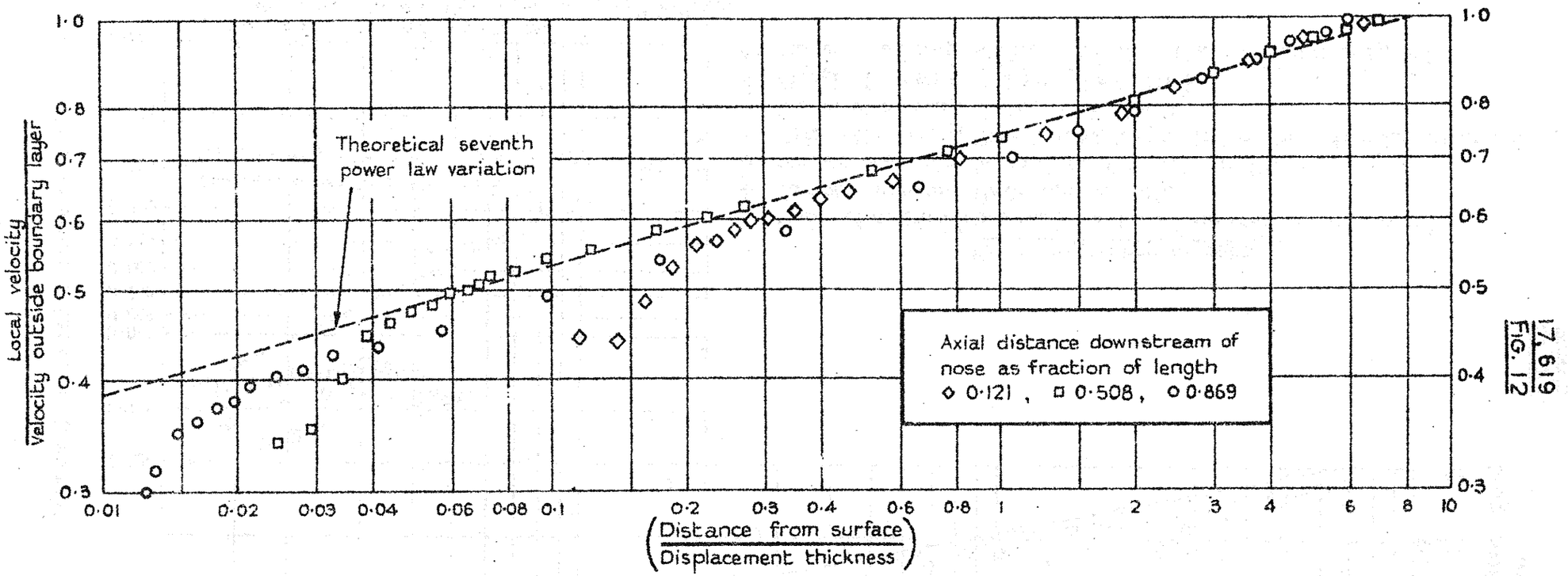

17,619
FIG. 12

Velocity distribution within boundary layer over hull of airship "Akron" in axi-symmetric flow at a Reynolds number of 18 million based on hull length.

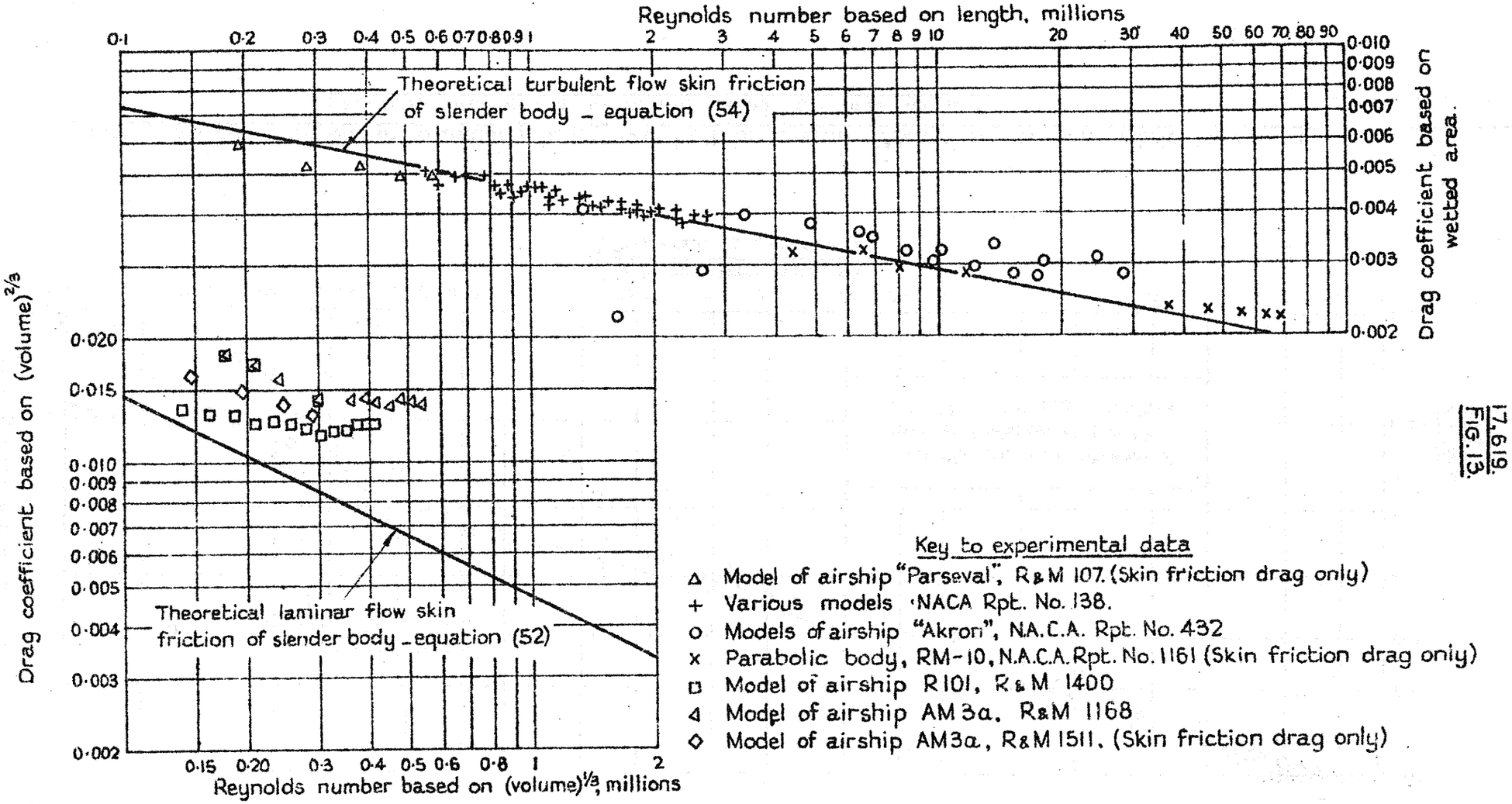

17.619.
Fig. 13.

Drag of various bodies of revolution in axi-symmetric motion, with laminar or turbulent boundary layer flow

17, 619.
FIG. 14.

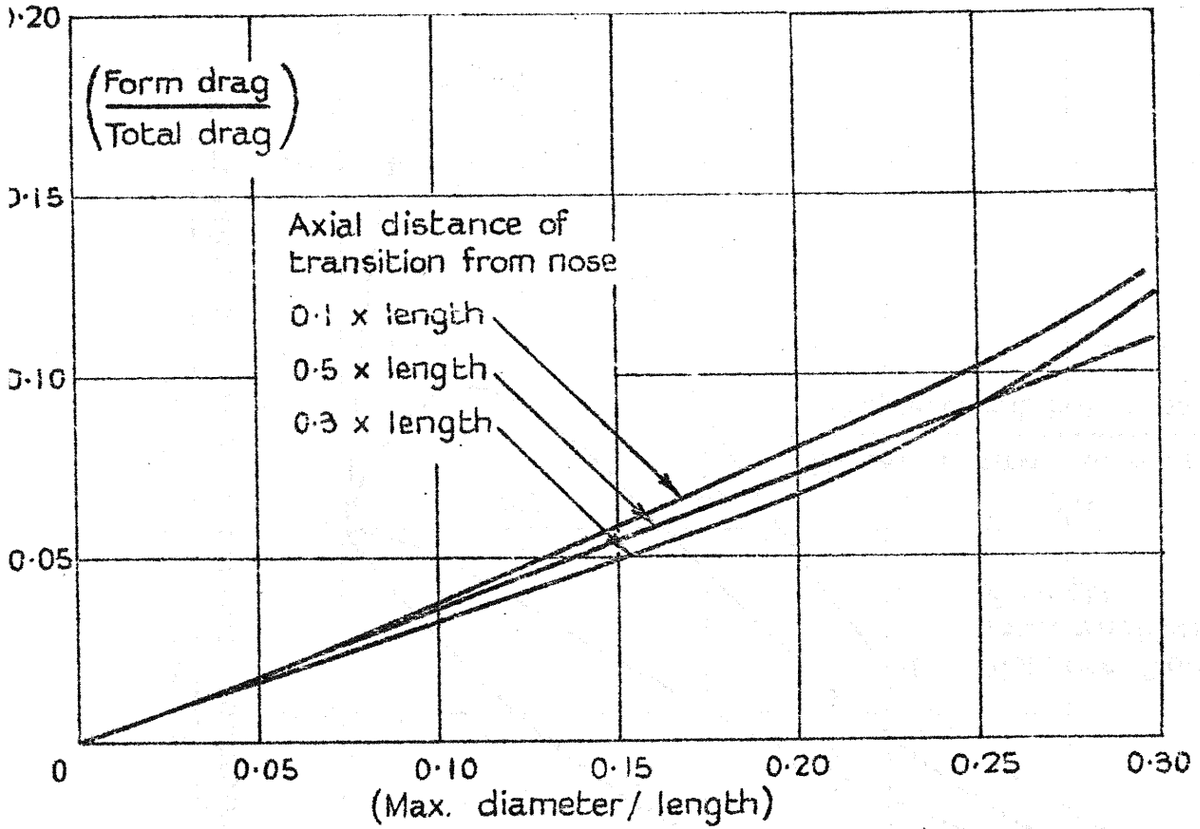

Calculated form drag of bodies in axi-symmetric flow.

(Reynolds numbers between 10^6 and 10^8)

17,619
Fig. 15

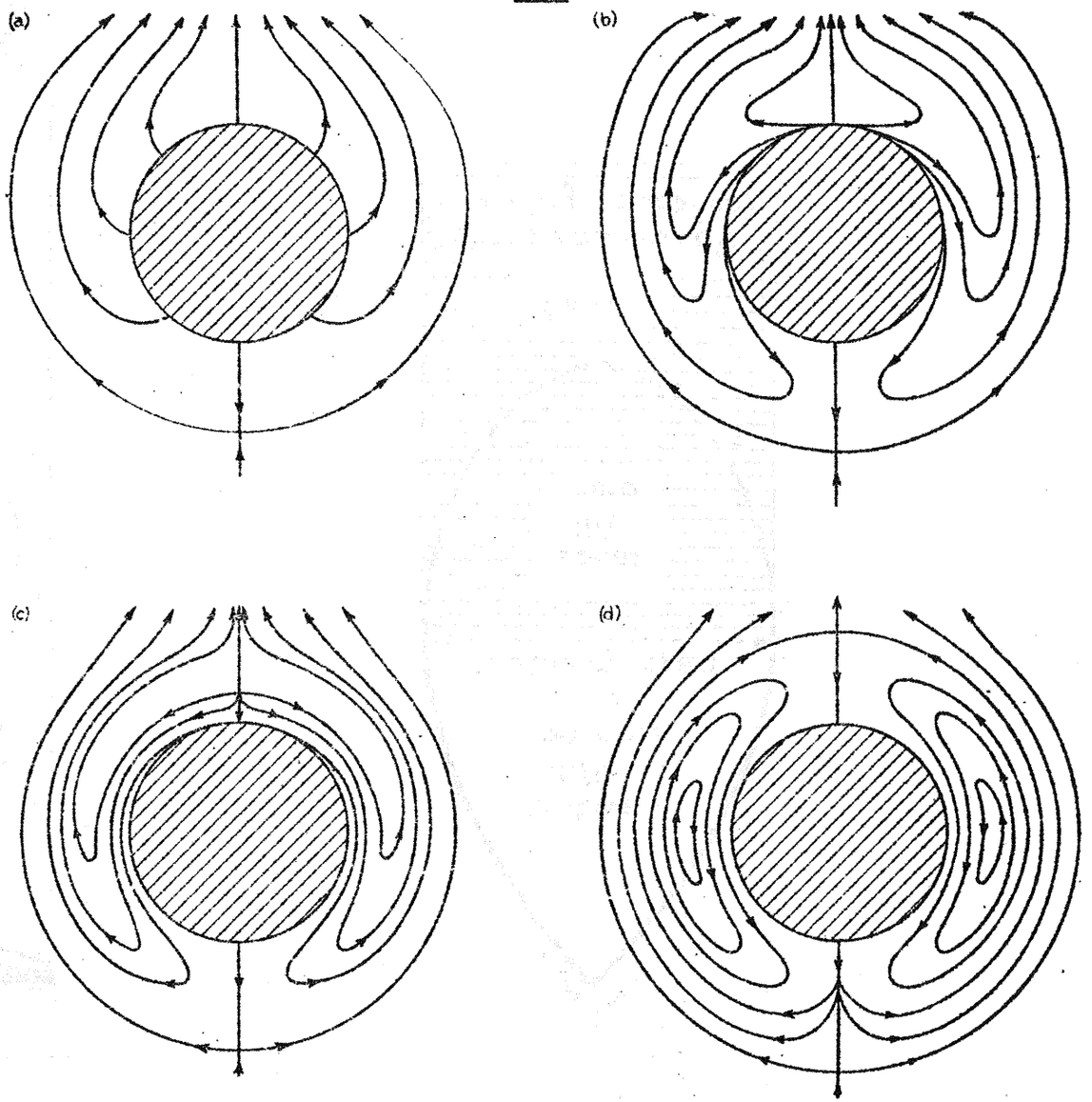

Sketches showing progressive downstream development of the streamlines in the boundary layer of a body of revolution at small incidence. Diagrammatic representation of theoretical results.

FIG. 16.

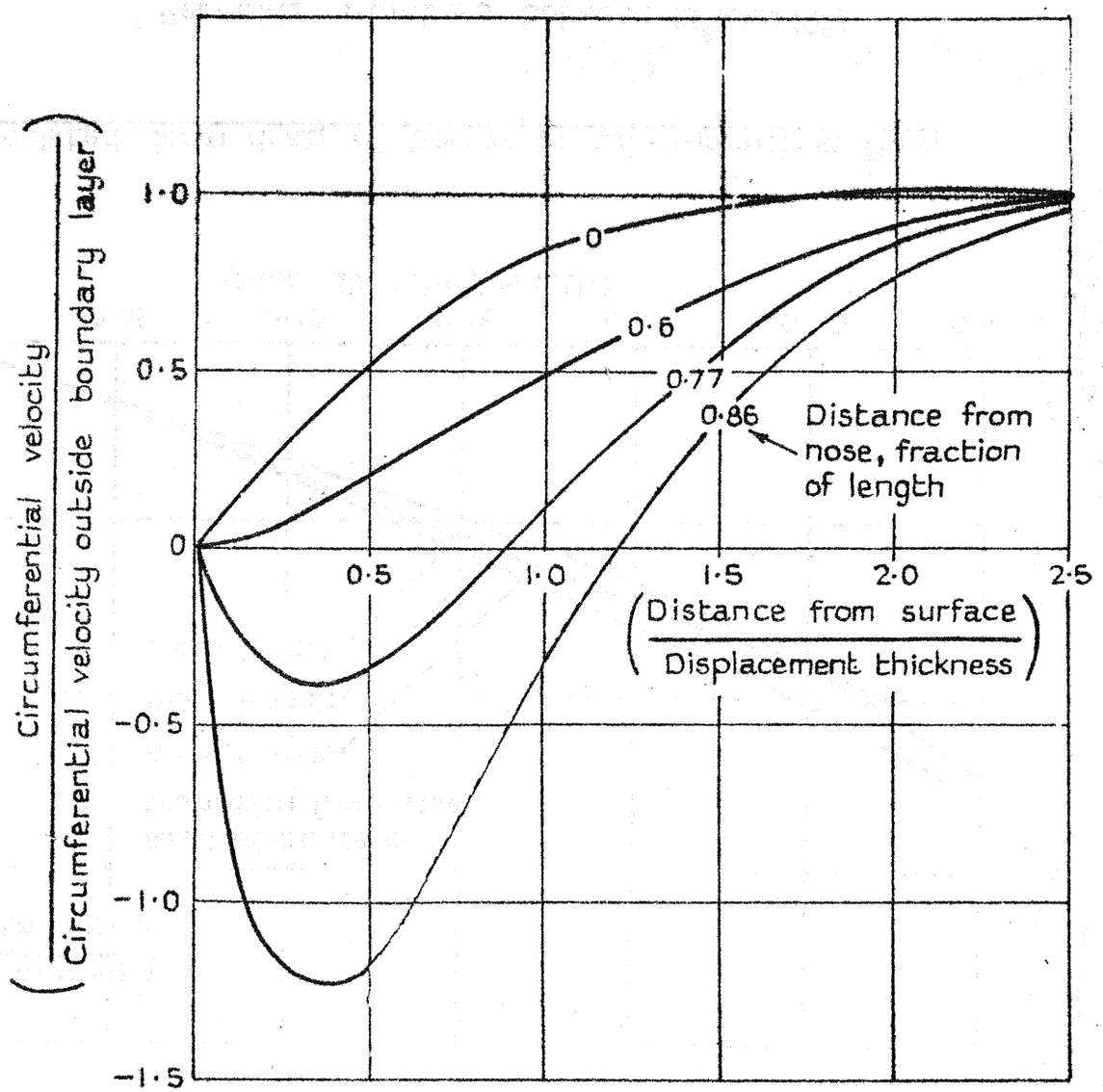

Circumferential velocity distributions on hull of airship "Akron", theoretical calculations for laminar boundary layer.

FIG. 17.

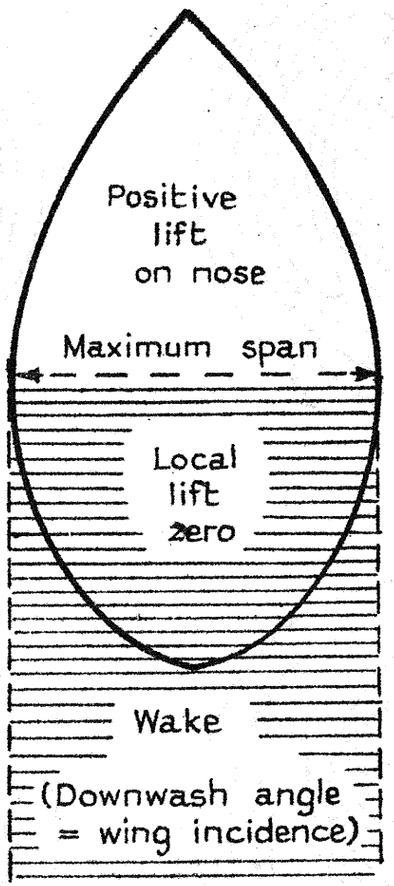

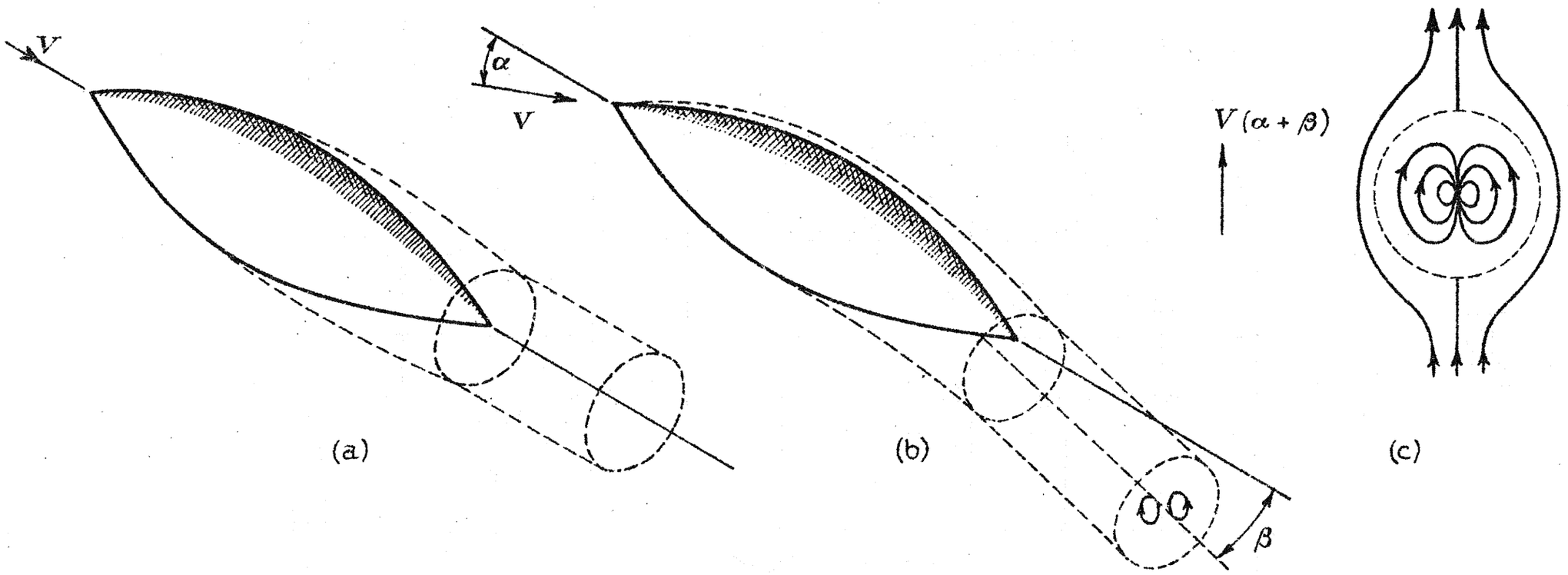

Sketches showing displacement surfaces of boundary layer and wake.

17.6.19.
FIG. 18.

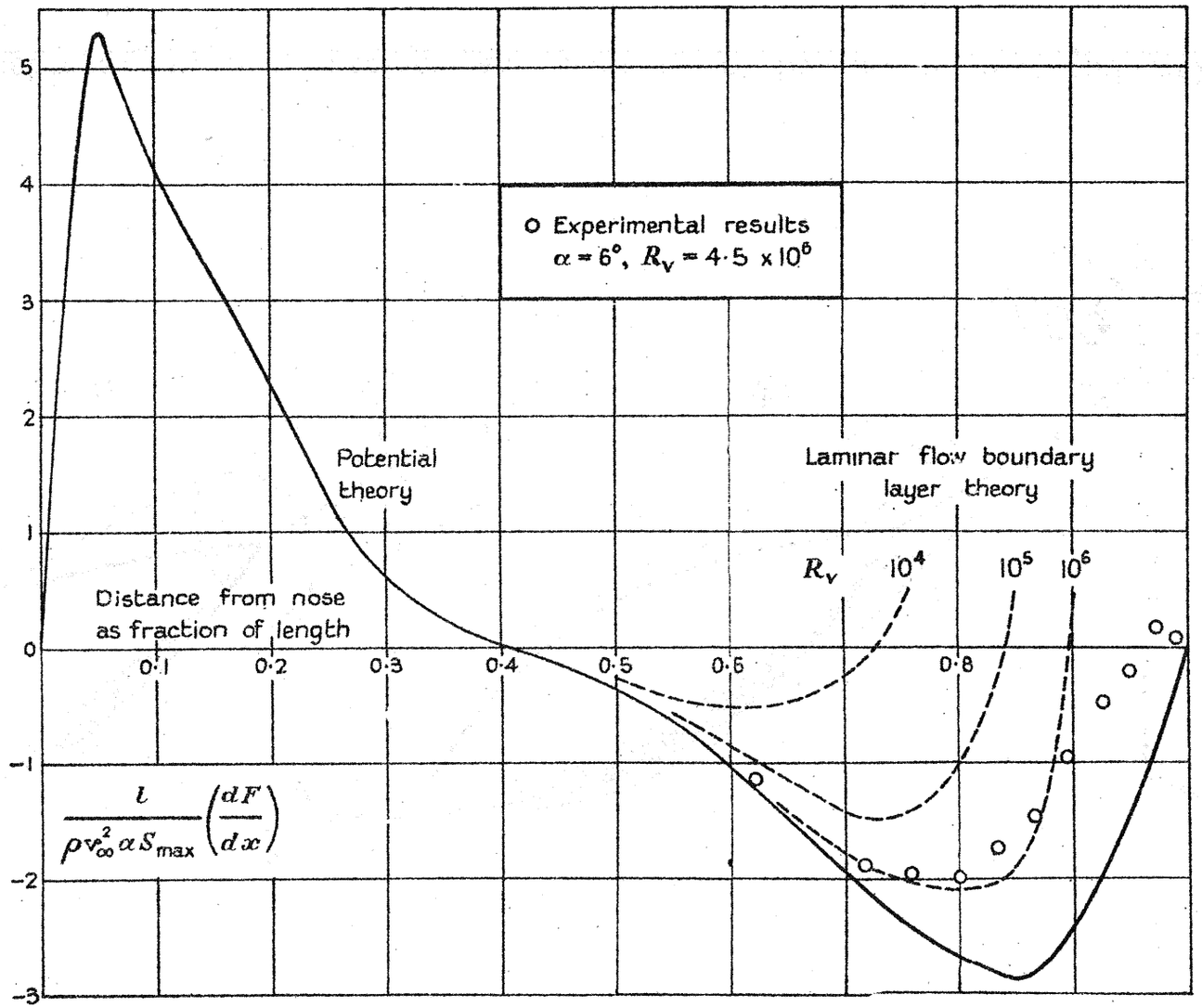

Theoretical calculations showing effect of boundary layer on side force distribution

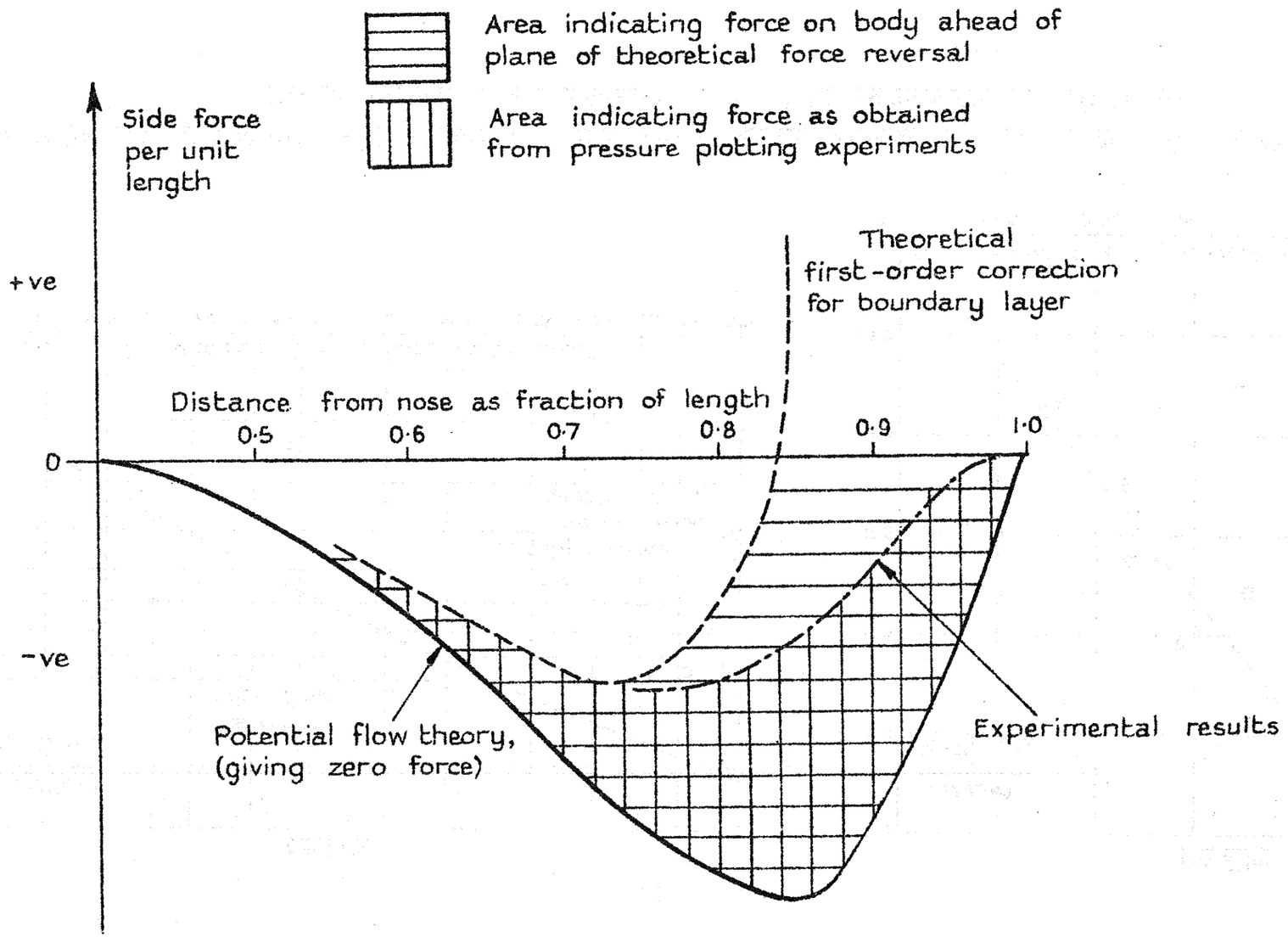
Area indicating force on body ahead of plane of theoretical force reversal
Area indicating force as obtained from pressure plotting experiments
Side force per unit length
+ve
0
-ve
Theoretical first-order correction for boundary layer
Distance from nose as fraction of length
0·5
0·6
0·7
0·8
0·9
1·0
Potential flow theory, (giving zero force)
Experimental results

17,619.
FIG. 20.

Fig. 21 (a)

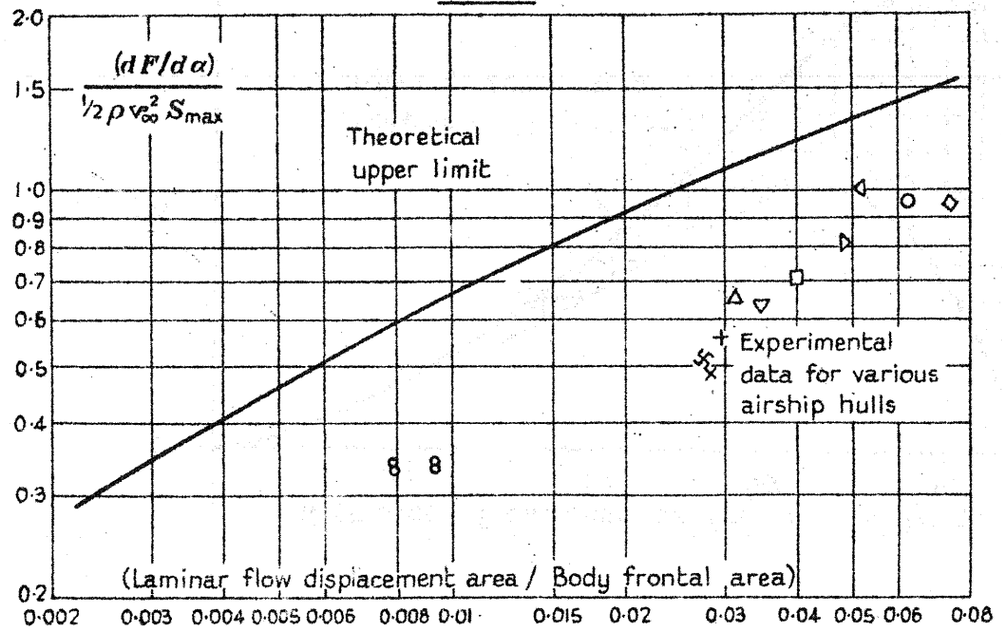

Fig. 21 (b)

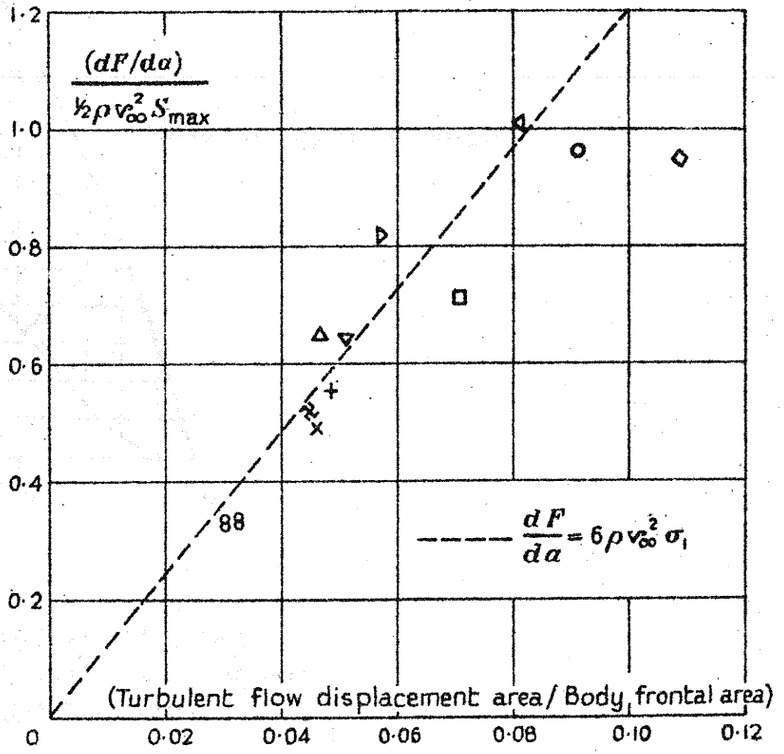

17,619
Fig. 21 (a & b)

Rate of increase of side force with incidence at $\alpha = 0$, as influenced by boundary layer displacement area calculated for (a) laminar and (b) turbulent flow conditions. (Key to data given in figure 28.)

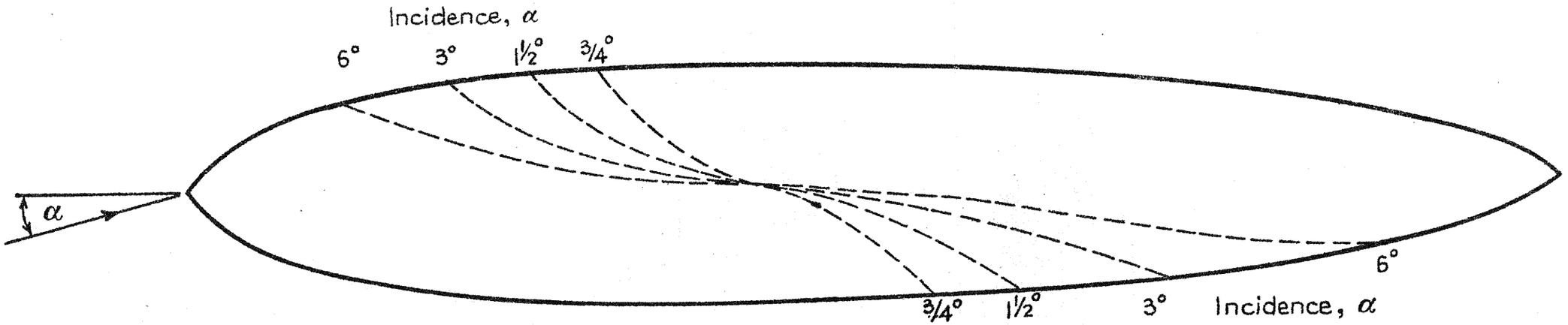

17,619.
FIG. 22.

Loci of theoretical positions of circumferential minimum pressure over hull of airship "Akron" at incidence.

Transverse planes showing
streamlines, boundary layer and vortices

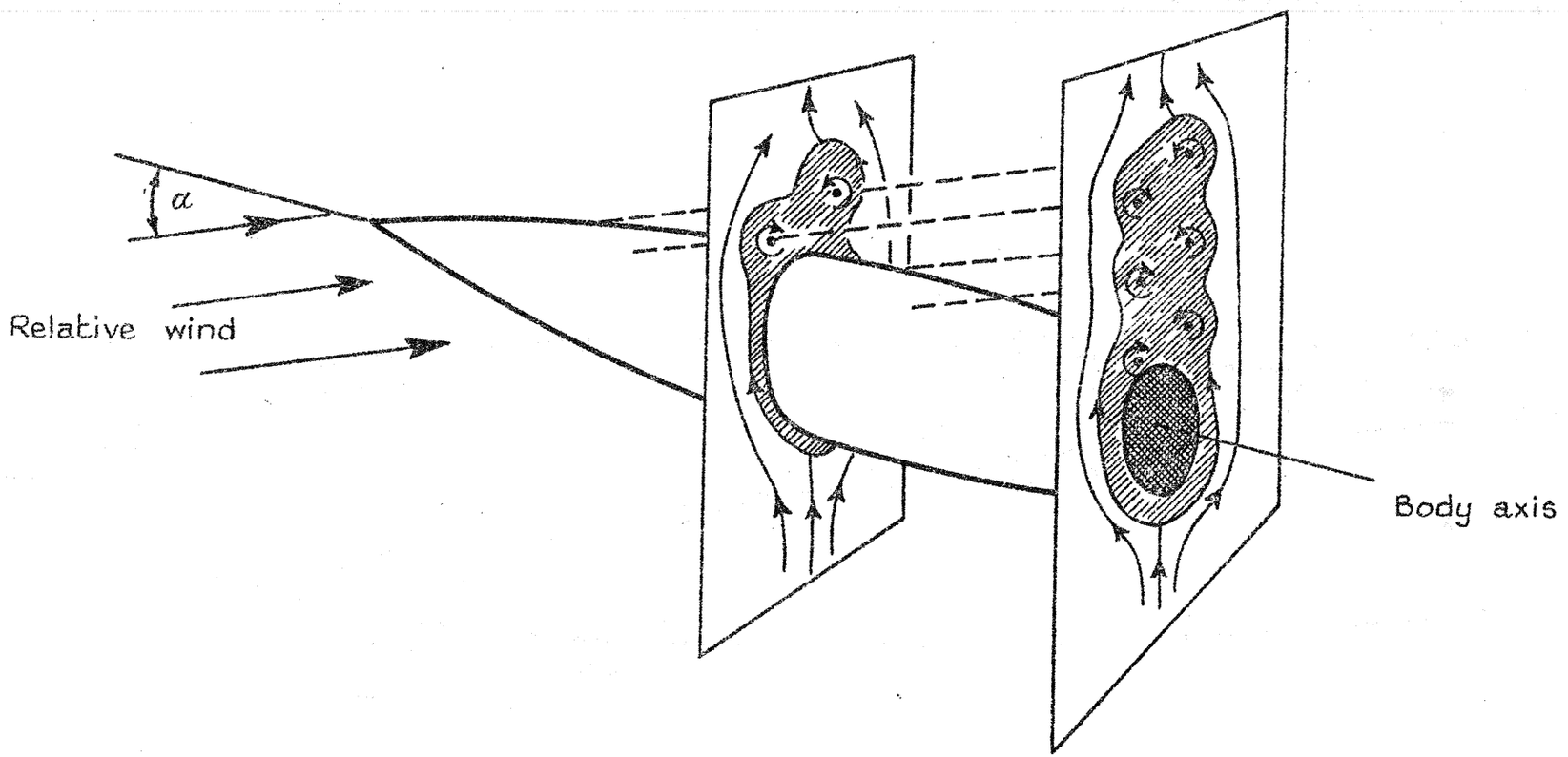

17,619.
FIG. 23.

Diagram showing progressive formation of vortex-street on body of revolution at incidence

17, 619.
FIG. 24.

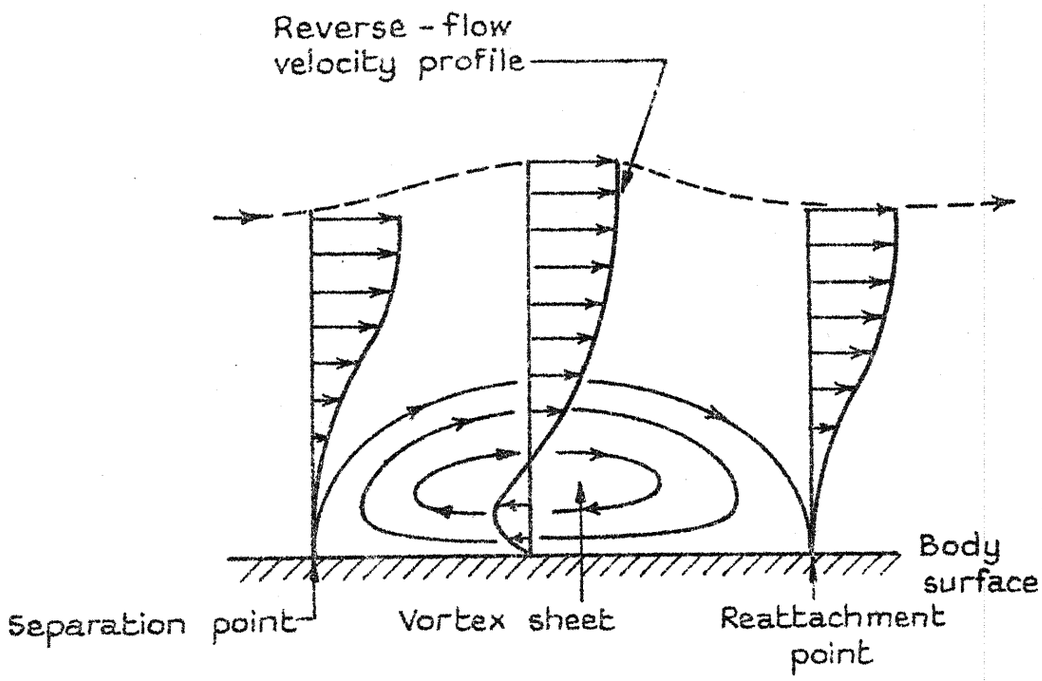

(a) Velocity profiles and streamlines within separation bubble

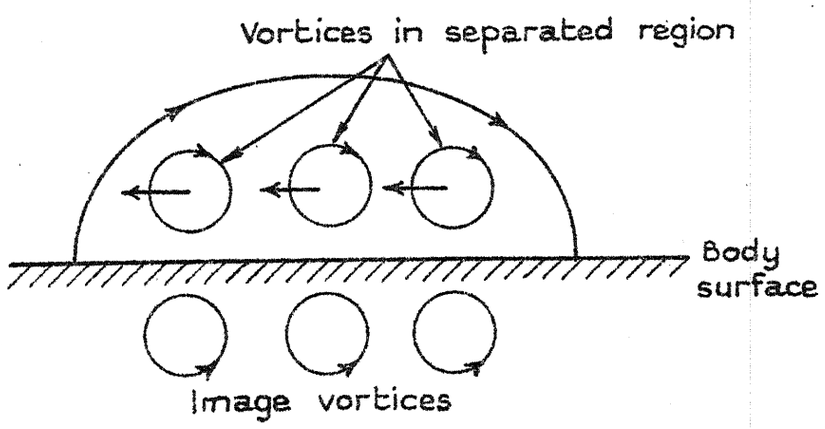

(b) Illustrating coalescence of vorticity in bubble under action of image system

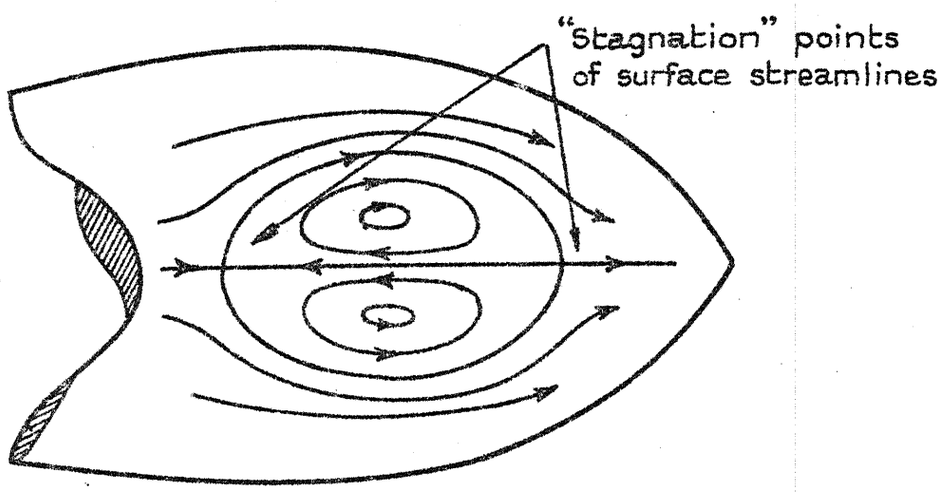

(c) Surface streamlines produced by bubble.

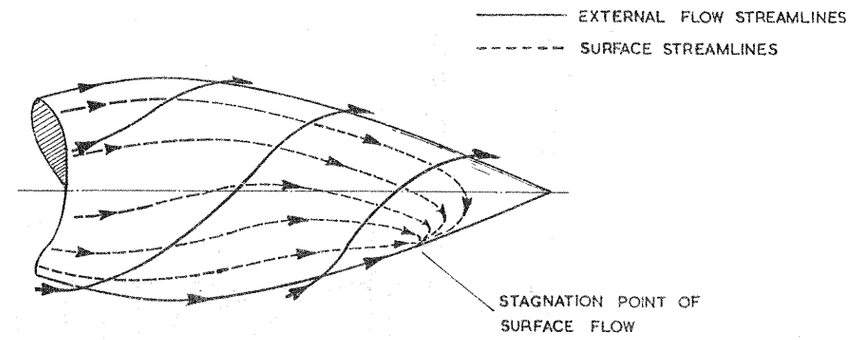

(A) SIDE VIEW OF BODY SHOWING SURFACE FLOW

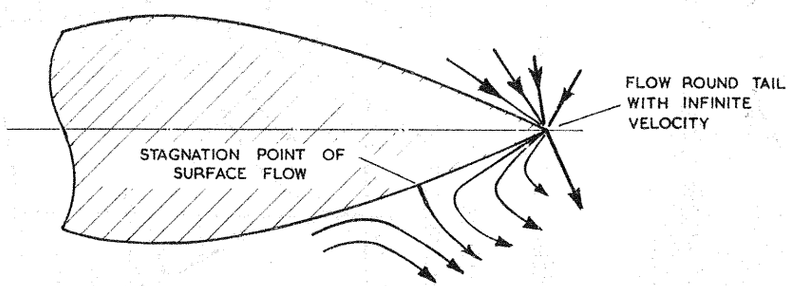

(B) STREAMLINES IN MERIDIAN PLANE

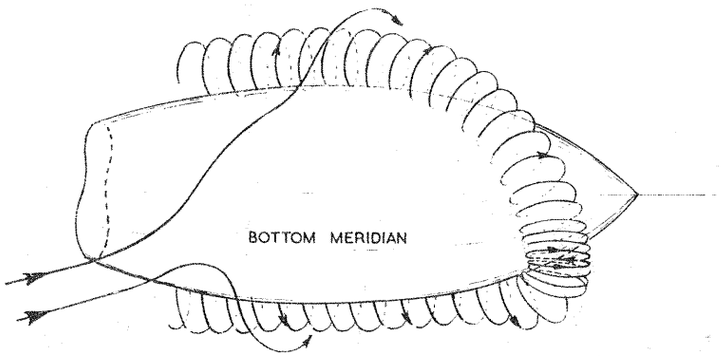

(C) THREE QUARTER VIEW FROM BELOW SHOWING THEORETICAL VORTEX FORMATION

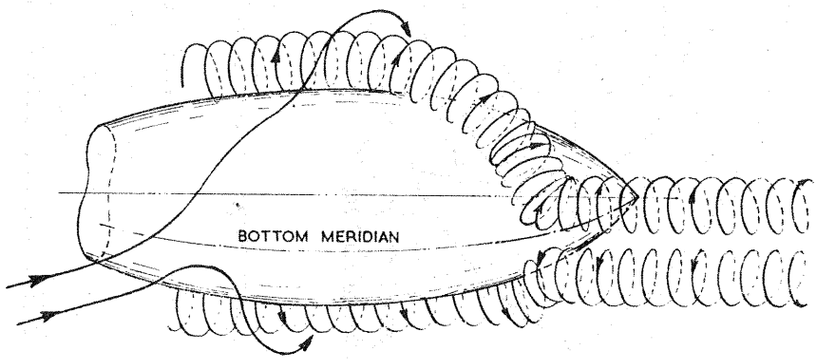

(D) THREE QUARTER VIEW FROM BELOW SUGGESTING ACTUAL VORTEX FORMATION

THEORETICAL BOUNDARY LAYER FLOW ABOUT A SLENDER BODY AT LOW INCIDENCE

FIG. 25.

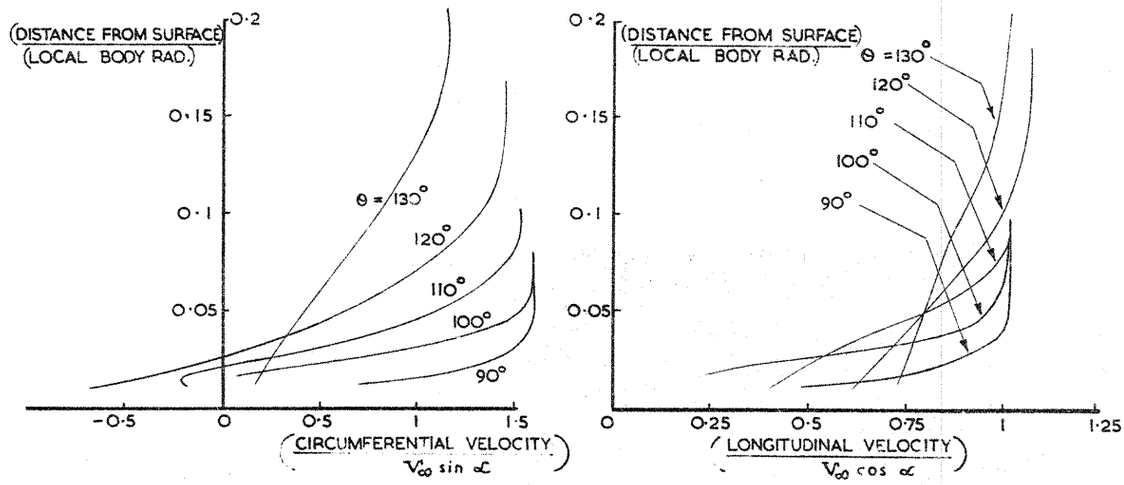

(A) $\theta = 90° - 135°$
SHOWING VORTEX ON SIDE OF BODY AND REGION OF RETARDED FLOW

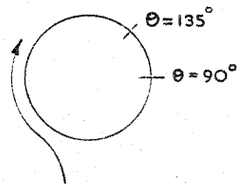

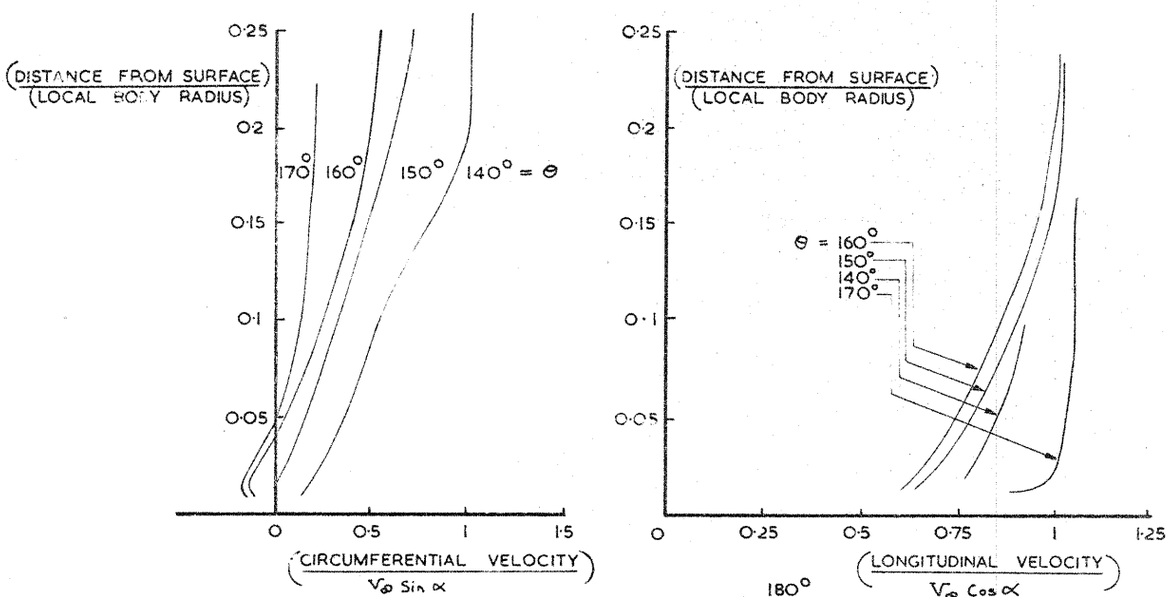

(B) $\theta = 135° - 180°$
SHOWING WEAK VORTEX NEAR UPPER MERIDIAN.

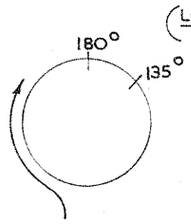

VELOCITY DISTRIBUTIONS INSIDE BOUNDARY LAYER AT A CROSS SECTION MIDWAY ALONG BODY, SIMILAR TO THAT SHOWN ON PLATE I, AT INCIDENCE 20° AND OF FINENESS RATIO 5:1. (REYNOLDS NUMBER R_ℓ = 1 MILLION)

FIG. 26.

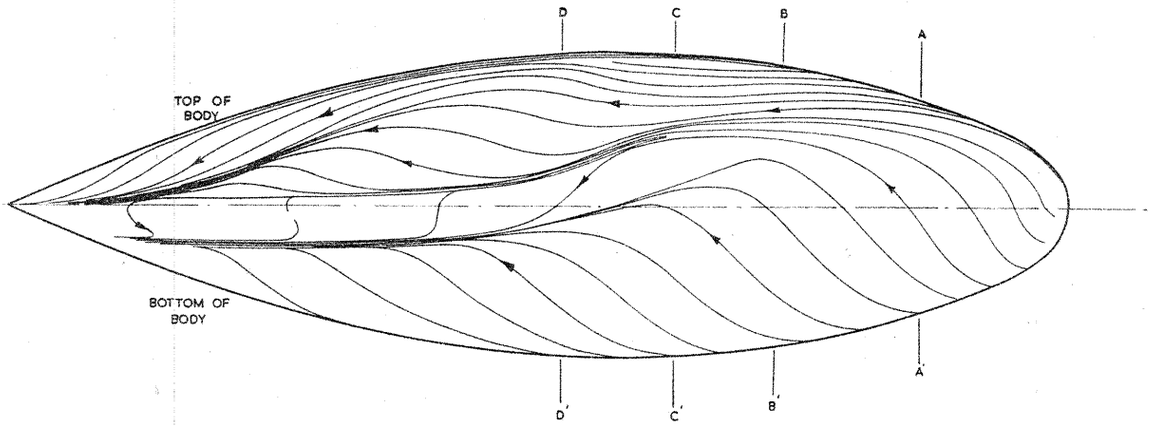

(A) SIDE VIEW OF BODY SHOWING SURFACE STREAMLINES

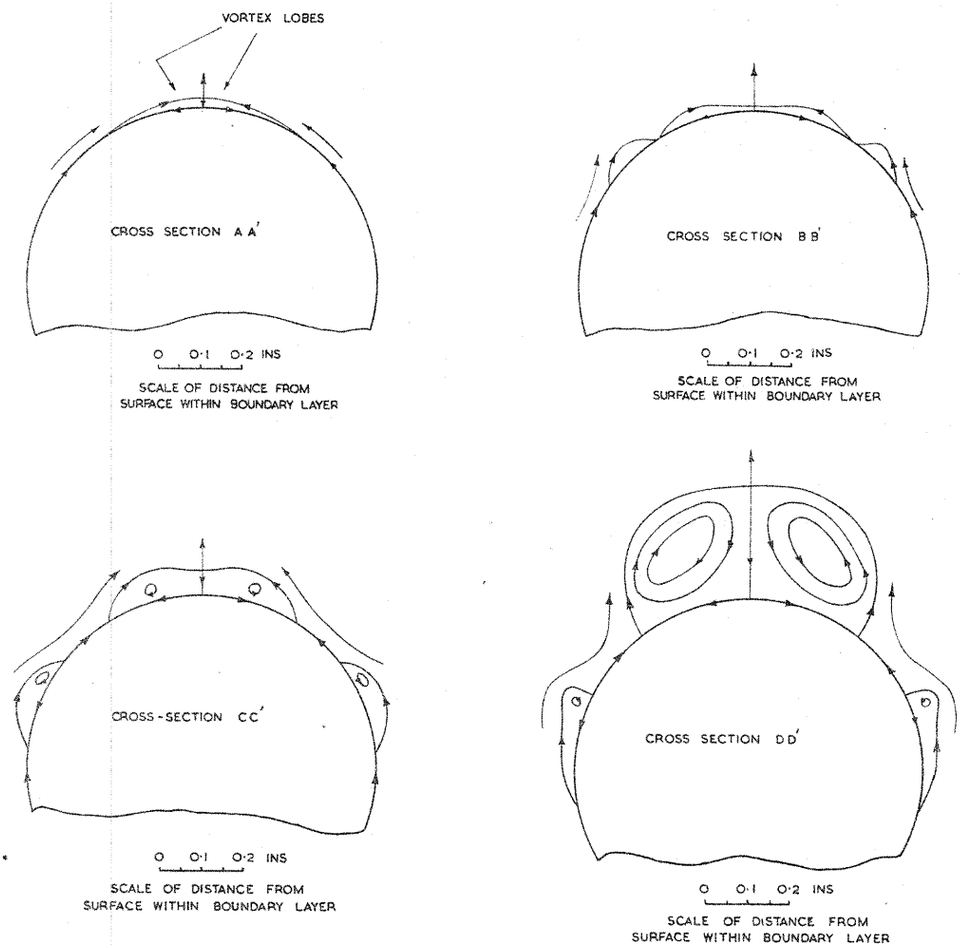

(B) PROGRESSIVE FORMATION OF CROSS FLOW VORTICES
(NB BOUNDARY LAYER THICKNESS MAGNIFIED LENGTH OF BODY = 18 INCHES)

SCHEMATIC INTERPRETATION OF EXPERIMENTED DATA ON BOUNDARY LAYER FLOW STREAMLINES ABOUT A BODY OF REVOLUTION AT INCIDENCE OF ABOUT 20° (REYNOLDS No. R_ℓ = 1 MILLION)

FIG.27.

17, 619.

FIG. 28 (a & b)

FIG. 28 a.

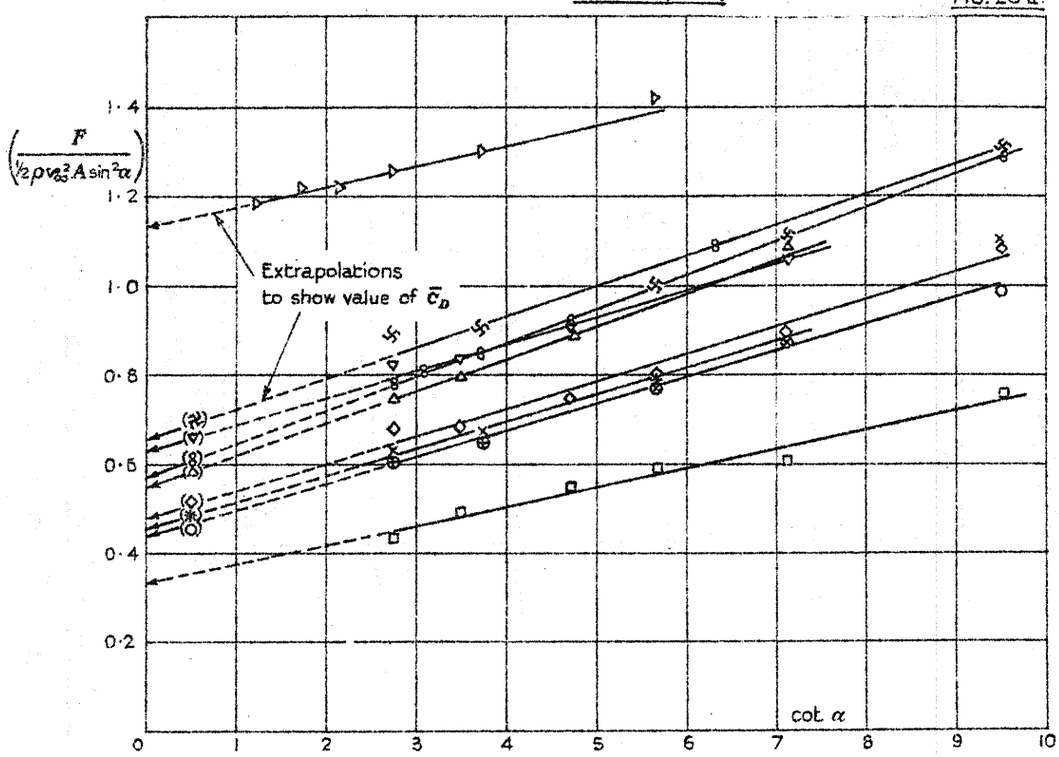

Experimental values of side force, and fitted relations of the type,
$\frac{F}{\frac{1}{2}\rho v_\infty^2 A \sin^2\alpha} = a_0 \cot\alpha + \bar{c}_D$, ($a_0$ constant), to determine the value of $\bar{c}_D$.

FIG. 28 b.

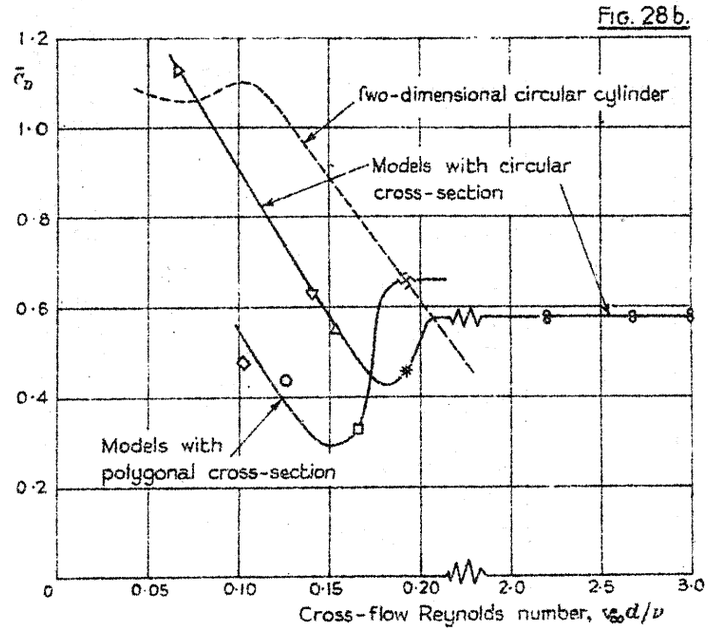

Key to data			
Airship model	Length / diameter	R_e million	Cross-section shape
▷ Parseval	5·68	0·38	Circular
▽ S.S.	5·2	0·73	Circular
△ S.S.Z.	4·75	0·73	Circular
× A.M.3 (α)	5·5	1·06	Circular
+ R.101	5·9	1·14	Circular
8 Akron	5·91	13–18	Circular
◇ R. 29	10·1	1·03	Polygonal *
○ R. 32	9·4	1·18	Polygonal *
□ R. 33	8·15	1·35	Polygonal *
⋛ A.M.3 (α)	5·5	1·06	Polygonal *
* Between 15 and 19 sides			

Tentative variation of cross-flow drag coefficient, $\bar{c}_D$, with Reynolds number.

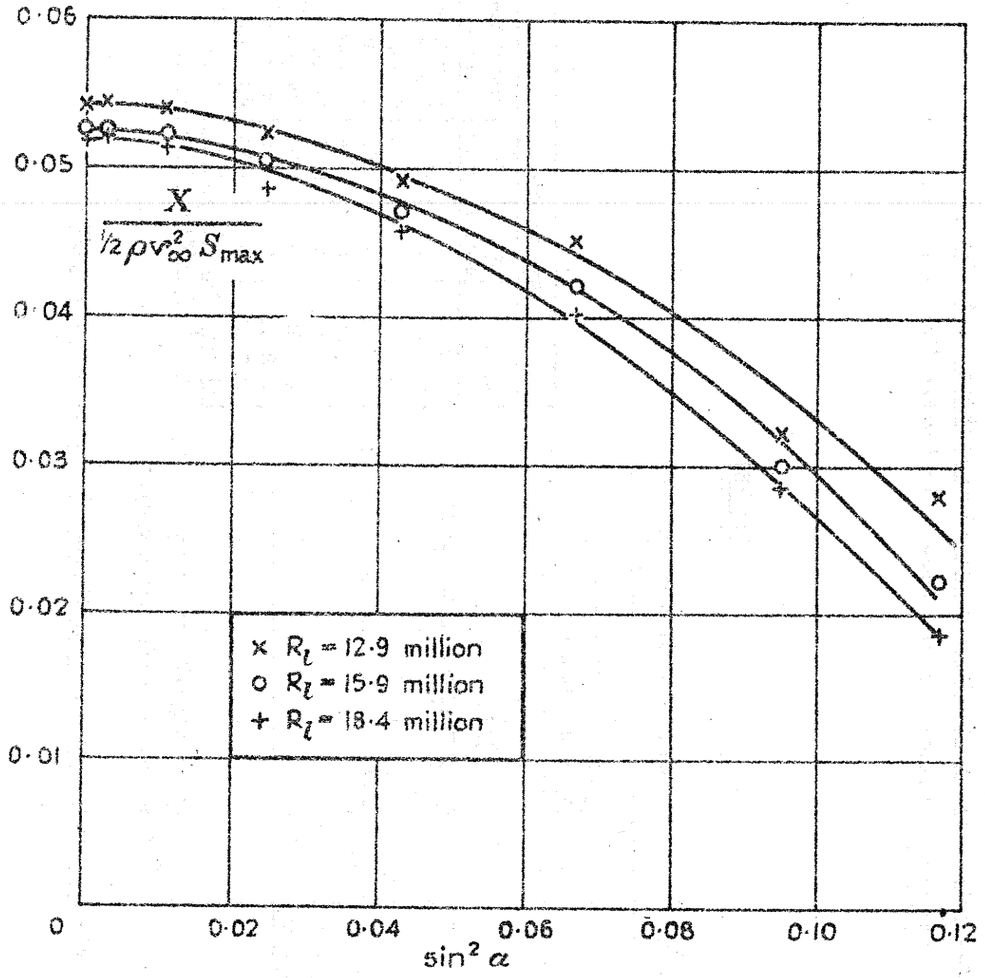

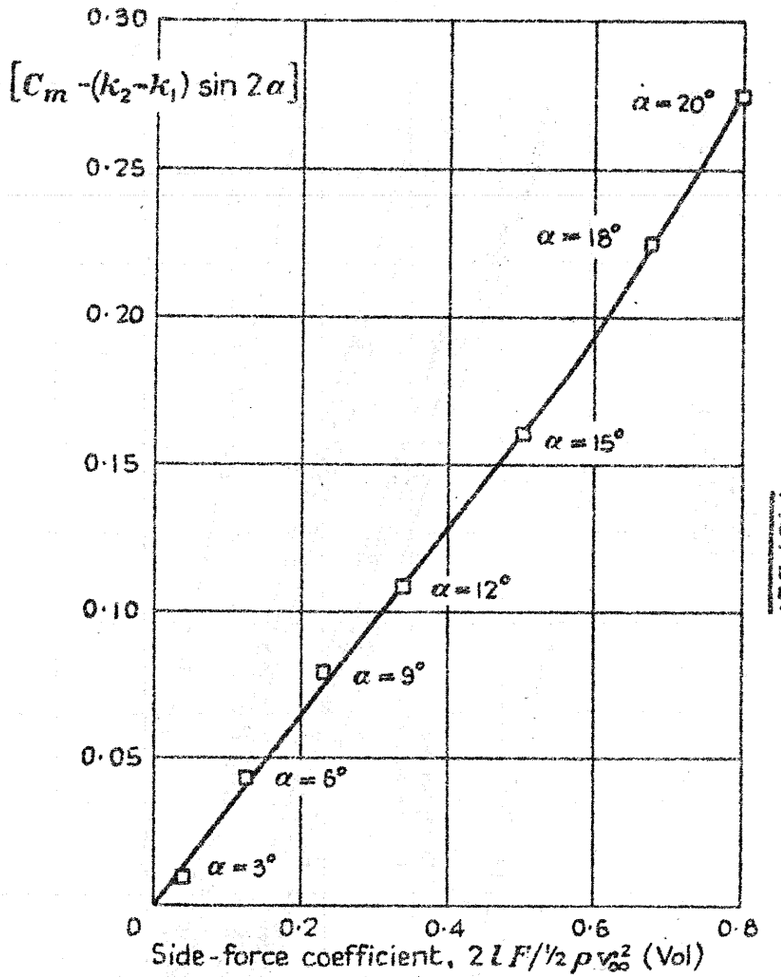

17.619.
FIG. 29.

Longitudinal force and moment characteristics of a model of the airship Akron

[Pitching moment coefficient C_m referred to tail. Estimated value of (k_2-k_1) used is 0·817]

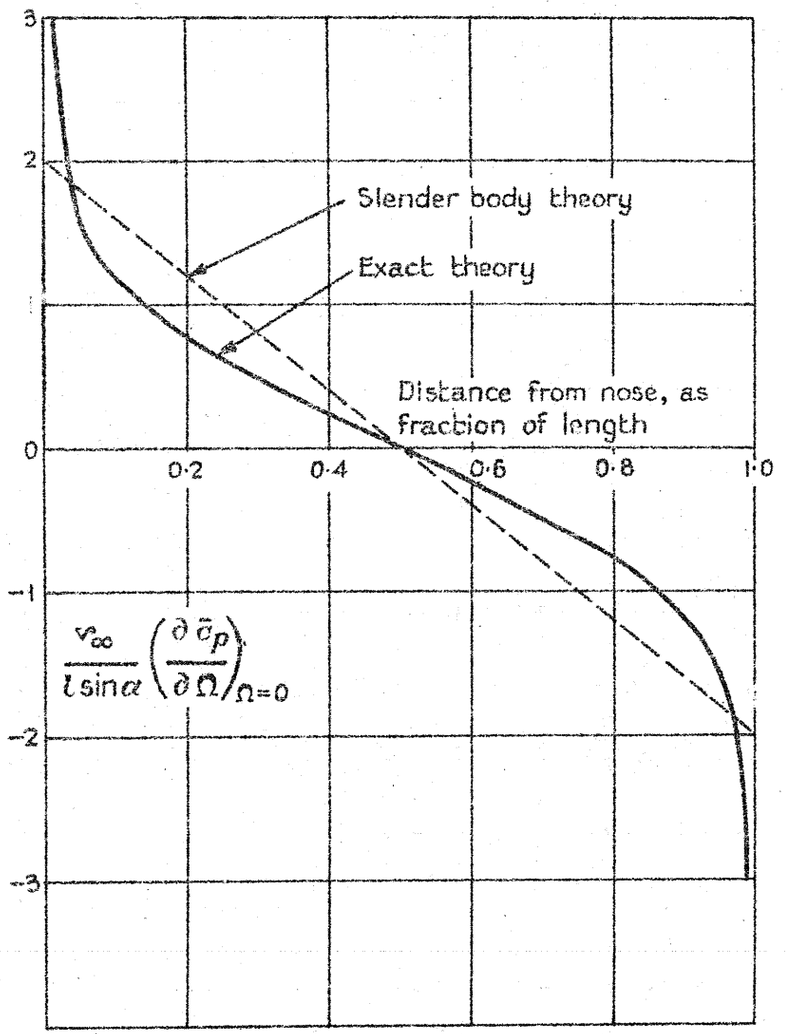

(a) Average pressures

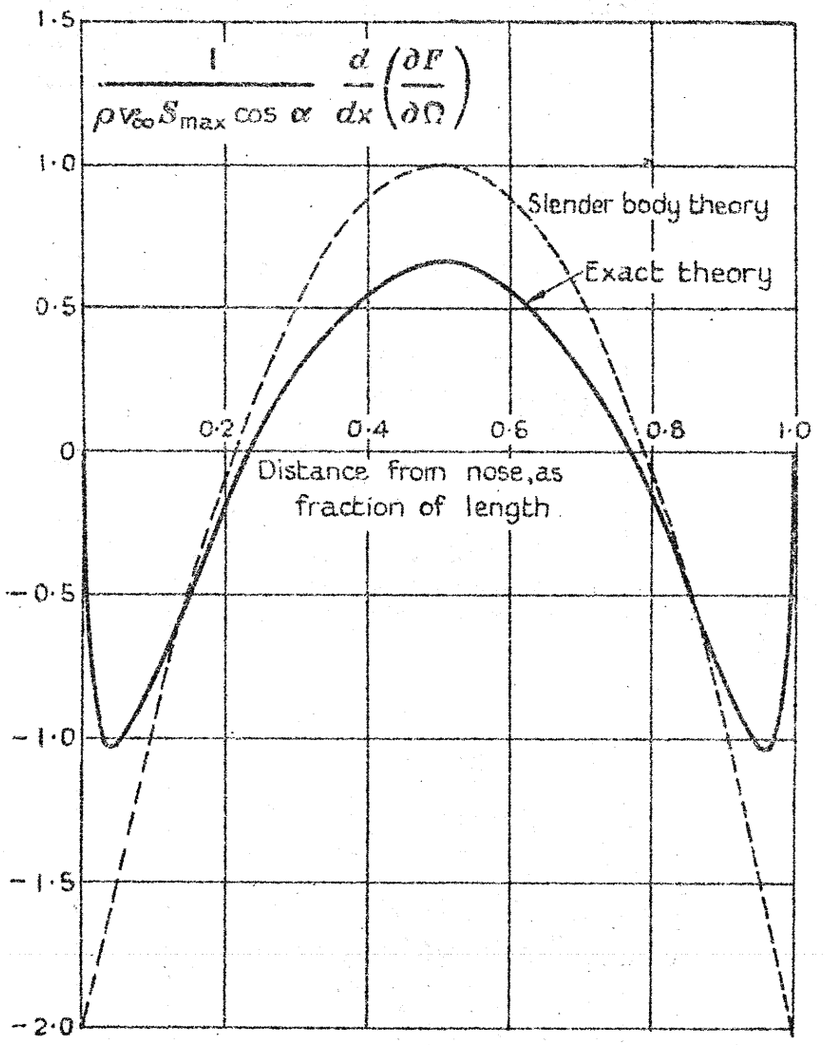

(b) Resultant side force per unit length

17,619.
Fig. 30.

Average pressure and resultant side force on a spheroid of fineness ratio 4:1.

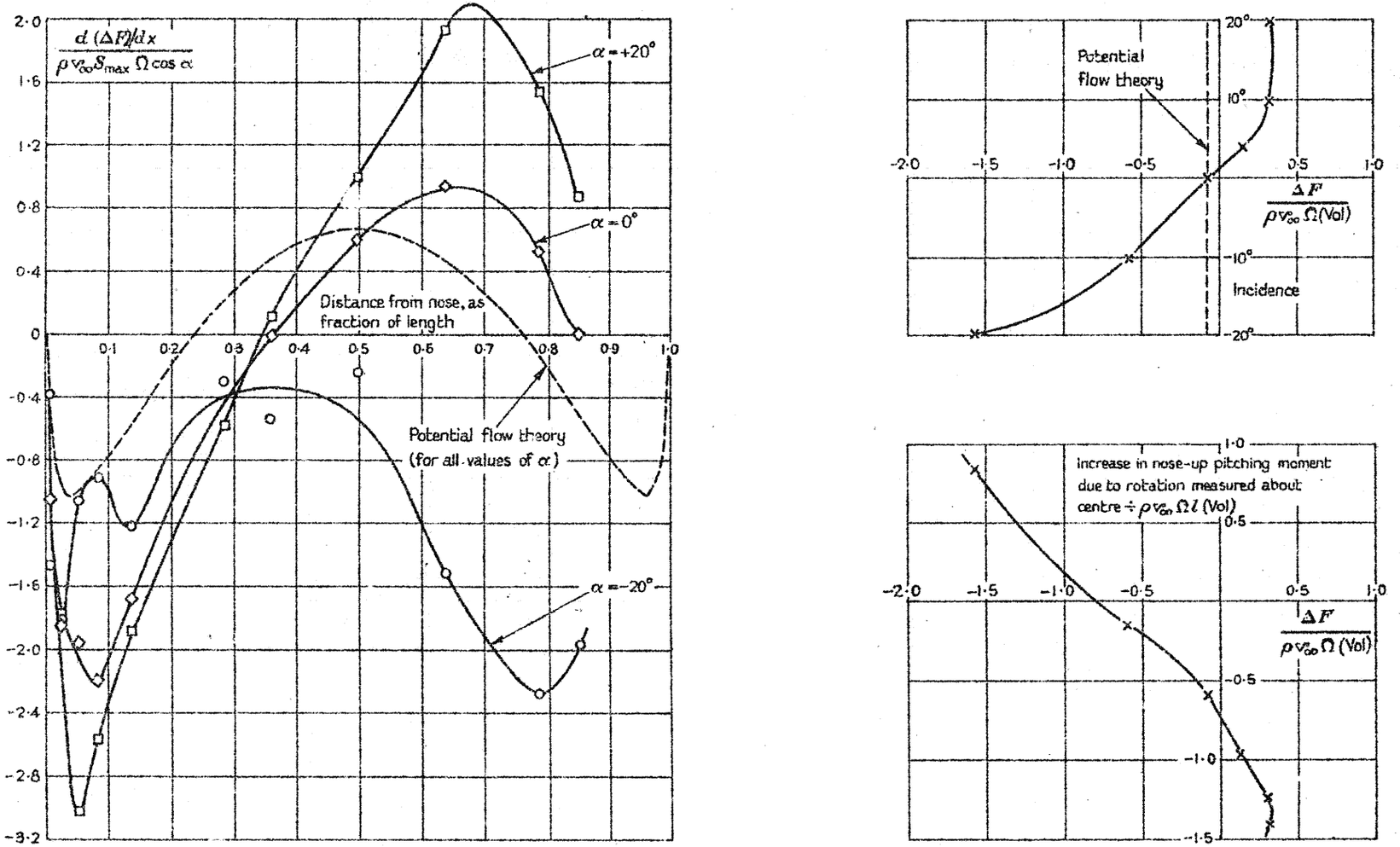

17.619.
FIG. 31.

Side force distribution and total side force and pitching moment increments due to the rotation of a spheroid in the plane of motion. (Fineness ratio of spheroid 4:1. Rate of rotation Ω given by $\Omega l/V_\infty = +1/28$. Reynolds number of tests, $R_l = 0{\cdot}51$ million. Axis of rotation passes through centre of spheroid)

17.619.
FIG. 32.

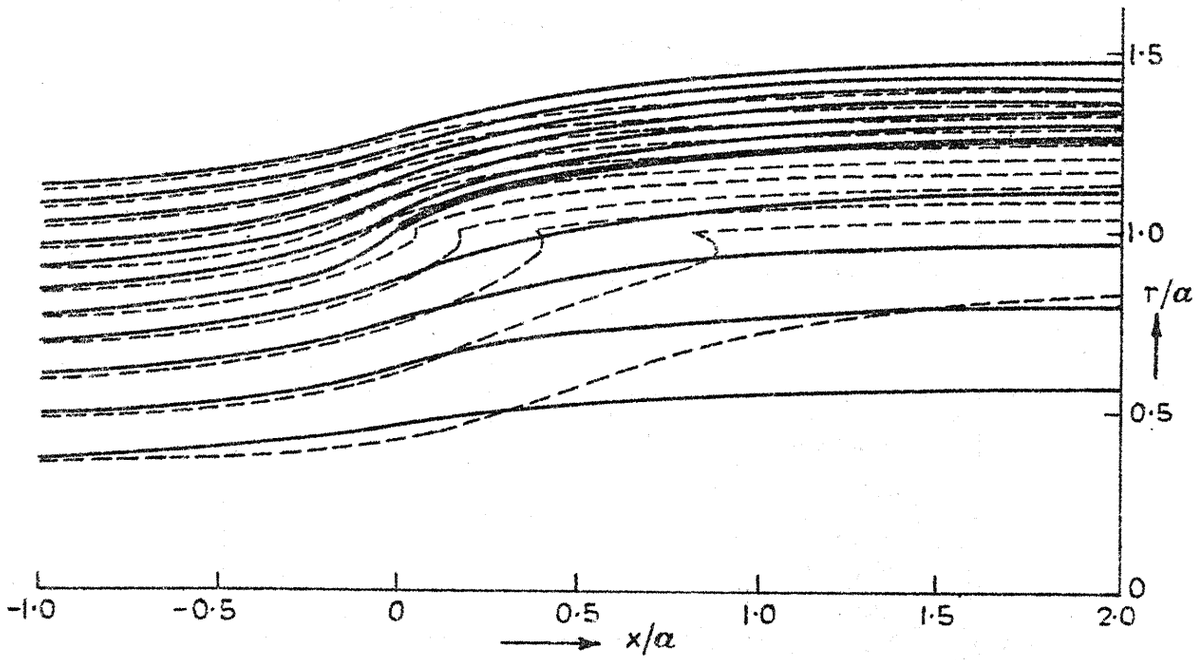

Streamlines due to a semi-infinite vortex ring distribution of constant strength in a uniform stream parallel to the axis. Broken lines show streamlines due to vortex distribution on the circular cylinder $r = a$. Full lines show streamlines due to same vortex distribution on a stream surface originating at $x = 0$, $r = a$.

17,619.
FIG. 33.

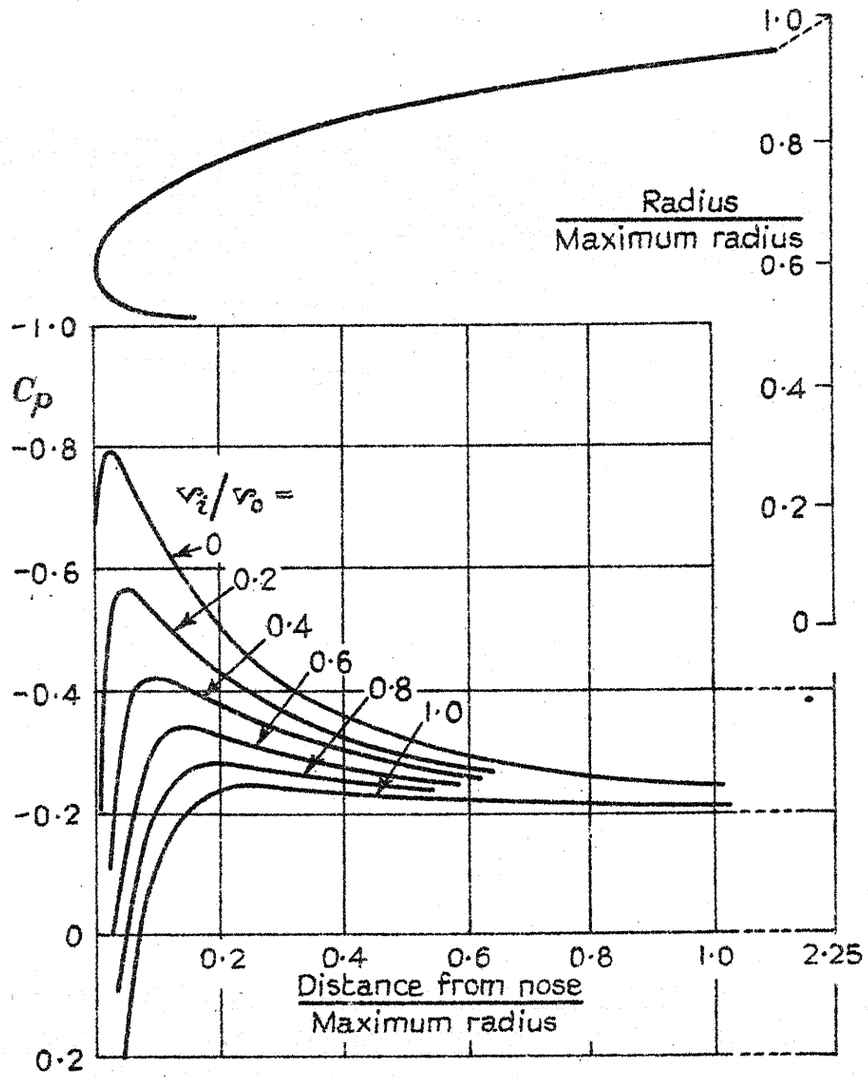

Typical experimental pressure distributions over exterior of semi-infinite duct as influenced by intake velocity, v_i. (Intake area / Maximum frontal area = 0·27) From Kuchemann and Weber 1953.

17,619.
FIG. 34.

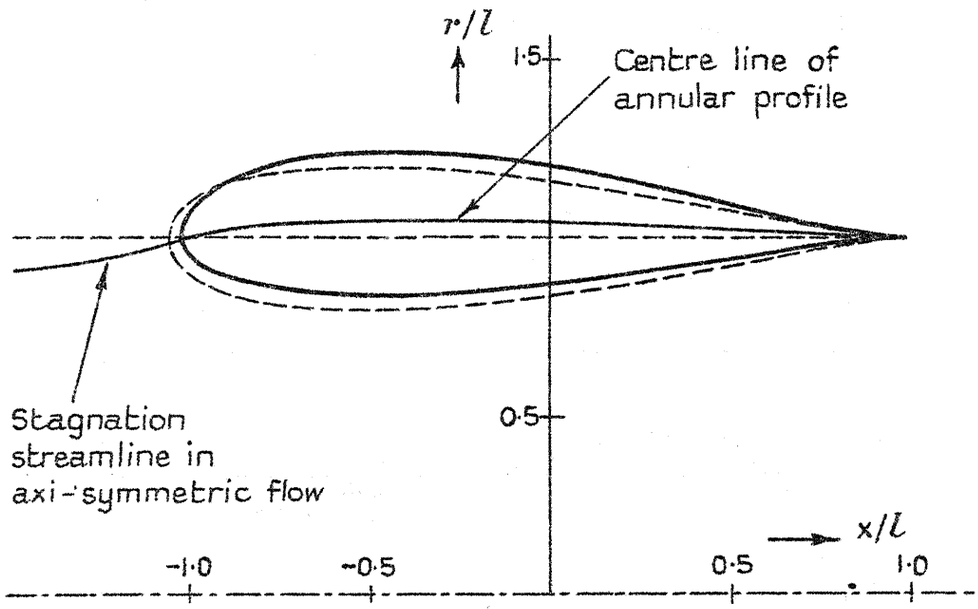

Duct shape produced by distribution of sources on cylinder r/l, whose intensity is adjusted to yield thickness distribution of Joukowsky profile (shown in broken lines), placed in a uniform stream parallel to axis of symmetry.

17,619.
FIG. 35.

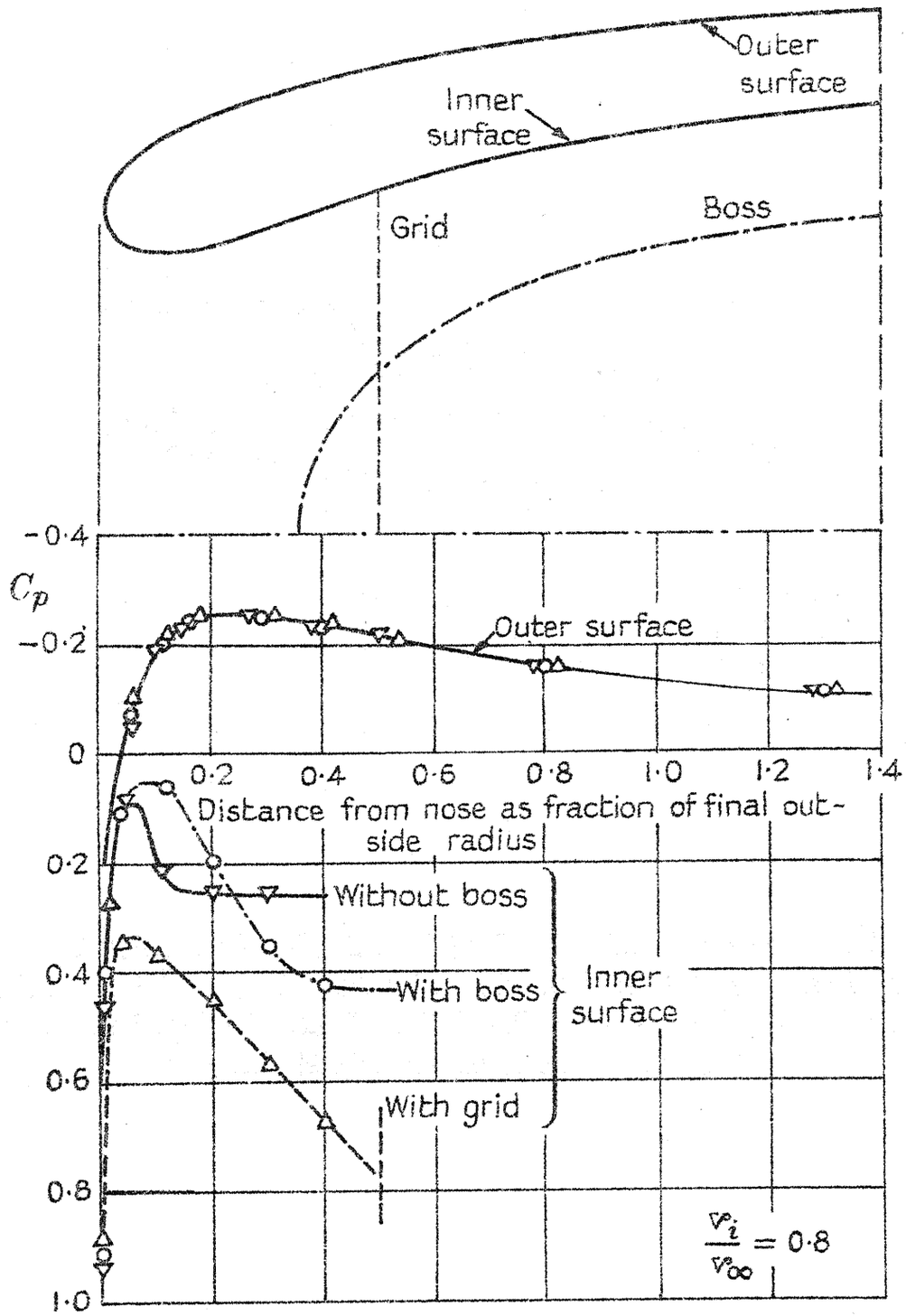

Independence of the pressure distribution along the outer surface from conditions in the internal duct.
(From Kuchemann, 1953).

17, 619.
Fig. 36.

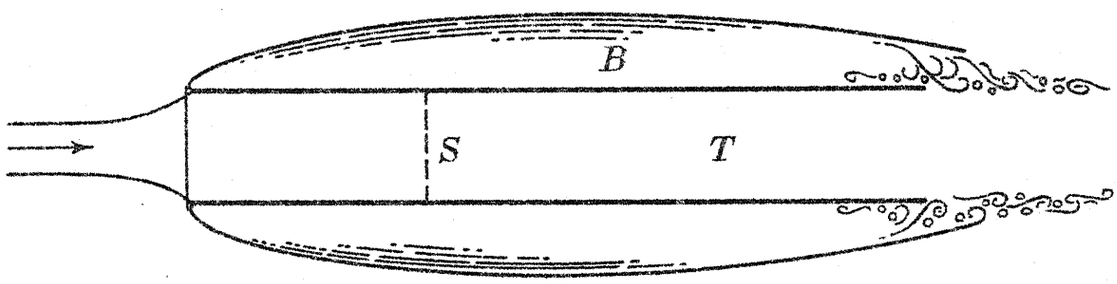

T: Tube *B*: Bubble *S*: Screen

The cavitation method of duct design.

17,619.
FIG. 37.

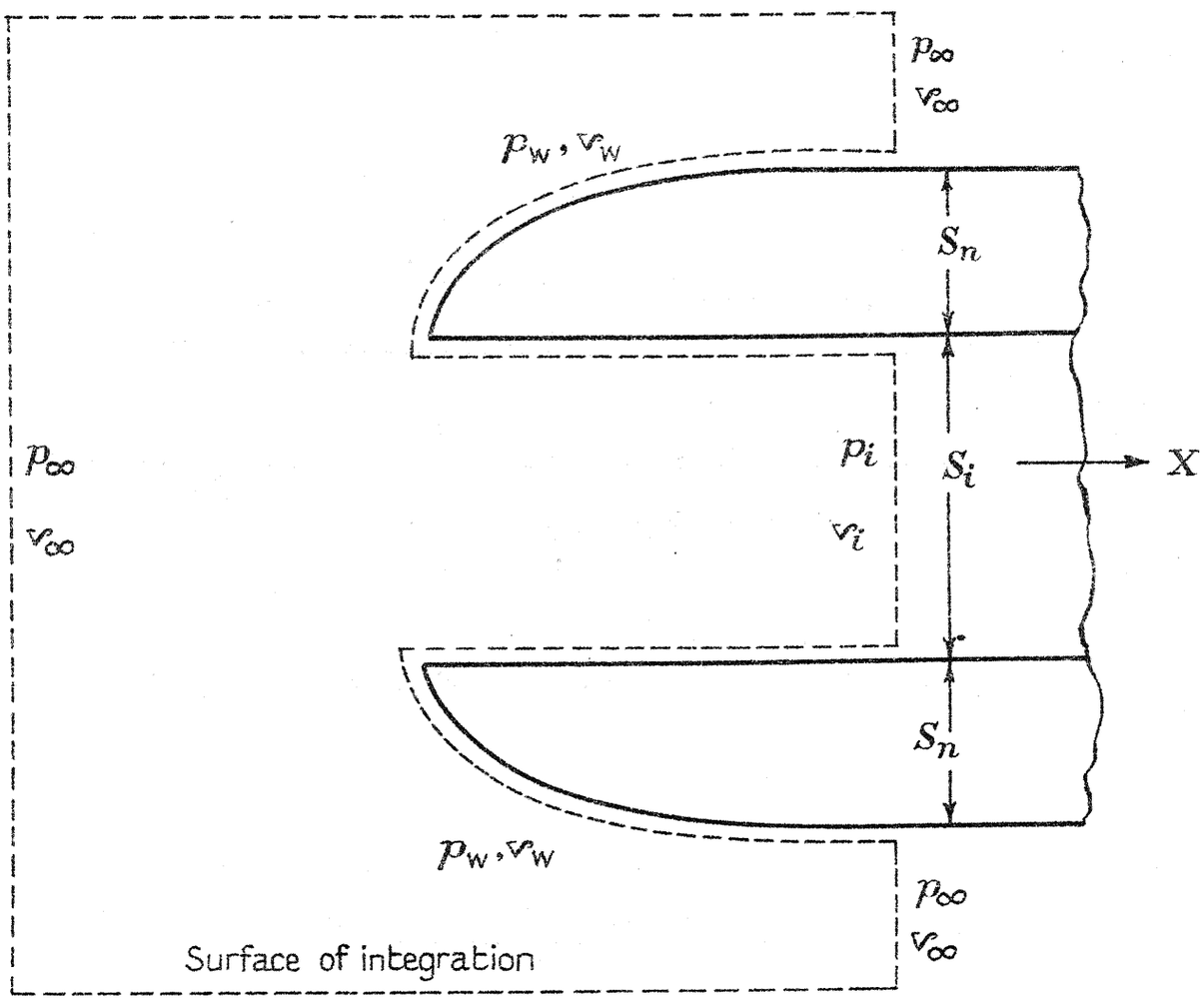

Control surface and symbols for momentum theorem

17,619.
FIG. 38.

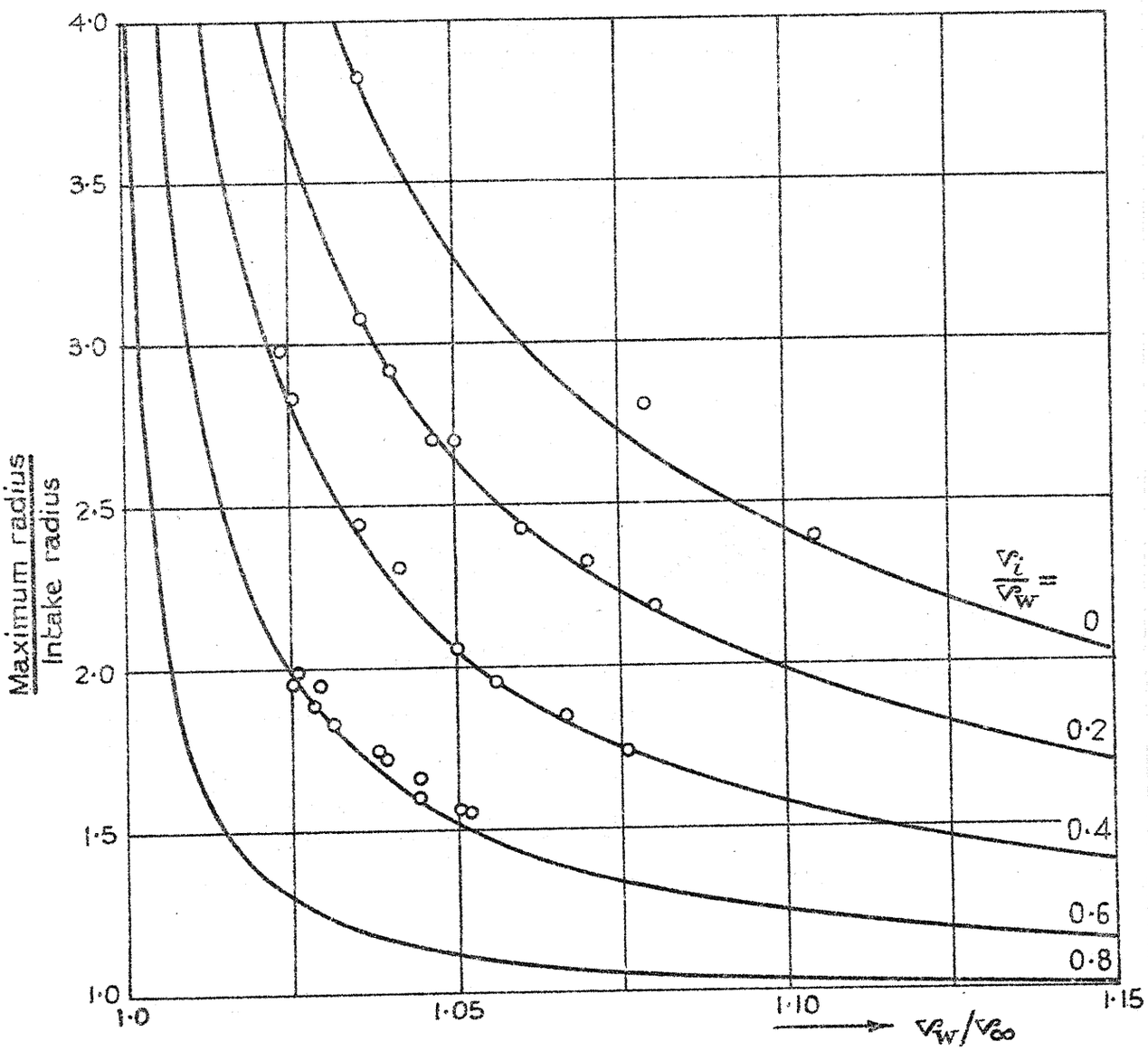

Experimental values of the contraction ratios of cavitation bubbles compared with theoretically determined values.

17,619.
FIG. 39.

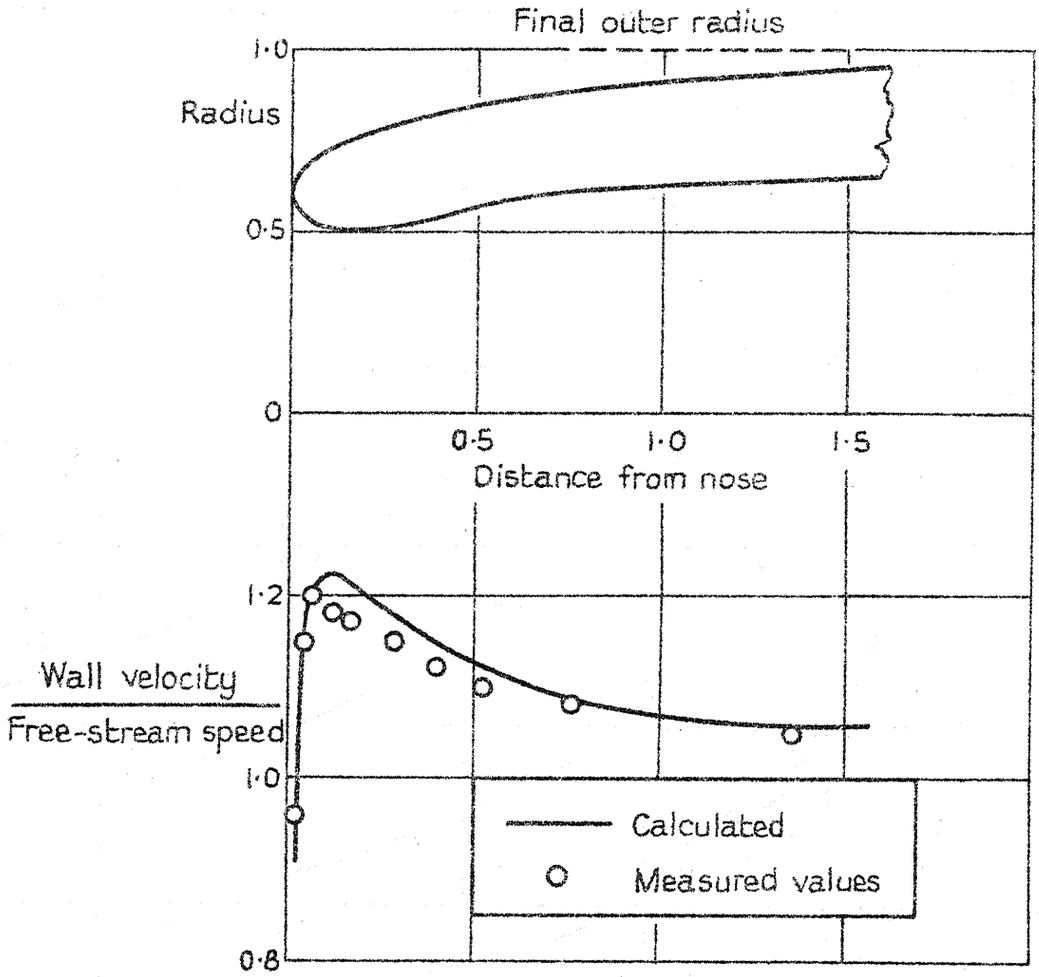

Shape of duct calculated by iterative procedure from stipulated vortex and source ring distribution, together with the theoretical velocity distribution over its outer surface compared with measured values at corresponding intake velocity

17, 619.
FIG. 40.

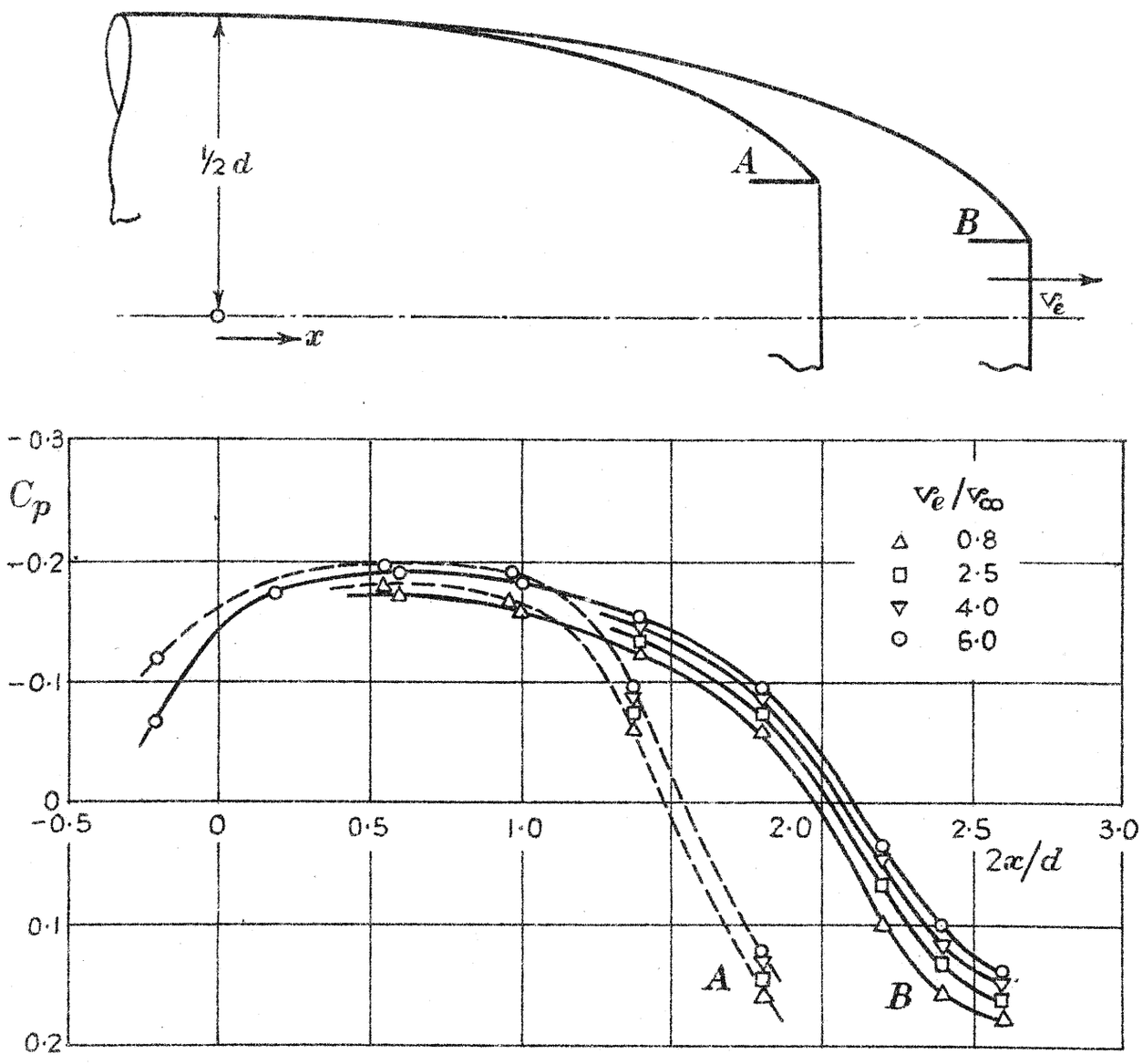

Pressure distribution over exterior of base of semi-infinite duct showing effect of exhaust velocity, due to the turbulent mixing process.
From Kuchemann and Weber, 1953.